# Lab-On-Chip for *Ex-Vivo* study of morphogenesis of tip growing cells of pollen tube

Mahmood Ghanbari Mardasi

A Thesis

in

the Department

of

Mechanical and Industrial Engineering

Presented in partial fulfillment of the requirements for the
Degree of Doctor of Philosophy (Mechanical Engineering) at
Concordia University
Montreal, Quebec, Canada

**CONCORDIA UNIVERSITY**

**SCHOOL OF GRADUATE STUDIES**

This is to certify that the thesis prepared

By: **Mahmood Ghanbari Mardasi**

Entitled: **Lab-On-Chip for Ex-Vivo study of morphogenesis of tip growing cells of pollen tube**

and submitted in partial fulfillment of the requirements for the degree of

DOCTOR OF PHILOSOPHY (Mechanical Engineering)

complies with the regulations of the University and meets the accepted standards with respect to originality and quality.

Signed by the final examining committee:

_____ Chair
Dr. Z. Chen

_____ External Examiner
Dr. R. Selvaganapathy

_____ External to Program
Dr. P. Valizadeh

_____ Examiner
Dr. A. Dolatabadi

_____ Examiner
Dr. R. Bhat

_____ Examiner
Dr. A. Geitman

_____ Thesis Supervisor
Dr. M. Packirisamy

Approved by _____
Dr. A. Dolatabadi, Graduate Program Director

January 10, 2014

_____
Dr. C. Trueman, Interim Dean
Faculty of Engineering & Computer Science

# *ABSTRACT*

## Lab-On-Chip for *Ex-Vivo* study of morphogenesis of tip growing cells of pollen tube

***Mahmood Ghanbari Mardasi, Ph.D.***
***Concordia University, 2014***

The purpose of the thesis is to develop a microfluidic based *lab-on-chip* (LOC) platform providing an *Ex-Vivo*testing environment that is able to mimic certain aspects of the *in vivo* growth conditions of the pollen tube, a cellular protuberance formed by the male gametophyte in the flowering plants. The thesis focuses on design, fabrication, modeling and testing of various LOC devices for the study of static and dynamic behavior of pollen tubes in response to mechanical stimulation.

TipChip, an LOC platform, was developed to advance both experimentation and phenotyping in cell tip growth research. The platform enabled simultaneous testing of multiple pollen tubes. Using TipChip, we were able to answer several outstanding questions regarding pollen tube biology. We found that contrary to other types of tip growing cells such as root hairs and fungal hyphae, pollen tubes do not have a directional memory. Furthermore, we explored the effect of geometry of the microfluidic cell culture on pollen tube growth. We found that changing the width of the microfluidic channels does not have a significant effect on the pollen tube growth rate, while the growth rate was increased by increasing microchannel depth.

We modified the original TipChip design to ascertain identical growth conditions for sequentiallyarranged pollen tubes and to ensure even distribution of entrapment probabilities for all microchannels. The effect of different dimensions of the microfluidic network on cell trapping probability was assessed using computational fluid dynamics and verified by experimental testing. The design was optimized based on trapping probability and uniformity of fluid flow conditions within the microchannels.

This thesis also presents a novel method of fabricating a high aspect ratio horizontal PDMS microcantilever-based flow sensor integrated into a microfluidic device. The performance of the flow sensor was tested by introducing various flow rates into the microfluidic device and measuring the deflection of the cantilever's tip using an optical microscope.

The thesis addresses the quantification of cellular growth force of *Camellia* pollen tip growing cells using FlexChip, a flexure integrated LOC on polymer. We quantified the force that pollen tube is able to exert using a microfluidic lab-on-a-chip device integrated with flexural structure. The pollen grain is trapped in the microfluidic network and the growing tube is guided against a flexible microstructure that is monolithically integrated within the microfluidic chip. The invasive growth force of growing pollen tube was calculated from the maximal bending of microstructure modelled by Finite Element Analysis (FEA).

Furthermore, the effect of the mechanical obstacle on the pollen tube's growth dynamics was assessed by quantifying the shift in the peak frequency characterizing the oscillatory behavior of the pollen tube growth rate. Our detailed analysis of the pollen tube growth dynamic before and during the contact with microcantilever revealed that pollen tube growth rate was reduced by 44% during the contact with the microcantilever. Moreover,

the peak of oscillation frequency of pollen tube growth rate was reduced more dramatically by 70-75%. This suggests that the pollen tube actively changes its growth pattern to cope with the mechanical obstacle.

Our findings in this thesis are novel in terms of pollen biology, and we believe insights from this research will lead to a better understanding of morphogenesis of a kind of tip growing cells, namely, pollen tube.

# *ACKNOWLEDGEMENTS*

I would like to express my sincere thanks to Dr. Muthukumaran Packirisamy for being my thesis supervisor and giving me the opportunity to realize this work in Optical Bio-Microsystems laboratory MIE, Concordia University. Writing this thesis was definitely not possible without his technical, moral and financial support.

I especially thank Dr. Anja Geitmann for her great comments and her continuous attention and support. I had a lot of very interesting discussions with her throughout this work.

I would also like to thank the members of my defense committee, Dr. Ravi Selvaganapathy, Dr. Ali Dolatabadi, Dr. Rama Bhat, Dr. Pouya Valizadeh, for taking their valuable time to examine my thesis.

My thanks to the administrative staff at Concordia University: Leslie Hossein, Arlene Zimmerman, Sophie Mérineau and Maureen Thuringer. I also would like to thank technical staff of the department, Dainius Juras, Brad Luckhart, and Henry Szczawinski for their assistance and Dylan Lu for training me with the handling of microfabrication equipments in the clean room of Concordia University.

Very Special thanks to Amir Sanati Nezhad, Carlos Agudelo, and Mahsa Naghavi for helping me with their outstanding collaboration and valuable discussion at different stages of the thesis.

Special thanks to all of my friends and colleagues in the Optical-Bio MEMS laboratory: Simona, Hamid, Jayan, Roozbeh, Stefan, Pierre for all their help and also for making my PhD studies a joyful journey to remember.

The last, but of course not the least, my warmest appreciation goes to my family. My accomplishments are direct results of their love and support. My deepest gratitude goes to

my mother, Khadijeh. She has sacrificed many things throughout her life for my sake and I owe her all that I have. Her incredible love has always been a great source of support and motivation for me. I am very deeply grateful of my brothers, Amin and Amir and my sister, Azadeh for their strong supports, encouragements and for making the world a much happier place for me.

*Dedicated to my mother...*

## *TABLE OF CONTENTS*

## *LIST OF FIGURES*

# *LIST OF TABLES*

## *NOMENCLATURE*

| | |
|---|---|
| 2D | Two-Dimensional |
| 3D | Three-Dimensional |
| AFM | Atomic Force Microscope |
| BC | Before Contact |
| Ca | Calcium |
| CAD | Computer-Aided Design |
| CCD | Charge-Coupled Device |
| CFM | Cellular Force Microscopy |
| DC | During Contact |
| DFT | Discrete Fourier Transform |
| DWL | Direct Writing Laser |
| FEA | Finite Element Analysis |
| FEM | Finite Element Modeling |
| FFT | Fast Fourier Transform |
| FlexChip | Flexure Integrated Lab-on-a-chip |
| LOC | Lab-On-chip |
| MEMS | Micro-Electro-Mechanical Systems |
| MR | Mooney–Rivlin |
| PDMS | Polydimethylsiloxane |
| PGM | Pollen Growth Medium |
| PSD | Power Spectral Density |
| SCREAM | Single-Crystal Silicon Reactive Etch And Metal |

| | |
|---|---|
| SEM | Scanning Electron Micrograph |
| Sf9 | Spodoptera frugiperda |
| SU8 | Negative Photoresist |
| UV | Ultraviolet |

# *LIST OF SYMBOLS*

| | |
|---|---|
| A | Contact area |
| $D_1$ | Diameter of the curved notch |
| $D_2$ | *Camellia* pollen tube diameter |
| E | The elastic modulus of PDMS |
| F | Pollen tube force |
| h | Flattened height |
| H | Height of the microfluidic network |
| K | Cantilever Constant |
| L | Microcantilever length |
| $L_1$ | Appendix length |
| $P_A$ | Pressure at point A |
| $P_B$ | Pressure at point B |
| $P_C$ | Pressure at point C |
| $P_i$ | Trapping probability |
| $Q_i$ | flow rate at microchannel i |
| $Q_j$ | flow rate at microchannel j |
| $Q_T$ | Total flow rate at (Section A-A) |
| $R_1$ | Radius of rounded corner of notch entrance |
| R | Pollen tube radius |
| W | Microcantilever width |

| | | |
|---|---|---|
| $W_I$ | | Appendix width |
| $W_C$ | | Channel width |
| $W_D$ | | Distribution chamber width |
| WG | | Microchannel width |
| $W_O$ | | Outlet drain width |
| $W_T$ | | Transporting channel width |
| $X_I$ | | Longitudinal coordinate of Point I |
| $Y_I$ | | Lateral coordinate of Point I |
| θ | | Contact angle |
| δ | | Cantilever Deflection |
| | ΔX | Bending of horizontal glass cantilever |
| σ | | Trapping ratio |
| μ | | Fluid dynamic viscosity |
| υ | | Poisson ratio |

# Chapter 1

# Introduction

## 1.1 Introduction

The use of lab-on-a-chip or microfluidic chip for biological and biomedical research has attracted growing interest in recent years. In particular, employing microfluidic devices to perform biological experiments at cellular level has attracted significant attention (Andersson & Van den Berg, 2003; Beebe, Mensing, & Walker, 2002) because of their unique advantages including low cost, low reagent consumption, high separation efficiency, possibility of integrating micro sensors and actuators and performing parallel processing (Prokop et al., 2004; Wheeler et al., 2003). Moreover, the sizes of structural components of these devices match with dimensions of the cells. Therefore, using microfludic technology can provide more *in-vivo*-like growth microenvironment than conventional bulk assays for the cellular studies (Prokop et al., 2004). Microfluidic based platforms were employed in various cell biology research including cell trapping and sorting (Carlson et al., 1997; Chabert & Viovy, 2008; S. H. Kim, Yamamoto, Fourmy, & Fujii, 2011; Wilding et al., 1998), cell treatment (Huang & Rubinsky, 2001; Y.-C. Lin, Jen, Huang, Wu, & Lin, 2001; Strömberg et al., 2001; Taylor et al., 2001) and single cell analysis (Marcy et al., 2007; Ottesen, Hong, Quake, & Leadbetter, 2006; Zare & Kim, 2010).

Mechanical forces have central functions in regulating different biological processes at the cellular level. With recent advances in microfabrication techniques, different kinds of microfluidic devices have been developed which facilitate studying the cell

mechanobiology. These devices enable determination of type and magnitude of cellular forces which can improve our understanding of the roles of mechanical forces in the field of cell biology (D.-H. Kim, Wong, Park, Levchenko, & Sun, 2009).

## 1.2 Introduction to cell mechanobiology

Cell mechanobiology is an emerging multidisciplinary field of science which studies the function of mechanical forces in cell biology. Understanding the mechanisms by which cells sense and respond to mechanical forces and characterizing cell mechanical properties are two important aspects of cell mechanobiology. Although the effects of mechanical force on the cells mechanics and chemical signaling were experimentally demonstrated (Peyton, Ghajar, Khatiwala, & Putnam, 2007), the underlying mechanisms by which cells modulate their functions due to the mechanical forces is still poorly understood. Therefore, research on mechanotransduction, the mechanisms by which cells convert mechanical signal to biochemical activities, were subject of a great deal of research in the past decade (Jaalouk & Lammerding, 2009; Orr, Helmke, Blackman, & Schwartz, 2006; N. Wang, Tytell, & Ingber, 2009). Because of the importance of these mechanisms in various fundamental biological processes such as cell growth, differentiation and *morphogenesis*[1], this area is largely under explored. The main issue here is the difficulty in providing techniques to precisely change and manipulate the external mechanical stimulus influencing a cell. To address this issue, use of microelectromechanical systems (MEMS) in cell mechanobiology has rapidly evolved in the past decade.

[1]Morphogenesis is the biological process that causes a structure or entire organism to develop its shape.

### 1.2.1 MEMS for cell mechanobiology

Employing MEMS based platforms in cell mechanobiology studies has rapidly evolved in the past decade. These platforms enable precise manipulation of cells, determination of the type and magnitude of cellular forces, and accurate quantification of cellular responses with high resolution in high throughput experiments. Microcantilever based devices is a category of MEMS-based platforms which have been used to investigate cell mechanical responses to different types of forces such as stretch, indentation and contractile forces. Traction forces of fibroblasts were quantified using a micromachined device including microcantilevers of different lengths (Galbraith & Sheetz, 1997). The device enabled dynamic determination of the subcellular forces applied by small regions of fibroblasts to a calibrated microcantilever. Saif et al. (Saif, Sager, & Coyer, 2003) developed a microcantilever-based sensor that allows *in situ* measurement of force responses of a single bovine endothelial cell attached to a substrate. The microcantilever was fabricated from single crystal silicone coated with a thin layer of fibronectin. Using a piezoactuator, the micocantilever was moved to locally deform the cell. Image analysis technique was utilized to measure the deformation of the cantilever tip and quantification of the interaction force between the cantilever and the cell. The responses of fibroblasts to stretching forces were measured using a microfabricated force sensor by Yang et al (S. Yang & Saif, 2005). The force sensor consisted of a probe and flexible beams as sensing elements and was fabricated by single-crystal silicon reactive etch and metal (SCREAM) process. This technique allowed the authors to conclude that the actin filaments to be the main factor involved in resisting the cellular internal forces due to stretch.

Polymer-based microcantilevers have also been used in mechanobiology studies. Park et al. (Park et al., 2005) developed a hybrid biopolymer microcantilever that enabled real time determination of the contractile forces of self-organized cardiomyocytes. The microcantilever was fabricated from Polydimethylsiloxane (PDMS) using standard soft lithography process.

## 1.3 Pollen tube, a conduit to transport sperm cells

Pollen tubes are cellular protuberances involved in the reproductive process of flowering plants. They are formed upon germination of pollen grains on a receptive stigma. During the germination process, a pollen grain absorbs fluid secreted by the mature stigma and forms a tubular protrusion. A scanning electron micrograph of a *Camellia* pollen grain is shown in Figure 1.1. This tube grows through the pistil toward the ovule to deliver the sperm cells to the egg cell (Figure 1.2). Mechanical properties of the transmitting tissue varies significantly between species. In some species the tube has to penetrate a solid tissue (e.g. *Nicotiana, Arabidopsis*), whereas in other species such as *Lilium* or *camellia*, tubes grow through a hollow canal. In the case of solid transmitting tissue, the pollen tube softens these tissues during its way by secreting cell wall degrading enzymes or by inducing cell death. In addition to these chemical based efforts, the pollen tube needs to generate a considerable physical force to invade the tissues in its path to reach the target, ovule.

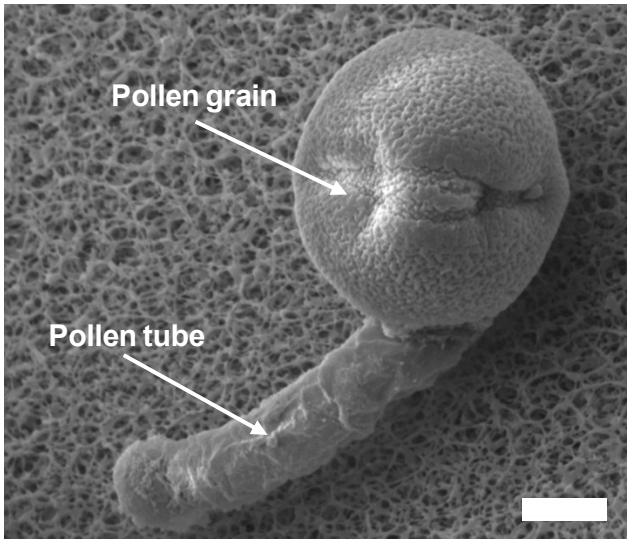


**Figure 1.1:** Scanning electron micrograph of a *Camellia* pollen grain germinated *in vitro*. Scale bar = 10µm.

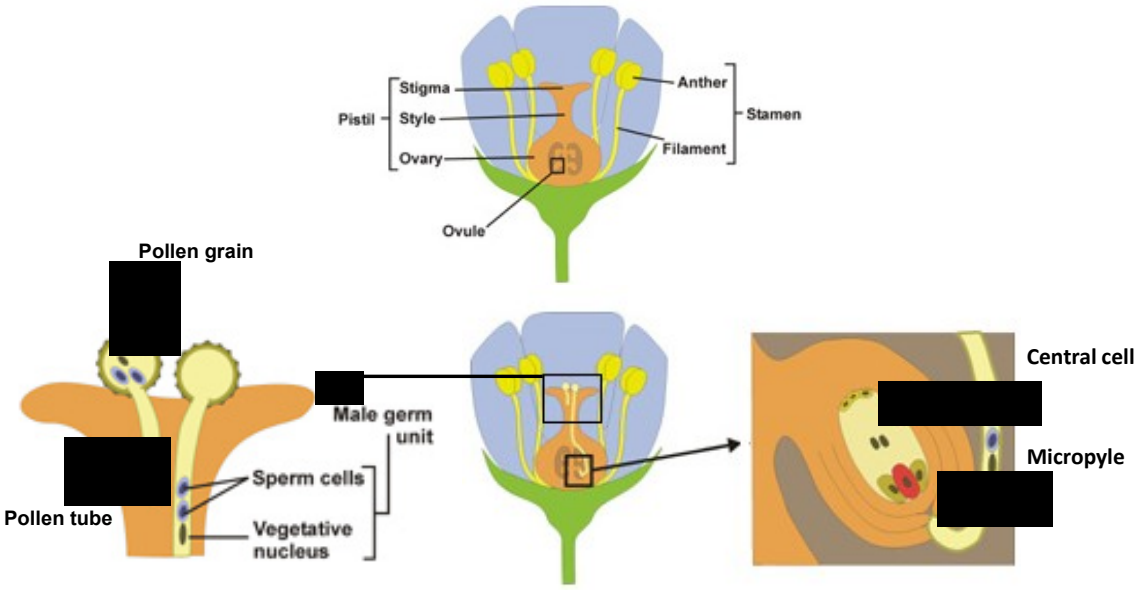


**Figure 1.2**: Fertilization in flowering plants (Courtesy of A. Geitmann)

in its path. Each pollen tube carries two sperm cells inside its cytoplasm[2]. When the pollen tube enters the ovule through the micropyle, an opening in the outer layers of the ovule, it bursts and the two sperm cells are released to achieve fertilization. One of them fertilizes the female gamete[3] and produces the embryo. The other one fuses with the central cell and forms the endosperm tissue which is responsible to provide nutrients for the embryo during its growth (Anja Geitmann & Ravishankar Palanivelu, 2007).

### 1.3.1 Pollen tube as a model system for the study of cellular growth

Pollen tubes are easily cultivated *in vitro* conditions, and they can grow extremely fast with rates up to tens and even hundreds of micrometers per minute in some species (Youssef Chebli & Anja Geitmann, 2007). They are easy to maintain and experimentally manipulate. All of these properties have made them an excellent model system to study cellular *morphogenesis* and growth (Feijo et al., 2001).

In most plant cells, growth happens by the expansion of cell wall over large portions of the cellular surface and simultaneous addition of new materials. In pollen tubes, the cell elongation is confined to a small region on cellular surface, the apex.

This tip focused growth process is shared by other cell types such as *root hairs*[4], fungal *hyphae*[5], and nerve cells (Youssef Chebli & Anja Geitmann, 2007). The exclusive expansion at the apex minimizes friction between the expanding cell and the surrounding growth matrix endowing tip growing cells with the capacity to invade a substrate or tissue.

---

[2] The cytoplasm is a thick, clear liquid that resides between the cell membrane and holds the cell organelles.
[3] A gamete is a cell that fuses with another cell during fertilization in organisms that reproduce sexually.
[4] A root hair is a tubular outgrowth of a hair-forming cell on the epidermis of a plant root.
[5] A hypha (plural hyphae) is a long, branching filamentous structure of a fungus.

Secondly, the tip-focused growth activity enables the rapid reorientation of growth and hence is responsible for tip growing cells to display chemotropism[6] or thigmotropism[7]. Hence, pollen tubes can also be considered as an important model system for studying polar cell growth, so-called tip growth.

### 1.3.2 Parameters involved in pollen tube growth

So far, a considerable number of studies has been conducted to understand the principal factors that regulate pollen tube growth. Among them we can mention the intracellular ion concentration, the actin filaments and microtubules in the *cytoskeleton*[8], the activity of ion transporters, the fusion of secretary vesicles and finally the *turgor pressure*[9]. While many of these factors governing pollen tube growth have been recognized, their exact role and precise interactions have not been fully elucidated yet.

In particular, the role of turgor pressure in pollen tube growth is a matter of intense discussion (J. H. Kroeger, Zerzour, & Geitmann, 2011; Lawrence J Winship, Obermeyer, Geitmann, & Hepler, 2010; Zonia, 2010; Zonia, Müller, & Munnik, 2006). Generally, turgor pressure is assumed to be the driving force for pollen tube growth but it is not clear whether it also regulates pollen tube growth (M. A. Messerli, Créton, Jaffe, & Robinson, 2000a; Plyushch, Willemse, Franssen-Verheijen, & Reinders, 1995). Since plant cell

---

[6] Chemotropism is the growth of organisms (or parts of an organism, including individual cells) such as bacteria and plants, navigated by chemical stimulus from outside of the organism or organism part.
[7]Thigmotropism is the ability of cells to orientate growth with respect to features of the physical environment.
[8] The cytoskeleton consists of rod shape protein polymers contained within the cytoplasm that provide the cell with structure and shape. The cytoskeleton plays an important role in cytomechanics or cell mechanics in animal cells, but in plant cells it has mostly the function to coordinate intracellular transport and the guidance or plasma membrane located enzymes.
[9]Turgor Pressure or turgidity is the main pressure of the cell contents against the cell wall in plant cells and bacteria cells, determined by the water content of the vacuole, resulting from osmotic pressure

growth results from the turgor driven expansion of the wall, a change in growth rate could be achieved either by a change in turgor or a change in the material properties of the cell wall. However, different approaches used to measure turgor pressure in pollen tubes have shown that there is no direct correlation between the turgor pressure and pollen tube's growth rate. For example a pollen tube sometimes exhibits pulsatile growth characteristic (Pierson et al., 1996), but no change in turgor pressure during its growth has been reported in the literature (Benkert, Obermeyer, & Bentrup, 1997; R. Zerzour, J. Kroeger, & A. Geitmann, 2009).

It is therefore reasonable to assume that acceleration of growth occurs due to cell wall relaxation. Relaxation of the wall entails a reduction of the material strength either due to enzymatic action or addition of soft cell wall material at the apex which in turn leads to water influx leading to cell growth (Elodie Parre & Anja Geitmann, 2005). Both parameters, cell wall stiffness and turgor, can be influenced by various cellular features such as the actin cytoskeleton which delivers the new cell wall material and cytosolic ion gradients which spatially and temporally regulate actin polymerization (Youssef Chebli & Anja Geitmann, 2007; Feijo et al., 2001).

## 1.4 Experimental approaches to quantify physical properties of cells

Although the important role of turgor pressure in plants growth has been known since the early 20th century, measuring turgor pressure in a single plant cell has remained challenging. For almost a century, only indirect methods have been used to quantify the turgor pressure in different plant cells. In these methods, the turgor pressure is quantified

based on the measurement of the difference between *osmotic pressure*[10] of the *protoplast*[11] and that of the surrounding medium, because osmotic pressure is approximately equal to turgor pressure in fully turgid cells.

The first direct measurement of turgor pressure in plant cells was the work of Paul Green (Green, 1968). He developed a method to measure the turgor pressure by using micromanometer in the giant-celled alga Nitella. In this method, the cell was impaled by a water and air-filled glass tube which was closed at one end. The high pressure in the cell leads to compression of the trapped gas. Using Boyle's law (Pressure × Volume = Constant), the pressure of the cell can easily be determined. The schematic of this method is shown in Figure 1.3.

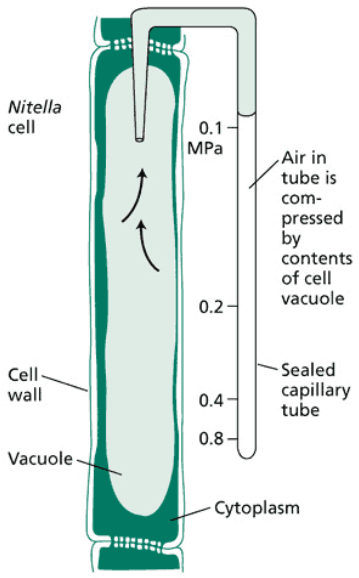


**Figure 1.3:** Use of the micromanometer, a pressure probe, to measure Nitella cell turgor pressure (Taiz & Zeiger, 2010).

[10]Osmotic pressure is the pressure which needs to be applied to a solution to prevent the inward flow of water across a semipermeable membrane

[11]A protoplast is a plant cell that had its cell wall completely or partially removed using either mechanical or enzymatic means.

In small cells, losing *cell sap*[12] into the glass tube, lead to the deflation of the cells and as a result measuring artifactually low pressures. So, this method is only applicable for cells of relatively large volume.

The pressure probe method was then improved by Zimmermann et al. in 1979 (Zimmermann & Steudle, 1979). They replaced the air bubble in micromanometer method by a silicone oil-filled microcapillary which was connected to a pressure sensor. Silicon oil is an incompressible fluid, and it transmits the applied pressure to the pressure sensor. They also used a plunger in this device that allowed applying pressure and displacing the cell sap-oil interface. In this method, the tip of the microcapillary is inserted into the cell. Because of the cell turgor pressure, the cell sap starts to come into the microcapillary. The boundary between the silicon oil and the cell sap is easily distinguishable under a microscope. Then by applying pressure to the plunger of the device, the cell sap-oil interface can be moved to the tip of the microcapillary making the cell return to its initial volume. Now, the cell turgor pressure which is balanced by the oil pressure inside the microcapillary, can be measured continuously by the pressure sensor. The schematic of the pressure probe method is shown inFigure 1.4.

The pressure probe method has been used to study the effect of turgor pressure in the growth of different kinds of fungi. Money et al. (Nicholas P Money & Harold, 1992, 1993)used this method to quantify the turgor pressure in *Saprolegnia ferax* and *Achlya*

[12] The liquid inside the large central vacuole of a plant cell that serves as storage of materials and provides mechanical support, especially in non-woody plants

*bisexualis*. They found that hyphal turgor pressure to be 0.7 MPa and 0.4 MPa for *A. bisexualis* and *S. ferax*, respectively.

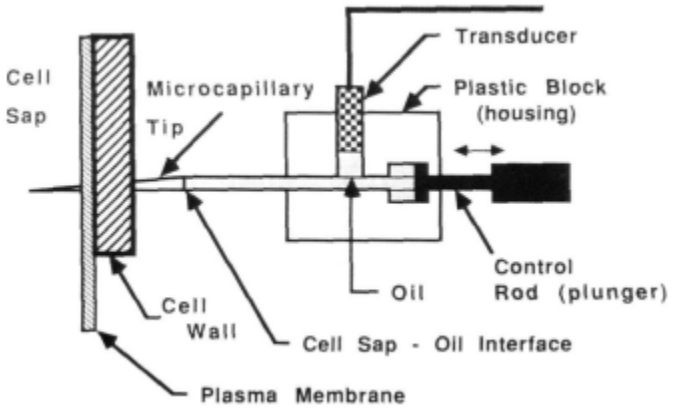


**Figure 1.4:** Schematic of the pressure probe method (Ortega, 1990).

In 1997, Benkert et al. (Benkert et al., 1997)used the modified version of the pressure probe developed by Zimmermann and co-workers to measure the turgor pressure of growing pollen tubes of lily *in vitro*. They also used incipient plasmolysis method to quantify the turgor pressure of lily pollen tubes during their growth and compared the results of this method with the turgor pressures measured by pressure probe. Using the pressure probe method to measure turgor pressure of growing pollen tubes includes several limitations. One main problem is to provide mechanical support for growing pollen tubes in a suspension culture so that they could be impaled by a glass microcapillary tip. To solve this problem, the authors mixed the germinated pollen grains in growth medium with 2% warm agarose. After solidification, agarose provided mechanical support for the pollen tubes. So, the microcappilary could be inserted into the pollen tubes. As the authors noted, by using this method, because of the very slow exchange rate of the solutions in agarose, the

immediate response of pollen tubes to the changing of growth medium composition cannot be quantified. Using the pressure probe method, the turgor pressure of lily pollen tube was recorded for 20 to 30 minutes. During this period, no transient changes in turgor pressure more than the resolution limit of this method (about 0.005 MPa) was reported by the authors. Also, no linear correlation between pollen tube growth rate and turgor pressure was noticed by the authors. They reported an average value of 0.22 MPa for the turgor pressure of lily pollen tubes, using the pressure probe technique, and 0.79 MPa using the incipient plasmolysis method. The authors suggest considerable forces might be necessary to overcome linkages between plasma membrane and cell wall as a reason of overestimating turgor pressure by incipient plasmolysis technique.

Wang et al. reported the use of micromanipulation to estimate turgor pressure in plant cells (L. Wang, Hukin, Pritchard, & Thomas, 2006). The micromanipulation method was initially developed to measure the mechanical properties of animal cells (Thomas, Zhang, & Cowen, 2000; Z. Zhang, Ferenczi, Lush, & Thomas, 1991), and was used to quantify mechanical properties of single tomato cell (Blewett, Burrows, & Thomas, 2000), but application of this technique to measure turgor pressure had not been reported before this work. In this method, a cell is located between the base of a chamber containing suspended in culture medium and the flat surface of a micromanipulation probe (an optical fiber). The probe is connected to a force transducer and can be driven a certain displacement at a chosen speed. When the probe is moved toward the cell, the cell is compressed between the two surfaces and the amount of the applied force is recorded by the force transducers. Using a side microscope allows the cell to be observed clearly form the side and the contact area between the probe and cell can be estimated. By dividing the applied force by the

contacted area, the turgor pressure of the cell was calculated. To validate this method, concomitant measurement of the turgor pressure by pressure probe also was used by the authors. Good agreement between these two methods was reported by the authors. A schematic diagram of the micromanipulation equipment and a micrograph of a single tomato cell under compression between glass surface and micromanipulation probe are shown inFigure 1.5 and Figure 1.6 respectively.

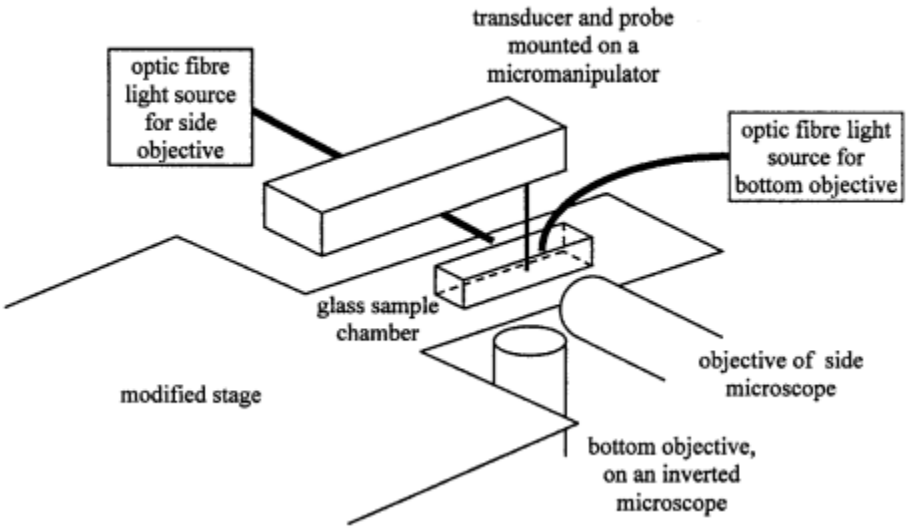


**Figure 1.5:** A schematic diagram of the micromanipulation equipment (Blewett et al., 2000).

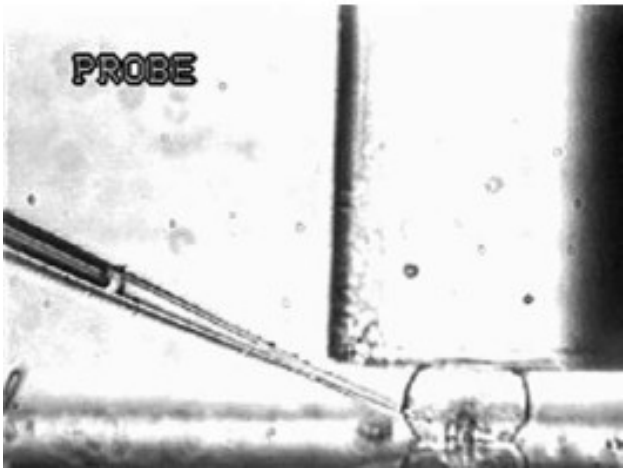


**Figure 1.6:** Single tomato cell compressed between a micromanipulation probe and the bottom of a glass chamber. The probe diameter was 200 µm. The pressure probe microcapillary has been inserted into the cell from the left (L. Wang et al., 2006).

In 2000, ball tonometry, a non-invasive method to quantify turgor pressure in a single cell, was developed by Lintilhac et al. (Lintilhac, Wei, Tanguay, & Outwater, 2000). In this method, a known load is applied by utilizing a spherical glass ball attached to a cantilever to the surface of a target cell. Then, the load-induced deformation of cell's surface is measured by analyzing captured images. The turgor pressure is calculated by dividing the applied load by the projected area of the contact patch. Given the non-destructive nature, repeated measurement of turgor pressure on a single cell is possible by using this technique. This method is only applicable for surface cells with thin cell walls and is not practical to measure turgor pressure of non-spherical cells. Therefore, this method is not applicable to measure turgor pressure of cylindrical shaped cells such as pollen tubes. Figure 1.7 shows the schematic diagram of the ball tonometry equipment.

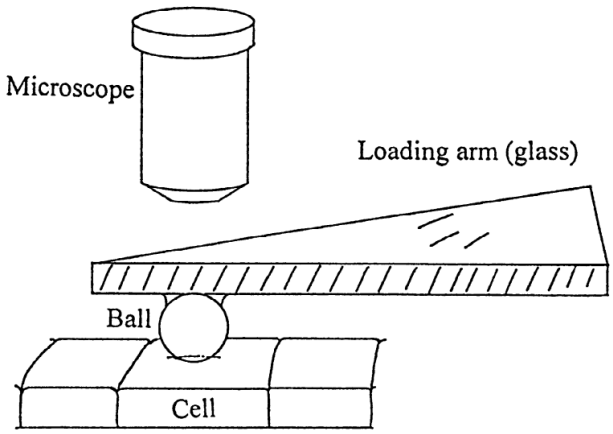


**Figure 1.7:** Schematic diagram of the ball tonometry equipment (Lintilhac et al., 2000).

In 2004, Geitmann et al. used a micro indentation technique to measure local stiffness of growing pollen tube along its longitudinal axis (Anja Geitmann, William McConnaughey, Ingeborg Lang-Pauluzzi, Vernonica E Franklin-Tong, & Anne Mie C Emons, 2004; Anja Geitmann & Parre, 2004). This technique was used earlier to characterize mechanical properties of animal cells (Petersen, McConnaughey, & Elson, 1982; Zahalak, McConnaughey, & Elson, 1990). But using of this method to measure mechanical properties of pollen tubes had not been reported before this work. In this method a vertical glass needle mounted at one end of a horizontal glass cantilever with known spring constant (K) was used to locally deform a pollen tube. The other end of the cantilever was connected to a piezoelectric motor which moves vertically. Vertical positions of the needle and the piezoelectric motor were monitored by using optical sensors. The amount of bending of the horizontal glass cantilever ($\Delta X$) is proportional to the force applied to the glass needle by the pollen tube and was determined from the displacement difference between the tip of the needle and the piezoelectric motor. By using the spring constant of

the cantilever, it is then possible to calculate the pollen tube's resistance force to deformation from F = K.ΔX. The slope of the linear section of the force-deformation graph was used to quantify the cellular stiffness. Results from experiments using micro-indentation on pollen tubes showed that local cellular stiffness at the apical region of the growing pollen tube is significantly less than that of the distal part of the tube. A schematic of the micro indentation technique, experimental setup, cantilever and attached needle, and microscope image of the micro-indenter needle touching a pollen tube are shown in Figure 1.8.

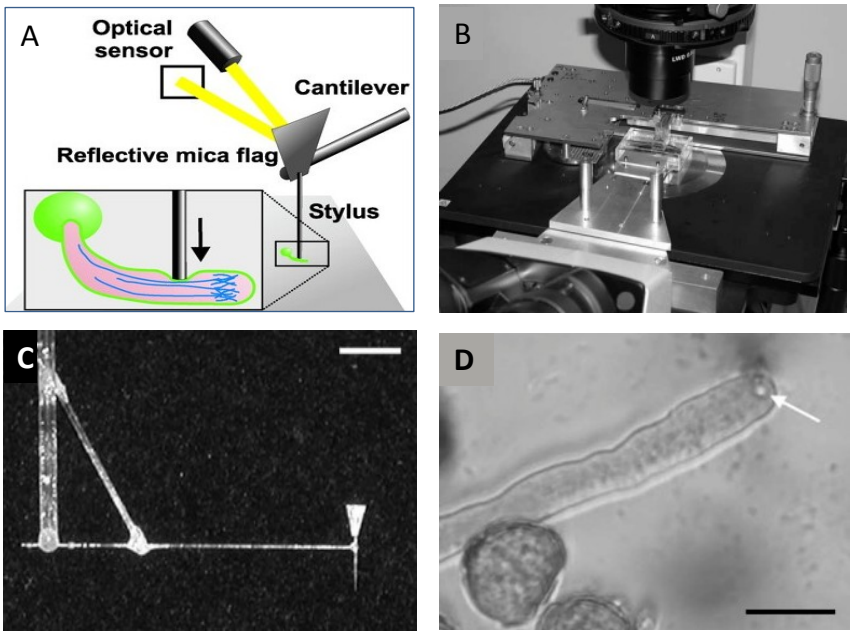


**Figure 1.8:** (A) A schematic of the micro-indentation technique. (B) Setup of the micro-indenter device on the stage of an inverted microscope. (C) Cantilever and attached needle. (D) Microscope image of the micro-indenter needle touching a pollen tube (arrow). Bars = 5mm (C), 20 µm (D). (Anja Geitmann, 2006).

Direct measurement of invasive forces produced by hyphae was reported by Money et al. in 2001 (Nicholas P Money, 2001). In order to quantify the invasive force of hyphae, a

miniature strain gauge was placed in front of a growing hyphal apex (Figure 1.9). Their strain gauge was composed of a silicon beam (100 μm thick and 10 mm wide) with a diffused electrical resistor. Using a micromanipulator, the strain gauge was located in front of the growing hyphae in culture medium. When the hypha pushes the silicon beam, the beam is deflected and the output voltage of the strain gauge changes immediately. The amount of deflection of the beam is proportional to the exerted force by the cell. In this manner, the authors were able to measure the invasive force applied by the hyphae to the strain gauge. The authors reported that typical hyphae with diameters 15 to 25 μm exerteda mean force of 12 μN to the strain gauge. The pressure exerted by a hypha is estimated by dividing the measured force by the contact area between the cell and the beam.

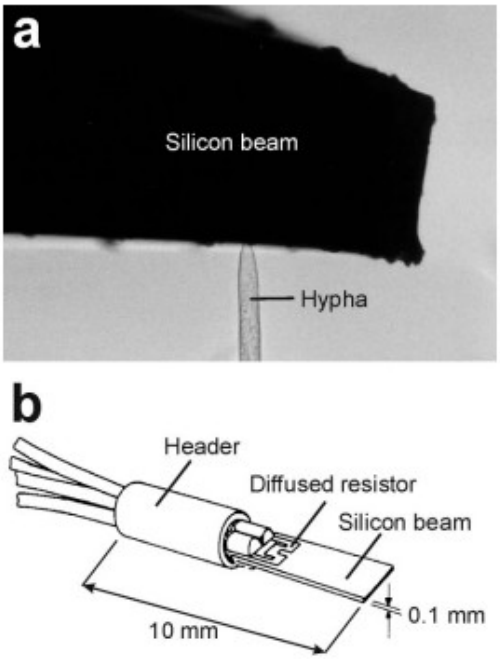

**Figure 1.9:** Force measurements with strain gauge. (a) Hyphal apex making contact with silicon beam strain gauge. (b) Schematic drawing of the stain gauge composed of a silicon beam with a diffused electrical resistor (Bastmeyer, Deising, & Bechinger, 2002).

The results from this study showed that the growth forces in hyphae have a pulsatory nature which corresponds to pulses in hyphal growth rate. Also, estimation of the pressure applied by the hyphal apex to the beam suggests that 10% or less of the force available from turgor is exerted by hyphal apex against the strain gauge which suggests that in addition to turgor pressure, mechanical properties of the fungal cell wall may influence the magnitude of invasive force (Nicholas P Money, 2001).

Although the hyphal invasive force could be quantified with a resolution better than 1 μN with this technique, experiments with miniature strain gauge and interpretation of the results obtained using this method are difficult. The difficulty of estimating the contact area between the hypha and the beam is another problem associated with this technique, because the contact surface between the cell and the beam is usually obscured by the vastness of the beam in comparison with the hypha.

In addition to direct measurement techniques, indirect methods can be utilized to measure growth forces in cells. One of the indirect methods used to quantify invasive forces of tip growing cells is the agar penetration technique. This method has been applied to both pollen tubes (Olivier Gossot & Anja Geitmann, 2007) and fungal hyphae (Bastmeyer et al., 2002; Brush & Money, 1999; N. Money, 2007). In this method, the ability of pollen tubes, or other kinds of tip growing cell, to penetrate media hardened with different concentrations of agarose is utilized to study the importance of various factors such as cell wall, cytoskeleton, or turgor pressure for the exertion of an invasive force.As the stiffness

of media with different concentrations of agarose can be determined by different means, such as penetrometers, the force or pressure applied by the elongating cell can be estimated. In 2007, Gossot et al. used this method to investigate the role of cytoskeletal elements, microtubules and actin filaments, in coping with mechanical obstacles and in the determination of the growth direction (Olivier Gossot & Anja Geitmann, 2007). To fabricate a mechanical obstacle for *in vitro* growing pollen tubes, the authors created an interface between two growth media stiffened by 1% and 2% concentration of agarose (Figure 1.10). The ability of pollen tubes to invade the obstacle was determined by the ratio between tubes that have crossed the interface and all tubes that have been deviated when touched the interface. However, this approach did not yield quantitative data about the invasive forces or pressures that pollen tubes need during penetration with different agarose concentrations.

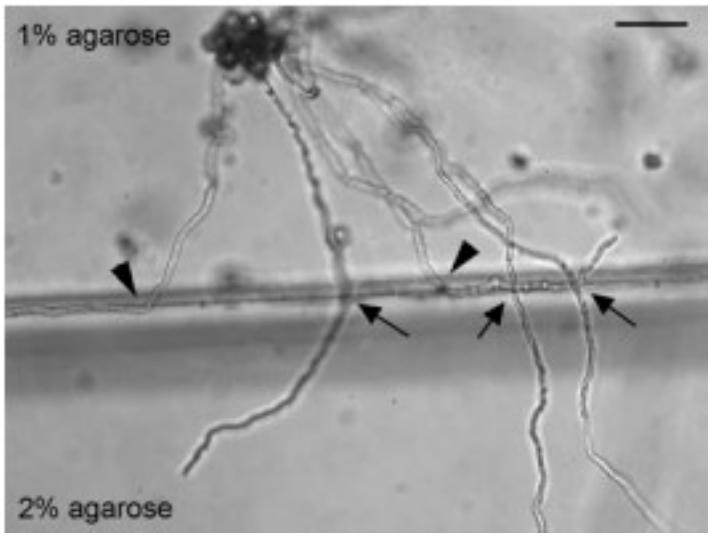


**Figure 1.10:** Micrograph of pollen tubes grown in the in vitro obstacle assay. The ratio between tubes that have crossed the interface (arrows) and all tubes that either crossed or touched the interface while being deviated (arrowheads) is calculated and reflects the

ability of pollen tubes to invade the obstacle. Bar=100 µm (Olivier Gossot & Anja Geitmann, 2007).

## 1.5 Challenges in *in vitro* study of pollen tubes

Because of difficulty and limitation associated with studying pollen tubes in *in vivo* conditions, research on pollen tubes growth has been done *in vitro* conditions for many years. Usually the cells are cultured in bulk conditions in a Petri dish, on a microscope slide or in an Erlenmeyer. The pollen growth medium (PGM) is either liquid or solidified by agarose. Given the size of the container relative to the size of the cell, this type of *in vitro* environment is essentially isotropic and uniform. While this is appropriate for many tests, this environment is not conducive to investigating the pollen tube's behavior when navigating a structured environment such as a flower pistil. To perform tests at cellular scale, microstructures at the same length scale need to be constructed. This can easily be done using microfluidic based platforms. The sizes of the structural components of these platforms can be designed to match the dimensions of pollen tubes providing microenvironments that can be made to resemble the *in vivo* conditions more accurately than conventional plate assays, leading to *ex-vivo* conditions. The microfluidic based *lab-on-a-chip*[13] (LOC) provides*ex-vivo*study environment compared to *in vitro* study like petri dish as it can provide (*i*) optimum conditions of nutrients such as $Ca^{2+}$, glucose and etc. similar to pistil (*ii*) softness of microfluidic structures are similar to pistil's softness. (*iii*) Single cell studies without interaction with other cells as in pistil (*iv*) continuous supply of nutrients with microflow.

[13]A lab-on-a-chip (LOC) is a device that integrates one or several laboratory functions on a single chip of only millimeters to a few square centimeters in size.

Most importantly, these platforms enable integration of various kinds of micro sensors within the microchannels to measure different biological parameters of a single pollen tube which was not possible in conventional *in vitro* plate assay.

## 1.6 Microfluidics-based platforms for plant cells studies

Over the past decade, microfluidics platforms have been used widely in cell biology research. However, only few studies have been published reporting the use of microfluidic devices for plant cells research (Grossmann et al., 2011; Ko, Ju, Lee, & Cha, 2006; Yetisen et al., 2011b). A polydimethylsiloxane (PDMS) microfluidic chip with integrated microfilter was used to culture *Nicotiana tabacum*protoplasts by Ko and colleagues (Ko et al., 2006). Grossmann et al. used a microfludic device which enabled control of root culture and live-cell imaging of the growth of *Arabidopsis thaliana* roots (Grossmann et al., 2011).

The use of a Microsystems-based assay for pollen tube research has been reported for the first time by group of Ravi Palanivelu at the University of Arizona (Yetisen et al., 2011b). They developed a device that can resemble the in vivo microenvironment of pollen tubes growth. The aim of their research was to test the targeting of ovules by pollen tubes. Using a usual plate assay method cannot satisfy appropriate conditions to perform this test. For example it is not possible to have control over pollen tubes growth direction or putting micro barriers in their growth direction in the plate assay. So, they developed a PDMS microdevice consisting of a microgroove and two chambers on each side into which ovules can be placed. The main groove width was about 1000 μm to have capacity for placing a cut pistil, but the area of side chambers varied from 250×250 $\mu m^2$ to 1000×1000 $\mu m^2$ to provide the possibility of placing different numbers of ovules. First the groove and the chambers were filled with PGM which is necessary for pollen tube growth. Then, a

pollinated and cut pistil of young *A. thaliana* flower was located on the PGM in the main groove and aligned such that the pistil cut edge is perpendicular to the groove axis as shown in Figure 1.11.

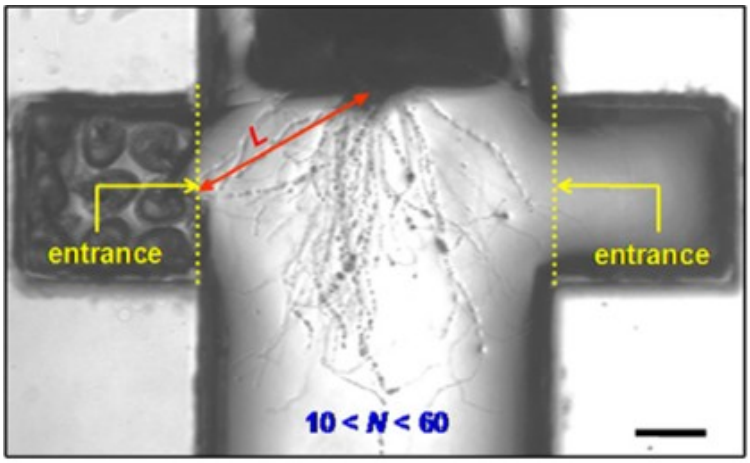


**Figure 1.11:** Microdevice developed by Palanivelu's group at the University of Arizona. Most pollen tubes grow towards the ovule-containing chamber. Scale bar = 200 μm (Yetisen et al., 2011b).

For quantitative investigation of the responses of pollen tubes to the ovule-derived attractants *in vitro*, they put unfertilized ovules in one chamber and left the other one empty. The authors reported that about 67% of pollen tubes turned toward the chamber with ovules. The data obtained with this device allowed to conclude that the pollen tubes sense the concentration gradient and respond to the chemoattractants secreted by unfertilized ovules. These studies have made important contributions to our knowledge of pollen tube mechanobiology and illustrate the power and potential of microfluidic techniques for this field.

## 1.7 Rationale and scope of the thesis

Both biochemical and biomechanical signals are involved in the morphogenesis of the pollen tubes. During the past decades, considerable amounts of research have been dedicated to understanding the role of biochemical signals in pollen tubes morphogenesis (Li, Lin, Heath, Zhu, & Yang, 1999; Michard, Alves, & Feijó, 2009), but the role of the mechanical signals has remained largely unexplored. It is believed that mechanical forces might be an important factor in pollen tube morphogenesis (Harold, 2002). However, it is not clear how these mechanical forces contribute to pollen tubes morphogenesis. Moreover, the impact of these forces on known major morphogenetic effectors has not been elucidated yet.

Despite the importance of the invasive force in pollen tubes growth, no quantitative data on the growth force of pollen tubes are available up until now. Thus, to develop techniques that allow direct measurement of force exerted by individual pollen tubes will be necessary for analyzing and characterizing pollen tubes growth.

It is believed that most, if not the whole, invasive force exerted by pollen tubes onto the surrounding tissue during the growth process is generated by the internal turgor pressure. Therefore, quantification of this force can help estimate the turgor pressure and will assist bringing consensus in the literature about the exact role of turgor pressure in pollen tube growth.

Only rough estimations of invasive growth force based on the turgor pressure measurement could be found in the literature. Also, because of significant discrepancies between the measured values of turgor pressures in different approaches, there is no definitive quantitative data for turgor pressure and as a result the role of this factor in pollen tube

growth has not been elucidated yet. The resolution of existing measurement techniques are poor and not enough to show possible fluctuations in turgor pressure and growth force in pollen tubes. Also, due to technical limitations doing measurement exactly at the tip of a growing pollen tube has not been attainable yet.

There is a lack of understanding of *thigmotropism* in pollen tubes. It is not completely clear how individual pollen tubes behave when mechanical obstacles in its growth direction are encountered. No comprehensive study has been performed to investigate the effect of mechanical stimulus on pollen tube growth dynamic.

Therefore the purpose of the thesis is to develop a microfluidic based *lab-on-chip* (LOC) platform providing an *ex-vivo* testing environment that physically resembles the in vivo growth conditions of the pollen tube. We consider the platform as an *ex-vivo* environment, since pollen grainsarecollected from a growing plant and will be cultured inside the platform. In addition, the platform enables to locally change the growth environment of growing pollen tubes, something that was not possible using the existing *in vitro* techniques used for studying pollen tube biology.

The platform enables more efficient experimentation on individual tip growing pollen tubes under precisely controlled and reproducible conditions. Moreover, the platform allows for investigation on the effect of mechanical stimulation on pollen tube growth dynamics and quantification of the invasive growth force of growing pollen tubes through analyzing bio-micromechanical interaction.

Additionally, the LOC platform facilitates studying the effect of microenvironment geometries on pollen tube growth rate and investigation of existence of directional memory

in tip growing pollen tubes. Insights from this research will lead to a better understanding of the mechanical aspects of tip growing cell physiology such as cellular growth and *mechanotransduction*[14].

## 1.8 Objectives and outline of the thesis

The purpose of this research is to employ microsystems technology to develop a platform providing an *ex-vivo* testing environment that physically resembles the *in vivo* growth conditions of the pollen tube. The main objective of the present thesis is to develop a flexible microstructure integrated microfluidic based *lab-on-chip* (LOC) platform for the study of morphogenesis of pollen tubes.

More specifically, the objectives of this work are:

1. Design, fabricate and test a LOC platform that enables characterizing a single pollen tube growth under precisely controlled and reproducible conditions.

2. Study the effect of geometry and shape of the *ex-vivo* growth microenvironment on pollen tube growth behavior.

3. Characterizing the biomechanical interaction of pollen tube with flexible micromechanical elements to quantify the invasive growth force of expanding pollen tube at different stages of its growth, and to study static and dynamic behavior of pollen tube in response to mechanical stimulation. The study will help to improve our understanding on the role of mechanical force in pollen tube morphogenesis.

[14]Mechanotransduction refers to the many mechanisms by which cells convert mechanical stimulus into chemical activity

## 1.9 Organization of the thesis

This thesis is submitted in a manuscript-based format. In another word, all the chapters (excluding first and last chapter) of this thesis, are duplicated from the manuscripts were published, accepted or manuscripts which are under reviewing process for publication in scientific journals.

The thesis is organized as follows:

Chapter 2 presents the TipChip, an LOC platform that has been developed based on MEMS technology to advance both experimentation and phenotyping in tip growth research. Here we describe the overall design, geometry and fluid flow conditions used to fabricate and test the LOC that was specifically developed to allow simultaneous testing of multiple pollen tubes. The effect of geometry of the microfluidic networks on the fluid velocity at the entrances of individual microchannels is numerically analyzed and experimentally tested. The fabrication process of the TipChip through two different methods of photomask production is discussed and the best method is selected. The versatility of the device is illustrated by several experimental assays included in the modular set-up. Two different microchannel configurations are utilized to assess the directional behavior of *Camellia* pollen tubes.

Chapter 3 describes an LOC device with a knot shaped microfluidic network that enables trapping of single pollen grains at the entrances of a series of microchannels. Here we present a significant modification to the TipChip design to create identical growth conditions for serially arranged pollen tubes and to ensure even distribution of entrapment probabilities for all microchannels. Two different criteria were established to assess the cell

trapping probability of each microchannel. The performance of different geometries of the microfluidic network in terms of cell trapping probability was numerically analyzed and experimentally tested. The design was optimized based on trapping probability and uniformity of fluid flow conditions within the microchannels.

Chapter 4 presents a microfluidic based Lab-on-a-chip platform to study the effect of the geometry of the microchannels on pollen tube growth. The device was fabricated using replica molding technique using polydimethylsiloxane (PDMS) and it comprises a network of micro fluidic channels with varying widths and depths. Here we compare the growth rates of pollen tube in traditional plate assays to those in microfluidic channels, and investigate the relationship between microchannel geometry and cell growth rate. The temperature effects on the growth behaviors is also detailed.

Chapter 5 presents a simple practical method to fabricate a high aspect ratio horizontal PDMS microcantilever-based flow sensor integrated into a microfluidic device. The performance of the flow sensor is tested by introducing various flow rates into the microfluidic device and measuring the deflection of the cantilever's tip using an optical microscope. The elasticity modulus of the cantilever is measured using a precision balance method developed in house to measure the sensitivity of the microcantilever to the flow drag force. Based on the elastic modulus of the cantilever and the deflection, the drag force applied on the cantilever is determined. The dynamic range of flow rates detectable using the flow sensor is found by both simulation and experimental methods and compared. This flow meter can be integrated into any type of microfluidic-based Lab-on-a-chip in which flow measurement is crucial such as flow cytometry and particle separation applications.

Chapter 6 introduces the FlexChip, a flexure integrated LOC on polymer for biomechanical study of cellular growth force of *Camellia* pollen tip growing cells. The chapter explains how the invasive growth force of growing pollen tubular cells is estimated by Finite Element Analysis (FEA) using the deflection of the flexible microstructure created by interaction with cellular growth and mechanical properties of the PDMS material. The maximum growth force of pollen tube is estimated just before bursting. Furthermore, in this chapter the effect of the interaction with mechanical obstacles on the pollen tube's growth dynamics is assessed through the shift in the peak frequency characterizing the pollen tube growth rate.

Chapter 7 presents the conclusions of this research and various potential research topics for further development of using LOC platforms in tip growing cell studies. The list of the journal and conference publications out of this research is also presented in this chapter.

Chapter 2

# TipChip - AModular, MEMS-Based Platform For Experimentation and Phenotyping of Tip Growing Cells

## 2.1 TipChip

In this chapter, we explain the overall design, geometry and fluid flow conditions used to fabricate and test a LOC, called TipChip, which is a novel and extremely powerful tool for multiple applications in research on polarly elongating cells. The results presented in this chapter have been published inthree Journals of *The plant Journal,vol: 73, pp:1057-1068, 2013*, with my equal contribution as the main author, *Biomed Microdevices*, *DOI 10.1007/s10544-013-9802-8* with my contribution as the second authorand*Journal of micromechanics and microengineering, vol. 22, 115009, 2011,*with my contribution as the thirdauthor. In the results section, only my contribution to this work is presented.

**Abstract**

Large scale phenotyping of tip growing cells such as pollen tubes has hitherto been limited to very crude parameters such as germination percentage and velocity of growth. To enable efficient and high throughput execution of more sophisticated assays, an experimental platform was developed based on microfluidic and MEMS technology, the TipChip. The device allows positioning of pollen grains or fungal spores at the entrances of serially arranged microchannels harboring microscopic experimental setups. The tip growing cells, pollen tubes, filamentous yeast or fungal hyphae, can be exposed to chemical gradients, microstructural features, integrated biosensors or directional triggers within the modular

microchannels. Using this platform we were able to answer several outstanding questions on pollen tube growth. We established that unlike root hairs and fungal hyphae, pollen tubes do not have a directional memory. The platform opens new avenues for both, more efficient experimentation and large scale phenotyping of tip growing cells under precisely controlled, reproducible conditions.

## 2.2Introduction

Tip growing plant and fungal cells have been widely used as model systems for the cellular morphogenesis in walled cells (Brand & Gow, 2008; N P Money, 2004; R Palanivelu & Johnson, 2011; L. J. Winship, Obermeyer, Geitmann, & Hepler, 2011). Growth in walled cells occurs through the turgor driven expansion of the cell wall and simultaneous assembly of new cell wall material. Tip growth is characterized by a spatial confinement of this cellular expansion process to the very end of the cell (A Geitmann & Dumais, 2009; A. Geitmann & Steer, 2006; F M Harold, R L Harold, & N P Money, 1995; Rojas, Hotton, & Dumais, 2011). The resulting structure is a perfectly cylindrical protuberance capped by a hemisphere- or oval-shaped apex. Among the hallmarks of tip growing cells are the speed of growth (up to 1 cm/h in pollen tubes and fungal hyphae) and the ability to control the direction of growth similar to neurons (R. Palanivelu & Preuss, 2000). How tip growing cells focus their growth activity onto a single site on their cellular surface and how they regulate growth dynamics through exerting temporal and spatial control has been the subject of a substantial body of research (Brand & Gow, 2008; A. Y. Cheung & Wu, 2007, 2008; J.A. Feijó et al., 2001; A Geitmann & R Palanivelu, 2007; Hepler, Vidali, & Cheung, 2001; R. Malhó, 2006; N.P. Money, 2001; N P Money, Davis, & Ravishankar, 2004; R

Palanivelu & Tsukamoto, 2011; Qin & Yang, 2011). Intriguingly, numerous genes have been found to be expressed exclusively in tip growing cells (Honys & Twell, 2003; Honys & Twell, 2004; Pina, Pinto, Feijó, & Becker, 2005; Y. Wang et al., 2008), but our understanding of the functions of many of the proteins encoded by these genes warrants major efforts. These will require developing methods for more sophisticated experimentation and for large scale phenotyping. Here we describe a platform that has been developed to advance both experimentation and phenotyping in tip growth research. The current version of the TipChip platform has been optimized and tested for use with pollen, but can be adapted easily to other tip growing cells produced from small cell bodies such as hyphae and protonemata generated by fungal and moss spores, respectively.

Large scale assessment of pollen tube performance in the past has largely been limited to quantifying seed set (*in vivo* approach) and to determining the percentage of germination, the average growth rate, and the morphology of the cell (*in vitro* approach). These parameters can be determined microscopically in bulk samples, and are based on simple *in vitro* cell culture techniques (Bou Daher, Chebli, & Geitmann, 2008). However, tip growth is a complex process and many other parameters have been studied using highly sophisticated methods with the aim to investigate pollen tube biology. These include monitoring ion fluxes with a vibrating probe (J A Feijó, Malhó, & Obermeyer, 1995; J. A. Feijó, Malhó, & Pais, 1995; M. Messerli & Robinson, 1997; M. Messerli & K. R. Robinson, 1998; M. A. Messerli & K. R. Robinson, 2003), measuring the biomechanical properties with a micro-indenter (A. Geitmann, W. McConnaughey, I. Lang-Pauluzzi, V.E. Franklin-Tong, & A. M. C. Emons, 2004; E. Parre & A. Geitmann, 2005; Elodie Parre & Anja Geitmann, 2005; R. Zerzour, J. H. Kroeger, & A. Geitmann, 2009), and

assessing invasive and tropic growth in experimental setups exposing pollen tubes to mechanical obstacles and directional triggers (F Bou Daher & A Geitmann, 2011; O. Gossot & A Geitmann, 2007; Higashiyama & Hamamura, 2008; Lord, 2003; R Malhó, Feijó, & Pais, 1992; Márton & Dresselhaus, 2010; R. Palanivelu & Preuss, 2000; R Palanivelu & Tsukamoto, 2011). These experimental approaches would be extremely useful as assays to discriminate between pollen tube phenotypes, but they are typically time-consuming (since only one cell can be tested at any given time) and associated with high variability. We therefore designed an experimental platform that allows for the simultaneous investigation of multiple tip growing cells, in a highly reproducible manner, under precisely controlled conditions. The modular nature of this platform makes it ideally suited both for phenotyping and for the development of new experimental approaches to study the biology of tip growing cells.

The TipChip platform is based on Micro-Electro-Mechanical Systems (MEMS) technology. This technology has been exploited in biological and medical applications to simplify sophisticated functions such as chemical reactions, drug development and bioassays by integrating them within a single micro-device, called a Lab-on-a-Chip (LOC) (K. Cheung & Renaud, 2006; Giouroudi, Kosel, & Scheffer, 2008; Nuxoll & Siegel, 2009). Here we describe the geometry, fluid flow conditions and materials of an LOC specifically developed to allow for simultaneous testing of multiple pollen tubes. The versatility of the device is illustrated by several experimental assays included in the modular setup. The data obtained with these configurations have yielded crucial and novel information on the biology and growth behavior of pollen tubes.

## 2.3Overall LOC design

The TipChip is specifically designed to enable investigation of longitudinally elongating cells for which commercially available microfluidic systems are not suitable (P. Lee, Helman, Lim, & Hung, 2008). The LOC allows high resolution brightfield and fluorescence imaging and multiple cells can be observed simultaneously. The setup was conceived to be modular to allow incorporation of various structural, micro-mechanical and chemical testing methods. Fabrication of the designs was done as explained briefly in Materials and Methods and in more detail in (C. Agudelo, Sanati Nezhad, Ghanbari, Packirisamy, & Geitmann, 2012). Tests using two different methods for photomask production (high-resolution digital printing at 3600 dpi and direct writing using laser lithography) revealed that to fabricate microchannels with surfaces that are sufficiently smooth compared to the dimensions of the pollen tube, the more expensive DWL 66FS laser lithography technology is required. In order to enable the simultaneous observation of multiple cells, the setup was designed to comprise a serial arrangement of microchannels through which the tip growing cells are guided to elongate. Cell bodies (pollen grains) are driven to the entrances of a series of these microchannels by laminar fluid flow. The overall microfluidic network consists of an inlet, a distribution chamber giving access to the entrances of the microchannels, and two types of outlets (Figure 2. **1**). One outlet allows for the evacuation of excess pollen from the distribution chamber, the second type of outlet drains liquid from the ends of the microchannels and thus allows for continuous liquid flow through the microchannels. The configuration encloses the cells from all sides thus preventing the evaporation of the growth medium, a phenomenon which has proved difficult to control in open assays (Yetisen et al., 2011c).

To avoid the accumulation of cells into stacks that would represent a mechanical impediment to fluid flow and a visual obtrusion preventing microscopical observation, the height of the distribution chamber was set to be between 1.2 and 1.5 times the diameter of the cells to be distributed. Here and in the following, optimized dimensions for pollen grains and tubes of the species *Camellia japonica* are provided. The grains typically have a diameter of 60 µm, therefore the height of the microfluidic network was set to 80 µm.The pollen tube of this species is between 14 and 20 µm large and grows extremely straight and rapidly thus making it an ideal model system for cytomechanical studies (F Bou Daher & A Geitmann, 2011). For pollen grains from other species or for fungal spores, the dimensions of the TipChip can be adjusted easily.

The principle of the setup is to inject a suspension of pollen or spores into the distribution chamber through the inlet and to trap individual cells at the entrances of each microchannel, similar to other setups developed in the past (Kobel, Valero, Latt, Renaud, & Lutolf, 2010; W. H. Tan & Takeuchi, 2007), but with the difference that the adjacent microchannels would have to be of substantial length thus requiring a novel design strategy. One of the main challenges was to design the distribution chamber such that most or ideally all entrances of the microchannels would be occupied by a single or very few cells after simple injection of the cell suspension. Large accumulations of cells were to be avoided, since they would hamper fluid flow through the microchannels thus affecting the experimental conditions and reproducibility. A simple rectangular shape geometry for the distribution chamber was tested (Figure 2. 1B). Trapping is achieved by pollen grains moving along the streamlines created by the laminar flow imposed by slow injection of the pollen suspension. To accomplish optimal trapping, the entrances were designed as a

curved notch, the narrow end of which is smaller in the x-y plane (30 µm) than the size of the pollen grain (Figure 2. 1C). The microchannels are narrow conduits through which pollen tubes are guided to grow. In modular manner, these microchannels can be equipped with the desired experimental configurations such as mechanical obstacles, microstructural features, chemical gradients, electric fields and other biosensors.

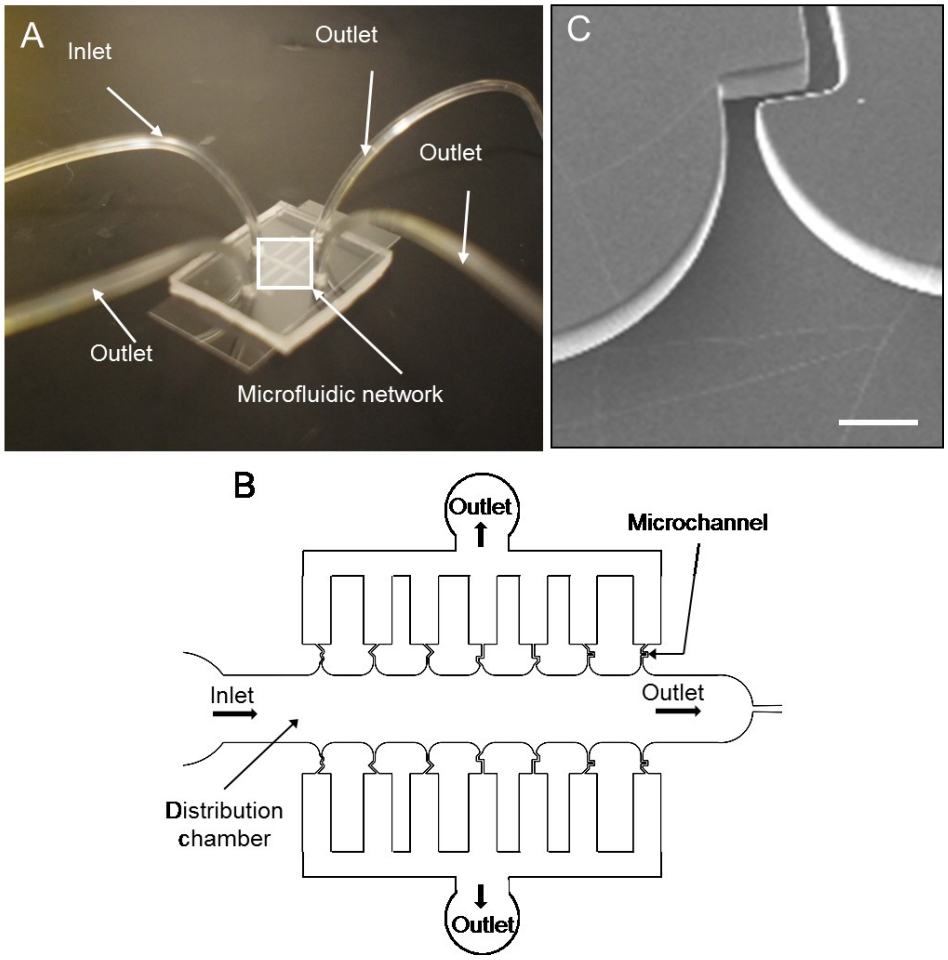


**Figure 2. 1** Overall design of the TipChip(**A**) Image of the TipChip showing the PDMS layer attached to a cover slip and the attached inlet and outlets
(**B**) General design principle of the microfluidic network in the TipChip. The pollen suspension is injected through the inlet and the pollen grains move through the distribution chamber and either get trapped at the entrances of the microchannels or evacuated through the distribution chamber outlet.(**C**) Scanning electron micrograph of trap entrance. Bar = 100 µm

## 2.4Effect of Width and Depth of Microchannels onPollen Tube Growth

For most of the envisaged applications, the microchannels would have to be only slightly bigger than the diameter of the tip growing cell. In the case of *Camellia*, a typical microchannel would measure 30 µm in width and 80 µm in depth. This is very different from conventional *in vitro* setups used for pollen tube culture, in which the elongating pollen tubes are surrounded by relatively large volumes of medium. This includes micro-structured devices such as the pollen tube guidance assay developed by Yetisen et al. (Yetisen et al., 2011c), since the pollen tubes in that device were surrounded by an amount of medium that was orders of magnitude bigger than the volume of the cell. The very limited volume of medium around the elongating cell in the TipChip could potentially have a negative effect on cellular growth, since supply of nutrients, minerals and oxygen might be limited. We therefore assessed the effect of the width (Figure 2.2A,B&C) and depth (Figure 2.2D) of the microchannel on pollen tube growth. Parallel channels were designed with constant dimensions to serve as reference to ensure that changes in pollen tube growth rate were not simply related to different stages of pollen tube maturation. Monitoring the growth rate of pollen tubes traversing the differently sized channel portions showed that varying width did not significantly affect pollen tube growth rate, but varying depth did. In channels with varying width the growth rate of *Camellia* pollen tubes remained very constant at velocities between 12 and 16 µm/min with temporal variations of less than ±1.5 µm/min vs. the average growth rate of the individual tube (n=3). Under no flow conditions, an increase in microchannel depth from 80 µm to 160 µm on the other hand, typically caused an increase of the pollen tube growth rate by up to 50% (n=3).

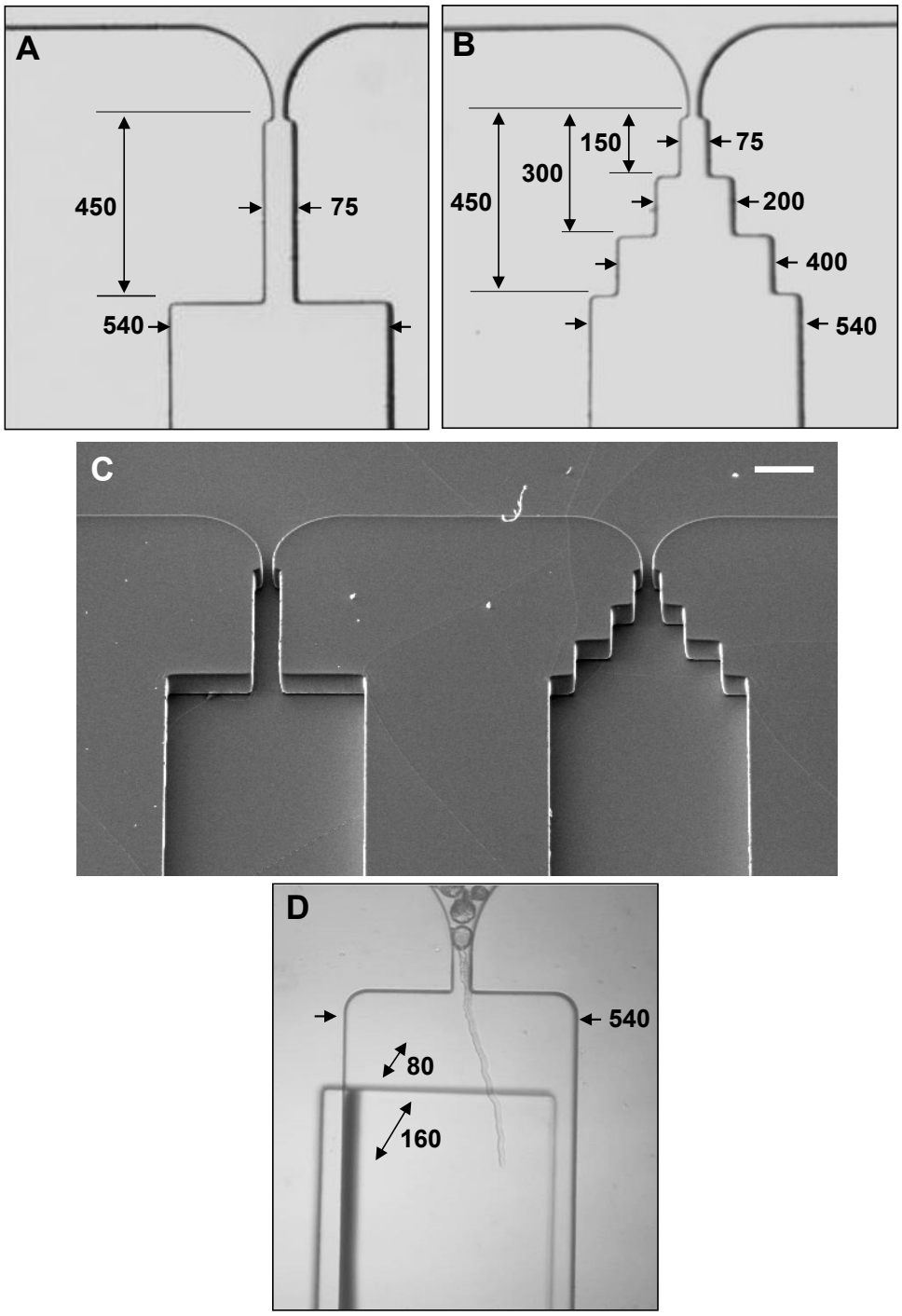


**Figure 2.2.** Effect of channel width on pollen tube growth(**A**) Microchannel with constant width over a length of 450 µm serving as control.(**B**) Microchannel with three different widths over a total length of 450 µm(**C**) Scanning electron micrograph of LOC used for channel width test. Bar = 200 µm(**D**) Microchannel with constant width but changing depth. All numbers are dimensions in µm.

Further investigation is warranted to address why pollen tube growth is more sensitive to the dimensions in z-direction than to those in-plane. However, the finding is consistent with other microfluidic applications (H. Yu, I. Meyvantsson, I. Shkel, & D. Beebe, 2005) and we hypothesize that this difference may be connected to convection of heat occurring primarily in z-direction under microscope. The finding that the in-plane dimensions of the microchannel have minor or no effects on pollen tube growth under no flow conditions is crucial for all further implementations of the TipChip, as incorporation of sensors and mechanical obstacles will inevitably necessitate varying these dimensions along the length of a microchannel. If the geometry *per se* would affect the growth rate, conclusions would be difficult to draw from such experiments.

## 2.5 Anchoring of Tip Growing Cell

The pollen grains are transported to the microchannel entrances by fluid flow and in experimental setups that allow for continuous flow, the fluid force keeps the grain at the entrance. However, in experiments that require absence of or a reverse direction of flow, or in experiments that expose elongating tubes to mechanical obstacles, the grain is not held in place but can either drift away or be pushed backwards by the reverse flow drag force or by the force generated by the growing tube hitting an obstacle, respectively (Figure 2.3). Therefore we conceived an additional feature to the microchannel design that prevents backward displacement. For this purpose a kink consisting of three consecutive 90° angles was incorporated into the microchannel shape (Figure 2.3C,E). Tests showed that this configuration was successful in preventing pushback of the grain and that it allowed for experiments in which the elongating tube was forced to negotiate mechanical obstacles.

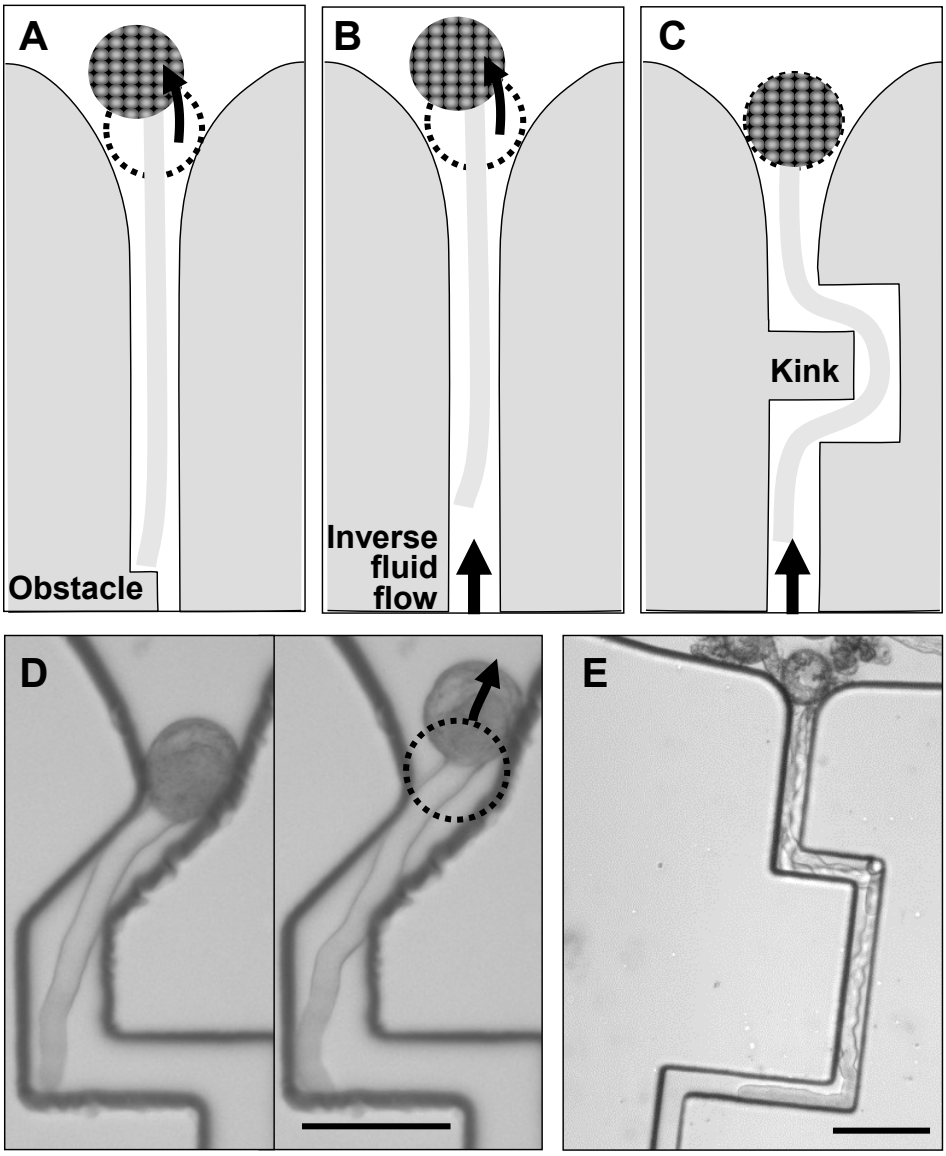


**Figure 2.3**Kink and serpentine features to prevent pushback (**A**) A pollen tube growing through a microchannel against a mechanical obstacle pushes back its grain and is thus unable to exert a mechanical force against the obstacle.(**B**) A pollen tube growing through a microchannel with inverse fluid flow is displaced backwards by the drag force.(**C**) Incorporation of a kink in the microchannel architecture enables fixing the pollen tube in place. Mechanical obstacles or inverse fluid flow encountered after passing this kink therefore do not cause a displacement of the grain allowing the tube to exert a pushing force.(**D**) A *Camellia* pollen tube growing through a microchannel against a mechanical obstacle pushes back its grain (original position marked by the dashed circle).(**E**) A *Camellia* pollen tube growing through a kink in the microchannel.Bars = 100 μm.

## 2.6 Pollen Tubes and Directional Memory

An important application of the TipChip is the investigation of the behavior of pollen tubes exposed to a chemical gradient. This includes testing the response of pollen tubes to signaling molecules produced by the pistillar tissues or by the female gametophyte (Higashiyama & Hamamura, 2008; Lord, 2003; R Palanivelu & Tsukamoto, 2011). Data obtained from experiments exposing pollen tubes to directional triggers could potentially be biased by an "inner memory" that determines the growth direction of the tube tip depending on the position of the pollen grain. In root hairs and fungal hyphae, such a directional memory, or endogenous polarity, has been observed (T N Bibikova, A Zhigilei, & S Gilroy, 1997; Held, Edwards, & Nicolau, 2011), but no information is available for pollen tubes. Therefore, we assessed the directional behavior of *Camellia* pollen tubes in two different microchannel configurations. The first setup exposed the tubes to a serpentine-like geometry with repeated changes in growth direction (Figure 2.4). In this configuration, growth was observed to occur in a "blind" fashion, meaning that a tube grew straight until it encountered a microchannel wall. It then slipped along the wall in the direction favored by the collision angle. In situations when the wall turned away sharply, the pollen tube maintained the last direction imposed by the wall indefinitely until another obstacle (or wall) was encountered (Figure 2.4B, n=20).

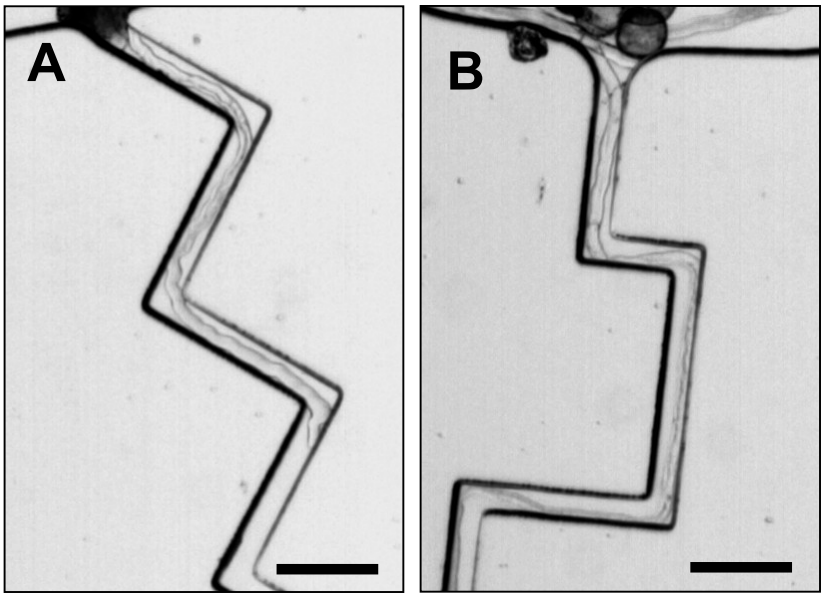


**Figure 2.4** (A,B) Pollen tubes growing through a serpentine like microchannel grow straight until they encounter an obstacle and deviate. Bars = 100 μm.

The second test consisted in exposing pollen tubes to repeated changes in growth direction prior to letting them enter a wide chamber (Figure 2.5A, B & C). Invariably, once they entered the wide chamber, the pollen tubes kept the last growth direction for extended periods of time. Contrary to root hairs (T N Bibikova et al., 1997) and fungal hyphae (Held et al., 2011), the pollen tubes did not return to the original growth direction after having cleared the microchannel maze (n=10). Both the presence and absence of a directional memory are consistent with the biological purpose of the respective cell types. Root hairs ideally need to grow away from the root to most efficiently accomplish their tasks consisting in water and nutrient uptake. An endogenous polarity ensures that even after navigating obstacles, the general growth direction of a root hair is maintained to be perpendicular to and away from the root. Similarly, a fungal mycelium expands most efficiently, if hyphae keep growing away from its center, even after having been temporarily deviated by an obstacle. Pollen tubes on the other hand must grow towards a

target, following external guidance cues. The position of the pollen grain is irrelevant for this targeting function and an endogenous directional memory would therefore be an impediment rather than an advantage. Its absence in pollen tubes is therefore consistent with the target finding function of this cell type.

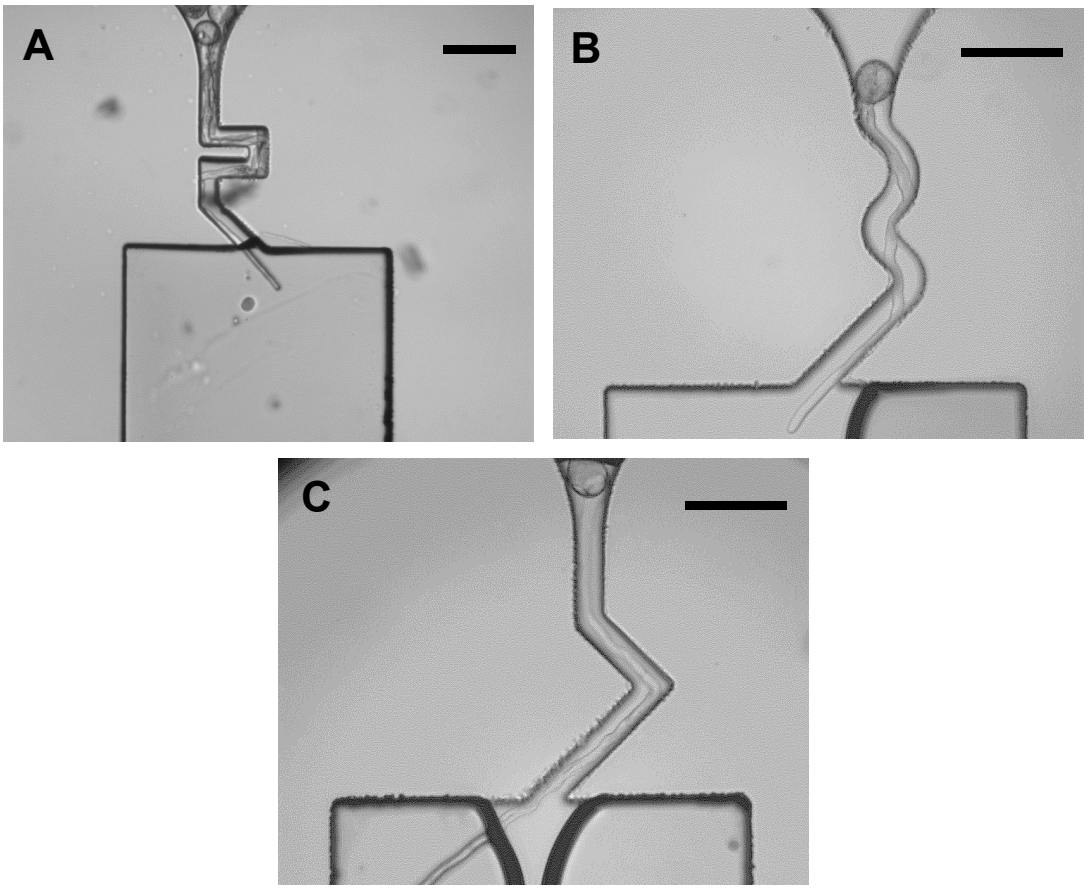


**Figure 2.5**(A, B & C) After multiple changes in growth direction, pollen tubes entering a wide channel grow in the direction they were last exposed to, independently of the position of the pollen grain. Bars = 100 µm.

## 2.7 Experimental Procedures

### 2.7.1 Fabrication of LOC Devices

The LOC was designed with CAD software and reproduced onto either a transparent film using digital printing or a glass mask with a direct-write lithography (DWL) system (DWL 66 FS - Heidelberg Instruments) to achieve higher resolution. Molds were fabricated as described in detail in (C. Agudelo, Sanati Nezhad, et al., 2012; Sanati Nezhad, Ghanbari, Agudelo, Naghavi, et al., submitted). Briefly, using a photolithographic technique a mold is fabricated with SU-8, a negative photoresist (MicroChem Corp.). To reach the thickness of 80 μm, SU-8 2035 is spin coated on 10 cm silicon wafers (WRS materials). After two soft-baking steps for 5 min at 65ºC and for 10 min at 95ºC in a hotplate the SU-8 is exposed to UV light using a photo mask. The SU-8 layer is then post-baked for 5 min at 65ºC and for 10 min at 95ºC in a hotplate and developed to obtain the SU-8 mold. The microfluidic device is next fabricated by curing a PDMS mixture of base and curing agent with a weight ratio of 10:1 on the SU-8 mold. The PDMS replica is peeled off from the mold, the inlet and outlets are drilled, and the layer is bonded to a cover slip using oxygen plasma bonding (Harrick Plasma PDC-001) to seal the fluidic network (Bubendorfer, Liu, &Ellis, 2007).

### 2.7.2 Pollen Culture and Germination

Pollen of *Camelliajaponica* was collected from a plant in the Montreal Botanical Garden, dehydrated and stored on silica gel at -20°C before until use. Prior to experimentation, few micrograms of the pollen were thawed and rehydrated in humid atmosphere for 1 hour and subsequently immersed in 1 mL liquid growth medium optimized for this species (F Bou Daher & A Geitmann, 2011).

### 2.7.3 Imaging

Brightfield imaging was done on an Olympus BX60M Brightfield microscope equipped with a Nikon Coolpix 4500 camera and with a Nikon Eclipse 80i digital imaging microscope system. Scanning electron microscopy was done on gold-palladium coated samples with a FEI Quanta 200 3D operated at 15 kV.

## 2.8 Conclusion

The presented microfluidics-based platform for tip growth research represents a novel and extremely powerful tool for multiple applications in research on pollen tubes, fungal and yeast hyphae and other polarly elongating cells. Its modular design allows for the incorporation of various features and future models will be equipped with flow sensors (Sanati Nezhad, Ghanbari, Agudelo, Packirisamy, et al., 2012), force sensors (Felekis et al., 2011), electric fields (Zou, Mellon, Syms, & Tanner, 2006) and other devices. Here we provided experimental proof of concept and we report a number of novel findings for the tested cell type pollen tube. *Camellia* pollen tubes were found to be able to grow in narrow microchannels. We established that contrary to other tip growing cells, pollen tubes do not have a directional memory. These findings are novel in terms of pollen biology and will be crucial for future application of microfluidics and MEMS-based techniques for tip growing cells.

# Chapter 3

## Microfluidic positioning of pollen grains in lab-on-a-chip for single cell analysis

### 3.1 Enhancing microfluidic platform for trapping of single pollen grains

The TipChip platform presented in Chapter 2 had a number of limitations which limited the performance of the device at large scale experiments. To provide reproducible and identical conditions, the fluid flow through all parallel microchannels would have to be similar, and each microchannel would have to be occupied by exactly one pollen grain. Both conditions were not met by the existing version of the TipChip. To address these issues, using numerical simulation and experimental testing, we modified the original TipChip platform to achieve uniform distribution of pollen grains within the microfluidic platform and to have reproducible and identical growth conditions for all the trapped pollen grains.

This work has been accepted for publication in *Journal of Bioscience and Bioengineering* (Ghanbari, Sanati Nezhad et al. 2013).

**Abstract**

A lab-on-a-chip device with a knot shaped microfluidic network is presented to enable trapping of single pollen grains at the entrances of a series of microchannels. This set-up serves to create identical growth conditions for serially arranged tip growing plant cells such as pollen tubes. The design consists of an inlet to introduce the pollen suspension into the chip, three outlets to evacuate excess medium or cells, a distribution chamber to guide

the pollen grains toward the growth microchannels and a serial arrangement of microchannels with different geometries connected to the distribution chamber. These microchannels are to harbor the individual pollen tubes. Two different criteria were established to assess the efficiency and optimize the device: trapping probability and uniformity of fluid flow conditions within the microchannels. The performance of different geometries of the microfluidic network was numerically analyzed and experimentally tested.

## 3.2Introduction

Lab-on-a-chip (LOC) devices can be used to perform biological experiments at the level of the individual cell thus providing the opportunity to examine cellular processes and properties that were inaccessible to experimentation hitherto (Andersson & Van den Berg, 2003; Beebe et al., 2002). Importantly, the dimensions of structural components of these devices match with the cellular dimensions providing microenvironments that are made to resemble the *in vivo* conditions more accurately than bulk experimental set-ups (Prokop et al., 2004). Furthermore, because of their design, LOC fabrication involves relatively low costs and experimentation requires only minute amounts of reagents. Finally, LOC technology offers the possibility of integrating micro sensors and actuators and it allows performing parallel processes (Prokop et al., 2004; Wheeler et al., 2003).

In conventional cell cultures, cells are in close physical contact with their neighbors and are thus exposed to the ions, proteins, hormones and other substances released by the adjacent cells. In addition, neighboring cells compete for nutrients provided in the medium. This generates complex, superimposing chemical gradients the effects of which may not be

negligible when assessing the behavior of an individual cell. In contrast, microfluidic-based cell culture can provide an autonomously controlled micro environment that eliminates the effect of neighboring cells which is essential to establish a precisely controlled and reproducible environment. To execute experiments on one or several individual cells within a micro-device, they typically need to be transported to a particular position, immobilized and manipulated. The design of the device has to cater for these transportation and positioning needs in addition to those required for the experimental procedure. Different principles have been employed for the purpose of positioning and trapping of particles or cells. These include mechanical (Chang, Lee, & Liepmann, 2005; Khademhosseini et al., 2004), electrical (Seger, Gawad, Johann, Bertsch, & Renaud, 2004; Voldman, Gray, Toner, & Schmidt, 2002), optical (Birkbeck et al., 2003; Chiou, Ohta, & Wu, 2005; Flynn et al., 2002), hydrodynamic (Gossett, Weaver, Ahmed, & Di Carlo, 2011; M. Yang, Li, & Yang, 2002) and magnetic (Furdui & Harrison, 2004; Grodzinski, Yang, Liu, & Ward, 2003; H. Lee, Purdon, & Westervelt, 2004) forces. Flow assisted cell trapping has the advantage of being simple, low cost, and it does not require any external control equipment or coupling electrical, magnetic or optical fields into the device which might create disturbance in the biological functions of the living cells. Flow assisted methods enable trapping of single cells without particular requirements on the material properties of the trapped objects even within a crowded cell suspension, a situation which is problematic when using force field based methods. However, since particles (cells) are moved passively by fluid flow, this method generally has limited precision and efficacy.

Various designs have been developed to trap particles based on directed fluid flow. Oleschuk et al. (Oleschuk, Shultz-Lockyear, Ning, & Harrison, 2000) reported the use of

weir structures oriented perpendicular to the fluid flow to trap octadecylsilane coated silica beads. One of the problems associated with this design was the difficulty to reproducibly generate a single layer of particles at the dam. Furthermore, high hydrodynamic pressure exerted on the trapped particles make culture conditions unstable for biological experiments. In addressing these problems, Yang et al. (M. Yang et al., 2002) demonstrated a parallel dam structure to immobilize cells within a microfluidic device that ensures minimal shear stress on the trapped cells and that allows for the generation of a concentration gradient through dilution of an analyte solution. However, these weir structures had relatively low capture efficiency making these approaches impractical for application with low cell numbers such as stem cells. To overcome this challenge, Skelley et al. (Skelley, Kirak, Suh, Jaenisch, & Voldman, 2009) devised an array of Polydimethylsiloxane (PDMS) weir structures with a trapping efficiency of ~70% when used on NIH3T3 fibroblasts, myeloma cells, B cells, mESCs and mouse embryonic fibroblasts. Chung and colleagues (Chung, Kim, & Yoon, 2011) integrated hydrodynamic guiding structures within the microfluidic device for high-throughput single cell trapping of prostate cancer PC3 cells to increase the capture efficiency to more than 80%. Cui et al. (Cui, Liu, Wang, Sun, & Fan, 2011) reported a microfluidic chip with a main channel and two suction microchannel networks at opposing sides of the main channel for highly efficient hydrodynamic trapping and pairing of cells. The effect of both flow rate and dimensions of the microchannels on the entrapment efficiency were studied and an efficiency of 100% for cell capture and 88% for cell pairing was reported.

The geometry of the trap has to be designed to be suitable for the size and shape of the cellular model system and for the type of experimental assay to which the cells are

subjected. U-shaped trap geometry has been used to trap single HeLa cells (Di Carlo, Aghdam, & Lee, 2006; Di Carlo, Wu, & Lee, 2006), whereas C-shaped and flat-type sieves have been developed for trapping small clusters of cells or 3T3 cells (M. C. Kim, Wang, Lam, &Thorsen, 2008). In these works, the criteria for optimal design were *1)* the optimization of capture efficiency of the microfluidic cell trapping device (particularly in the case of low cell numbers), and *2)* the degree of adaptation to the envisaged experimental assay.

In the present chapter, we present a hydrodynamic flow based trapping mechanism that is devised to suit the particular needs of a spherical cell that forms a very rapidly growing cylindrical protuberance. Rather than the spherical cell body, it is the cylindrical protuberance which is the object of the subsequent experimental studies. The particular challenge is therefore to trap the cell body at an opening of a microchannel into which the protuberance can elongate and where it can then be exposed to a variety of tests. These protuberances, or pollen tubes, are formed by pollen grains, the male gametophytes in the flowering plants. They are formed upon germination of pollen grains on a receptive stigma and serve to transport the sperm cells from the male gametophyte to the female gametophyte nestled within the pistillar tissues. Pollen tubes can grow extremely fast with rates up to tens and even hundreds of micrometers per minute in some species (Y. Chebli & A. Geitmann, 2007). They are easily cultured *in-vitro* and have become an excellent model system to study cellular morphogenesisand growth in walled cells (Feijo et al., 2001; J. Kroeger & Geitmann, 2012). The growth process in pollen tubes is confined to a small region on the cellular surface, the apex. This tip focused growth process is shared by other cell types such as root hairs, fungal hyphae, and nerve cells (Y. Chebli & A.

Geitmann, 2007) and enables the rapid reorientation of the growth direction. This reorientation allows pollen tubes to respond to external guidance cues rendering the cells able to perform chemotropism and thigmotropism.

The investigation of chemotropic and thigmotropic behavior necessitates an experimental setup that presents the elongating cells to potential guidance triggers. Yetisen et al. (Yetisen et al., 2011a) recently developed a microfluidic-based assay that exposes in bulk growing pollen tubes to a chemical gradient. However, the microstructure in this device was orders of magnitude bigger than the dimensions of the individual cells and did not allow for single cell analysis. To be able to conduct single cell analysis, we recently developed the TipChip, a microfluidic device designed to study individual pollen tubes (A Sanati Nezhad, Ghanbari, Agudelo, Packirisamy, & Bhat, 2012). In the TipChip, pollen tubes are guided to grow through individual microchannels. In order to achieve this, pollen grains must be positioned at the entrances of these microchannels. While performing successfully in preliminary tests, the TipChip had a number of limitations that made large scale experiments problematic. To provide reproducible and identical conditions, the fluid flow through all parallel microchannels would have to be similar, and each microchannel would have to be occupied by exactly one pollen grain. Both conditions were not met by the existing version of the TipChip and although functional, this limited the performance of the device at large scale. Most critically, differences in trapping efficiency between the microchannels led to the accumulation of several cells at the entrance of certain microchannels whereas others remained unoccupied. The accumulation of cells resulted in a narrowing of the passage and hence a change in the conditions regulating fluid flow through these microchannels.

Here we present a significant modification to the TipChip design which satisfies three different criteria: 1) entrapment of one but not more pollen grains at the entrance of each microchannel, 2) even distribution of entrapment probabilities for all microchannels 3) identical fluid flow conditions in all microchannels. The effect of different dimensions of the microfluidic network on cell trapping probability was assessed using computational fluid dynamics and verified by experimental testing.

## 3.3Device development

### 3.3.1 Design of Microfluidic Chip

The microfluidic network consists of an inlet for injection of the pollen grain suspension, a transporting channel to guide the pollen grains to the doughnut shaped distribution chamber, and two sets of microchannels with different geometries located at the outer face of the distribution chamber as shown in Figure 3.1A.

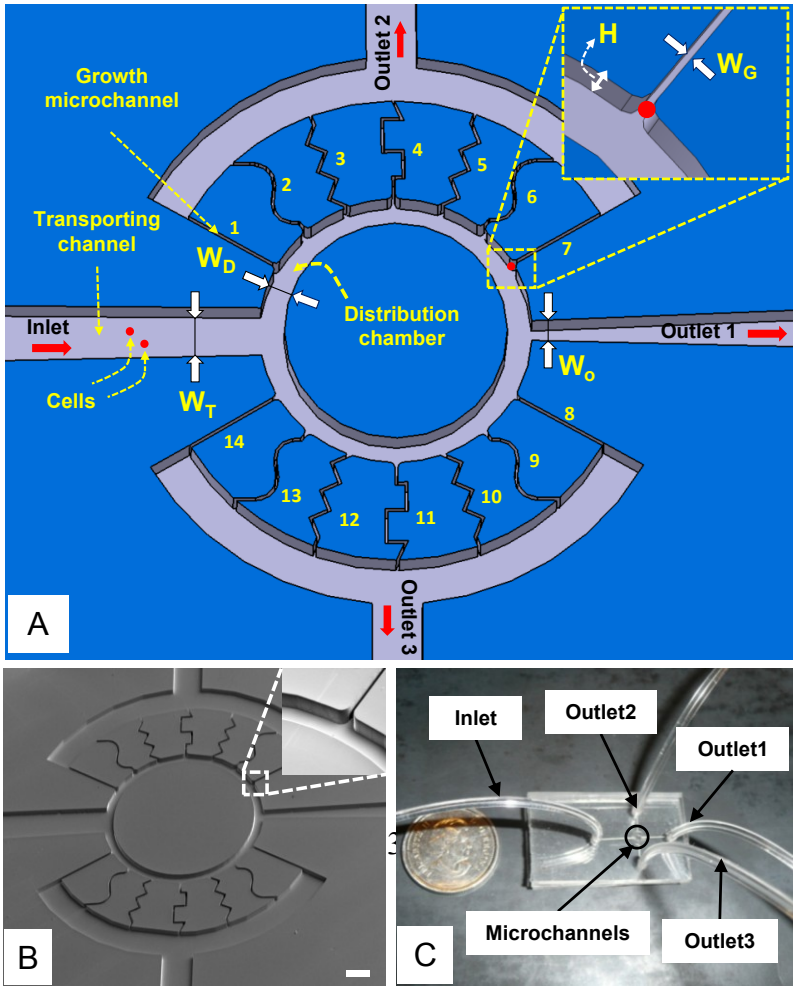

**Figure 3.1** (A) Schematic of the microfluidic network and magnified view of a pollen grain trapped at the entrance of a microchannel (B) Scanning electron micrograph of the PDMS-based microfluidic chip before bonding and magnified view of the trapping site at the entrance of a microchannel. Scale bar = 400 μm (C). Fabricated microfluidic chip of the primary design. A Canadian quarter coin is shown for reference.

The microchannels are meant to harbor the elongating pollen tubes so that it is possible to implement various experimental test assays in the same chip. In order to guide the pollen tubes into the microchannels, pollen grains have to be trapped at the entrances of these microchannels as shown in the inset of Figure. 3.1A. Three outlets remove medium from the distribution chamber and from the ends of the microchannels. The distribution chamber outlet (Outlet 1) is made large enough to allow the evacuation of excess pollen grains. Outlets 2 and 3 facilitate continuous fluid flow through the microchannels during experimentation, and also ensure the positioning of pollen grains at the entrances of the microchannels.

Several design features of the microfluidic network are chosen in accordance with the size of the particular cellular type used here. Pollen grains of *Camellia japonica* have a typical diameter of 50-60 μm. Therefore, the height (depth) of the entire microfluidic network (H) is set to be 80 μm in order to allow the grains to be transported freely by the fluid flow, without stacking along depth. In order to trap individual pollen grains at the entrances of the microchannels and to allow pollen tubes with a typical diameter of between 13-20 μm to enter these channels, the channel width ($W_G$) is set to 30 μm. The entrance of a microchannel is rounded with a radius of 50 μm to enable pollen grains to easily settle into a trap (inset of Figure 3.1B). Since the purpose of the present design was to study the directional control of pollen tube growth, microchannels with different geometries were used. Two identical sets of microchannels (top and bottom) were incorporated for

redundancy. Based on the aforementioned criteria, the transporting channel width ($W_T$), outlet drain width ($W_O$) and distribution chamber width ($W_D$) were selected as 500 μm, 200 μm and 150 μm, respectively, for the preliminary design.

### 3.3.2 Fabrication of the Microfluidic Chip

PDMS was used for the fabrication of the microfluidic chip due to its properties such as biocompatibility, transparency, low cost and ease of fabrication. Moreover, high gas permeability of PDMS ensures oxygen supply to the pollen tubes growing in the closed device (C. Agudelo, Sanati, Ghanbari, Packirisamy, & Geitmann, 2012). The chip was fabricated using replica molding technique (Xia & Whitesides, 1998). To fabricate the mold, SU-8 2035, a negative photoresist (MicroChem Corp., MA, USA) was spin coated onto a 4 inch silicon wafer and patterned using standard photolithography technique. A mixture of curing agent and PDMS prepolymer (Sylgard 184 silicone elastomer, Dow Corning Corporation, Midland, USA) at a weight ratio of 1:10 was poured onto the SU-8 mold. Then, the mixture was completely degassed in a desicator to remove any air bubbles and it was cured for 4 hours at 60ºC. After curing, the PDMS replica was peeled off the mold and the inlet and outlets were punched. In order to create an enclosed microfluidic network, a glass cover slip was bonded onto the PDMS replica using a plasma treatment method (Jo, Van Lerberghe, Motsegood, & Beebe, 2000). To perform the bonding, the surfaces of the PDMS and the glass cover slip were activated with oxygen plasma (40 seconds at 30 W, Harrick Plasma PDC-001) and then both surfaces were placed together face to face to form an irreversible bond. This closure significantly limits the evaporation of culture medium which poses a problem in open assays (Yetisen et al., 2011a). As the inlet and outlet tubes are attached to the PDMS layer, the glass bottom layer remained

smooth and flat for viewing under inverted microscope. Figure 3.1C shows the fabricated microfluidic chip of the preliminary design.

### 3.3.3 Pollen Culture and Germination

*Camellia japonica* pollen was dehydrated on silica gel for 2 h and stored at -20°C. Prior to each experiment, pollen was rehydrated in a humid chamber at room temperature for at least 30 min. Pollen grains were suspended in a liquid growth medium containing the following components: 2.54 mM of $Ca(NO_3)_2 \cdot 4H_2O$, 1.62 mM of $H_3BO_3$, 1 mM of $KNO_3$, 0.8 of mM $MgSO_4 \cdot 7H_2O$ and 8% sucrose (w/v).(F. Bou Daher & A. Geitmann, 2011) Pollen germination was monitored under the microscope and the pollen suspension was introduced into the microdevice upon initiation of germination.

### 3.3.4 Time-Lapse Microscopy

Time-lapse microscopy was conducted using an inverted microscope (Nikon TE2000) equipped with a cooled CCD camera (Roper fx) and ImagePro software (Media Cybernetics).

## 3.4. Results and Discussion

### 3.4.1 Preliminary test

To test the performance of the microfluidic device, the pollen suspension was injected into the microfluidic network of the preliminary design using a syringe pump. The distribution of pollen grains over the microchannel entrances was generally found to be uneven. At the near end of the distribution chamber several microchannel entrances remained unoccupied, whereas pollen grains accumulated at the entrances of the microchannels located at the far end. This accumulation of pollen grains must be avoided so as not to create a blockage for the flow of medium into the microchannel. Also, preliminary experiments suggest that

accumulation of the pollen grains at the entrances of microchannels increases the probability of more than one pollen tube to enter the same microchannel, a situation that prevents single cell analysis. To ensure a more even distribution of pollen grains, the widths of transporting channel, distribution chamber and outlet 1 were varied. In doing so, it was considered that if the widths of the distribution chamber and the outlet 1 are too large, almost all grains would be transported to the outlet drain, hence the chance of pollen grains to get trapped at the entrances of microchannels would be expected to decrease. To aid with the identification of suitable dimensions for the microfluidic network, computational fluid analysis was carried out.

### 3.4.2 Design Improvement

The design parameters of the microfluidic network have great influence on the flow behavior, and hence the trapping probability of the pollen grains. Two-dimensional (2D) finite element modeling was conducted to predict fluid behavior and optimize the preliminary design for different outlet drainwidth ($W_O$) and distribution chamber width ($W_D$). The width of the transporting channel ($W_T$) was set to 500 μm. Based on constraints explained in Section III, the width of the growth microchannels was set to 30 μm. $W_O$ was varied between 100 μm and 200 μm and $W_D$ was varied between 150 μm and 300 μm (Table 3.1).

**Table 3.1** Dimensions of the six different designs for the microfluidic device

| Design number | $W_O$ (μm) | $W_D$ (μm) |
|---|---|---|
| 1 | 200 | 150 |
| 2 | 200 | 300 |
| 3 | 150 | 150 |
| 4 | 150 | 300 |
| 5 | 100 | 150 |
| 6 | 100 | 300 |

Boundary conditions consisted of a constant velocity of 0.02 m/s at the inlet and atmospheric pressure at the outlets. No-slip boundary condition was considered for the channel walls. The medium is assumed to have properties similar to water with a dynamic viscosity of 0.001 Pa.s and a density of 1000 kg/m$^3$. The fluid domain was governed by the incompressible Navier-Stokes equations and the continuity equations. COMSOL Multiphysics software was employed to solve the governing equations.

A schematic of a pollen grain being transported by the fluid flow in the distribution chamber is shown in Figure 3.2.

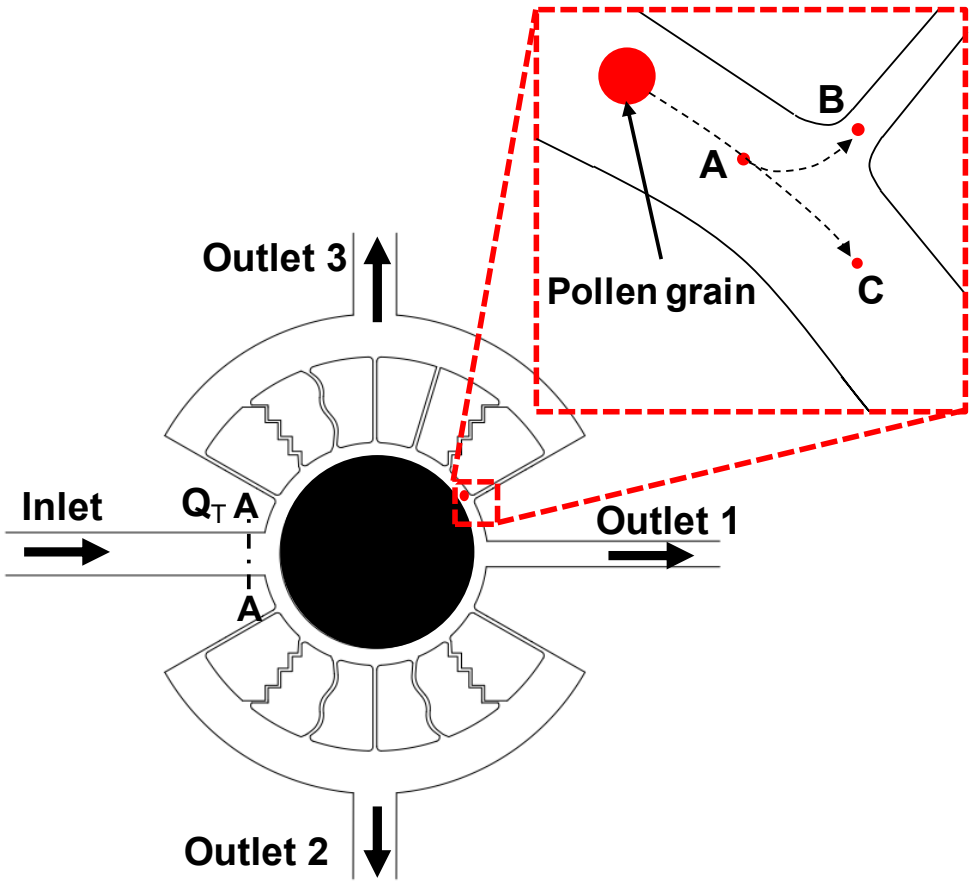


**Figure 3.2** Schematic of a pollen grain being transported by the fluid flow inside the distribution chamber. Points A and B were chosen such that the distance between A and B is identical to that between A and C. A, B and C are located 40 µm away from the outer wall of the distribution chamber.$Q_T$ is the total flow rate entering the distribution chamber at (Section A-A) of the transporting channel.

In order to evaluate the performance of six different designs proposed in Table 3.1, the trapping ratio (σ) was defined as the ratio of the pressure differences between points A and B to the pressure difference between points A and C (equation 3.1 andFigure 3.2).

$$\sigma = \frac{P_A - P_B}{P_A - P_C} \tag{3.1}$$

Where $P_A$, $P_B$ and $P_C$ are the pressures at points A, B and C respectively. The distances

between A and B and between A and C were identical. Furthermore, since preliminary experiments showed that only pollen grains at a distance less than 40 μm from the wall of the distribution chamber have the chance to be trapped, points A and B were chosen to be 40 μm away from the outer wall of the distribution chamber. It is assumed that a pollen grain passing in front of a microchannel follows the steepest pressure gradient. Trapping would therefore occur if the pressure difference between points A and B is bigger than that between points A and C or $\sigma>1$.

Computational fluid dynamics was applied to predict the flow velocities at the entrances of the microchannels and to identify σ for each channel. The simulated velocity field distribution for Designs 1 and 5 are shown in Figure 3.3A and Figure 3.3B. The simulation results clearly show that by varying the width of the outlet drain**,** the flow velocities at the entrances of the microchannels were changed. The predicted normalized flow velocities and the normalized trapping ratio (σ) for each microchannel are shown in Figure 3.4A and Figure 3.4B for all the selected Designs 1 to 6.

Among the six different designs proposed for the microfluidic network, Design 5 featured the smallest variations among flow velocities (20.9%) at the different channel entrances while the variations of flow velocities in microchannels for the other designs were between 64.7 to 79%. In terms of trapping ratio, Design 5 performed best since the maximum variation of the σ for the different channels in this design is less compared to the other designs. The value of σ indicates the capability of a channel to trap a pollen grain at its entrance. Therefore, the probability for each channel to trap a pollen grain at its entrance is similar for all the channels in Design 5, thus fulfilling one of the design criteria.

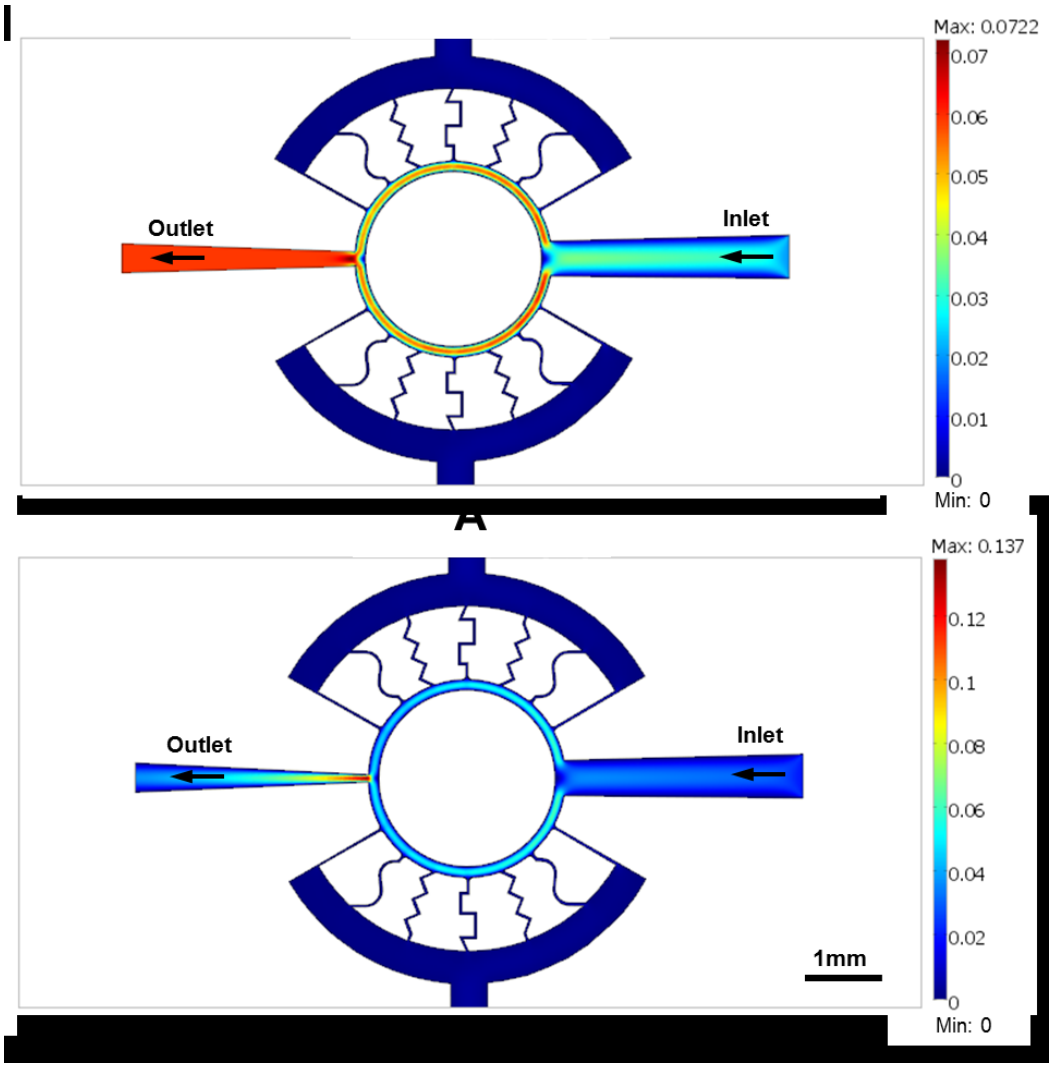


**Figure 3.3** Comparison of velocity field between (A) Design 1, (B) Design 5. The velocity gradient at the entrance of microchannels in Design 1 is much steeper than the gradient in Design 5. Color details flow velocity in m/s (Scale bar applies to both (A) and (B)).

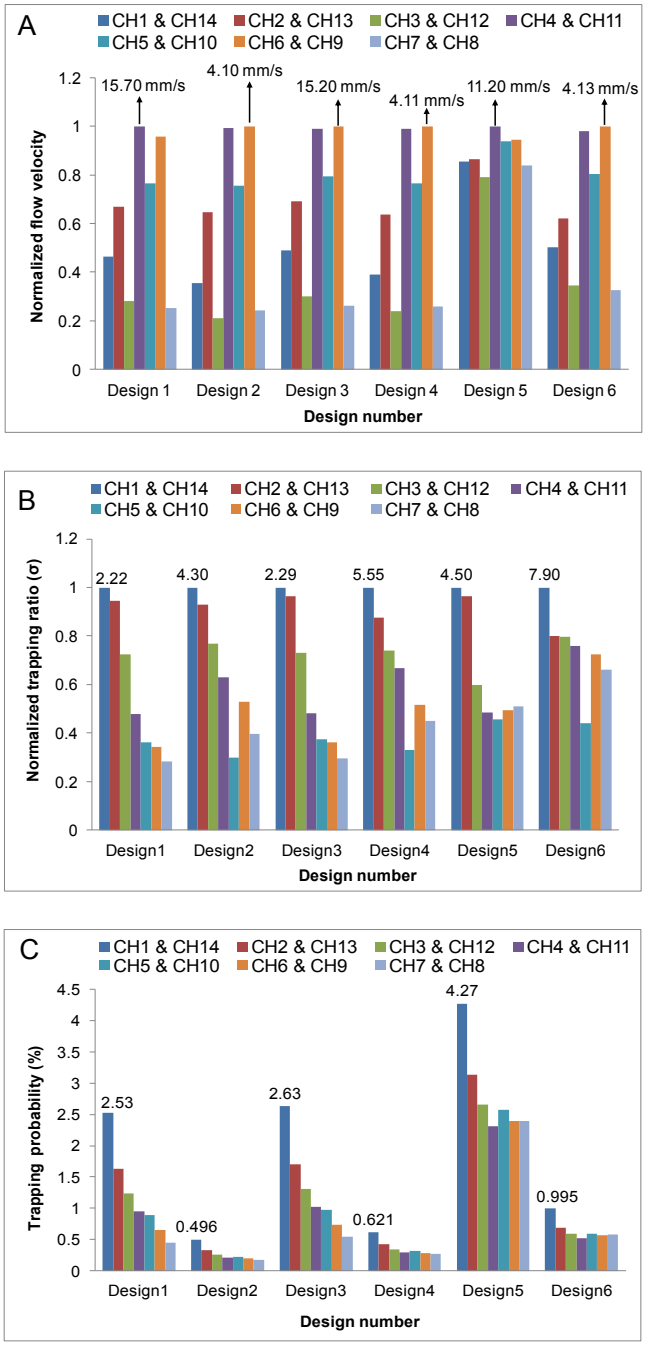


**Figure 3.4**The predicted (A) normalized entrance flow velocities (B) normalized trapping ratios (σ) (C) trapping probabilities for different channels of various designs. Data are normalized to the maximum flow velocity and maximum trapping ratio of each design in part A and B respectively. The maximum values of flow velocity, trapping ratio and trapping probability for each design are indicated numerically. Channel numbers are related to those shown in Figure 3.1A.

To corroborate these results, the trapping probability of the proposed designs was assessed in an alternative manner.Assuming uniform distribution of pollen grains across the distribution chamber width upon injection, the probability of trapping at each microchannel entrance was defined as the ratio of the fluid flow passing through the microchannel to the total fluid flow passing through the distribution chamber just before the microchannel as calculated by Eq. (3.2).

$$P_i = \frac{Q_i}{\frac{Q_T}{2} - \sum_{j=1}^{i-1} Q_j} \qquad 1 < i \leq 7 \qquad (3.2)$$

$$P_i = \frac{Q_i}{\frac{Q_T}{2}} \qquad i = 1$$

Where $P_i$ is the trapping probability for channel i, $Q_i$ and $Q_j$ are the flow rates at microchannel i and j, respectively, and $Q_T$ is the total flow rate entering the distribution chamber at (Section A-A) as shown in the schematic of the microfluidic network in Figure 3.2.

The numerical results for the trapping probabilities for different channels of various designs are estimated by Eq. 3.2 and presented in Figure 3.4C. They clearly show that the calculated probability values for the microchannels in Design 5 are higher as well as more uniform compared to the other designs. Both trapping probabilities and trapping ratio suggest that among the various options, this design will perform best in terms of trapping and uniformity of flow conditions. Therefore, Design 5 was chosen for experimental validation.

### 3.4.3 Experimental Performance of the Enhanced Design

In order to assess the performance of the improved design (Design 5), it was fabricated and tested by injecting a suspension of *Camellia* pollen grains using a syringe pump through the inlet with the velocity of 0.02 m/s. The results obtained from this experiment were compared with the results achieved with the preliminary design (Design 1). Contrary to the irregular distribution of pollen grains over the microchannel entrances in Design 1, each of the microchannels in Design 5 was occupied. Furthermore, all microchannel entrances were occupied by a single pollen grain only, and nowhere in the device did pollen grains accumulate and potentially alter fluid flow (Figure 3.5).

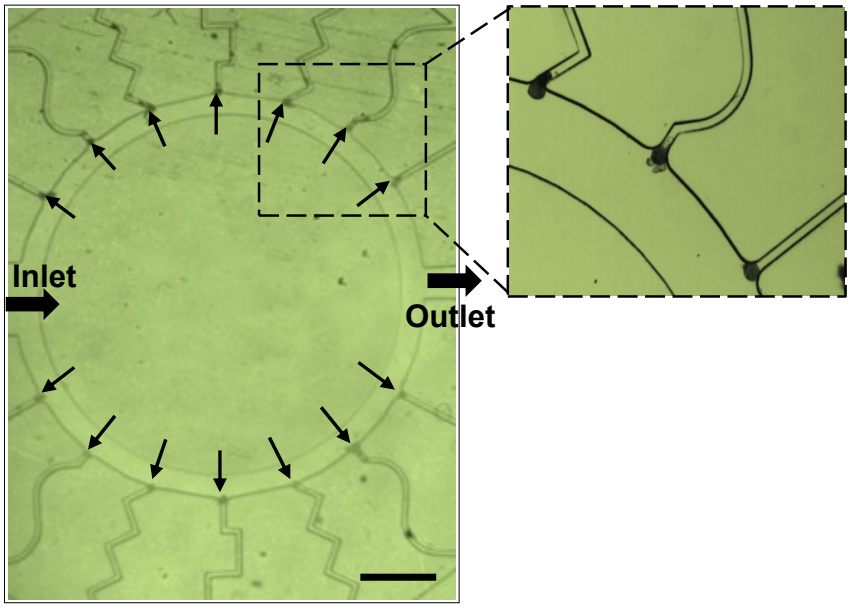


**Figure 3.5** Micrograph of the distribution chamber of Design 5 after injecting pollen suspension and magnified view of the pollen grains trapped at the entrance of the microchannels. A single pollen grain is seen trapped at each microchannel entrance. No accumulation of pollen grains was observed at the microchannel entrances or anywhere else in the distribution chamber. Scale bar= 500 μm.

### 3.4.4 Correlation of Trapping Probability with Trapping Time

Rather than relying only on the absence and presence of pollen grains at the microchannel entrances, the uniformity of trapping probabilities in the experimental situation was assessed using a more quantitative experimental approach. A microchannel with high trapping probability should trap a pollen grain within a shorter time interval after the beginning of injection compared to a microchannel with lower trapping probability. In order to validate and quantify the correlation of trapping probability with trapping time, Designs 5 and 1 were compared experimentally. Table 3.2 shows the experimental trapping times for all the microchannels in the two designs.

**Table 3.2** Experimental testing of trapping probabilities quantified by trapping time of individual microchannels.

| | | Experimental trapping time (s)[a] | | | | | | |
|---|---|---|---|---|---|---|---|---|
| Design | Test number | CH1 | CH2 | CH3 | CH4 | CH5 | CH6 | CH7 |
| Design 5 | Test 1 | 7 | 9 | 15 | 20 | 16 | 17 | 19 |
| | Test 2 | 4 | 7 | 14 | 17 | 12 | 19 | 18 |
| | Test 3 | 3 | 7 | 13 | 14 | 18 | 16 | 19 |
| Design 1 | Test 1 | 14 | 27 | 34 | 43 | 47 | 92 | - |
| | Test 2 | 16 | 33 | 37 | 48 | 44 | - | - |
| | Test 3 | 18 | 35 | 40 | 49 | 46 | 86 | - |

[a]The time indicates the duration from the start of the injection until a channel entrance is occupied by at least one pollen grain. Three runs were carried out for both Designs 1 and 5.

In Design 5, all of the microchannel entrances were occupied by at least one pollen grain after less than 20 s. On the other hand, in Design 1, the first channel was occupied by a pollen grain 14 s after starting the injection of pollen suspension and some microchannel entrances remained unoccupied even after injecting the total of 2 ml pollen suspension. Hence, as predicted, higher trapping probabilities of microchannels in Design 5 compared to the Design 1 correlate with shorter experimental trapping times of the microchannels in Design 5. Moreover, this confirms that the non-uniform distribution of trapping probability in Design 1 correlates with the non-uniform trapping times of its microchannels, whereas both parameters were uniform in Design 5. While injection of additional pollen grain suspension or a higher concentration of grains might remedy this situation in Design 1, this will also lead to the accumulation of pollen grains in the distribution chamber or microchannel entrances. The experimental results also showed that in Design 5, the time needed for the microchannels 1 and 2 to trap a pollen grain is less than the trapping time of the other microchannels which confirms the predictions made by the numerical analysis (Figures 3.4Band 3.4C). Moreover, channels 3 through 7, whose predicted trapping probabilities are very similar, were able to trap cells within a 6-second time period.

The trapping probabilities versus experimental trapping time for Design 1 and Design 5 are shown in Figure 3.6. For both tested Designs 1 and 5, the trapping probability is inversely related to the trapping time of pollen grain at the entrance of microchannels. This proves that the proposed numerical methods were able to properly predict the probability of pollen trapping for each design. In addition, regardless of the design type, the value of trapping probability was related to a defined range of trapping time. At the injection velocity used

here, the probability of 2.5% corresponded to a trapping time of approximately 12-18s. This applied to both, Designs 1 and 5.

### 3.4.5 Pollen Tube Growth Within the Microfluidic Chip

Results from the experiment show that the pollen tubes start to grow inside the microfluidic chip 30 minutes after the injection of pollen suspension and they can grow for more than three hours to reach a length of several millimeters. This confirms that the microfluidic device is conducive for pollen tube growth and that the behavior of the cells is similar to that observed in *in vitro* bulk assays (F. Bou Daher & A. Geitmann, 2011).

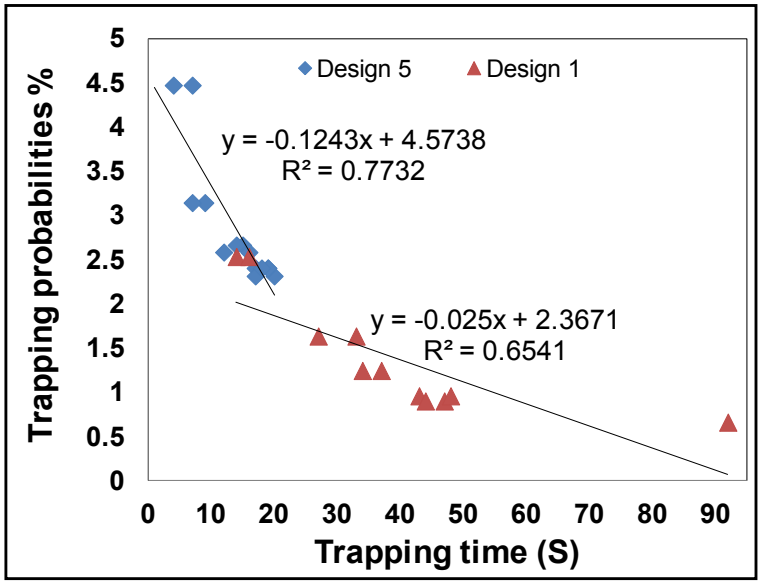


**Figure 3.6** Predicted trapping probabilities versus experimental trapping times for Design 5 and Design 1. The linear trend lines for both designs, equations of linear-fit lines and correlation coefficients (R) are also shown.

The extended length of the microchannels provides the possibility of integrating different kinds of micro sensors within the microchannels to measure various biological parameters of a single pollen tube which was not possible in conventional *in vitro* plate assay. For example, various microstructural features can be integrated at different locations of the microchannel to measure pollen tube invasive force or turgor pressure at different stages of its growth. Also, chemical and enzymatic reagents can be applied locally to individual pollen tubes to investigate their influence on pollen tube behavior.

The tests demonstrated that the pollen tubes follow the shape of the microchannels and are able to navigate simple and complex geometrical shapes (Figure 3.7A, Figure 3.7B and Figure 3.7C). It was observed that the tubes grow in straight lines as long as they do not encounter a mechanical obstacle. As soon as they hit the channel wall they change their growth direction to follow the direction imposed by the channel wall. Remarkably, they maintain this new direction dictated by channel even after exiting the channel, indicating that the pollen tube does not have an internal memory that forces it to return to its original growth direction. This behavior is very different from that of other tip growing cells such as root hairs and fungal hyphae (Tatiana N Bibikova, Angelica Zhigilei, & Simon Gilroy, 1997; K. Hanson, Filipponi, Lee, & Nicolau, 2005; K. L. Hanson, Nicolau, Filipponi, Wang, & Lee, 2006).

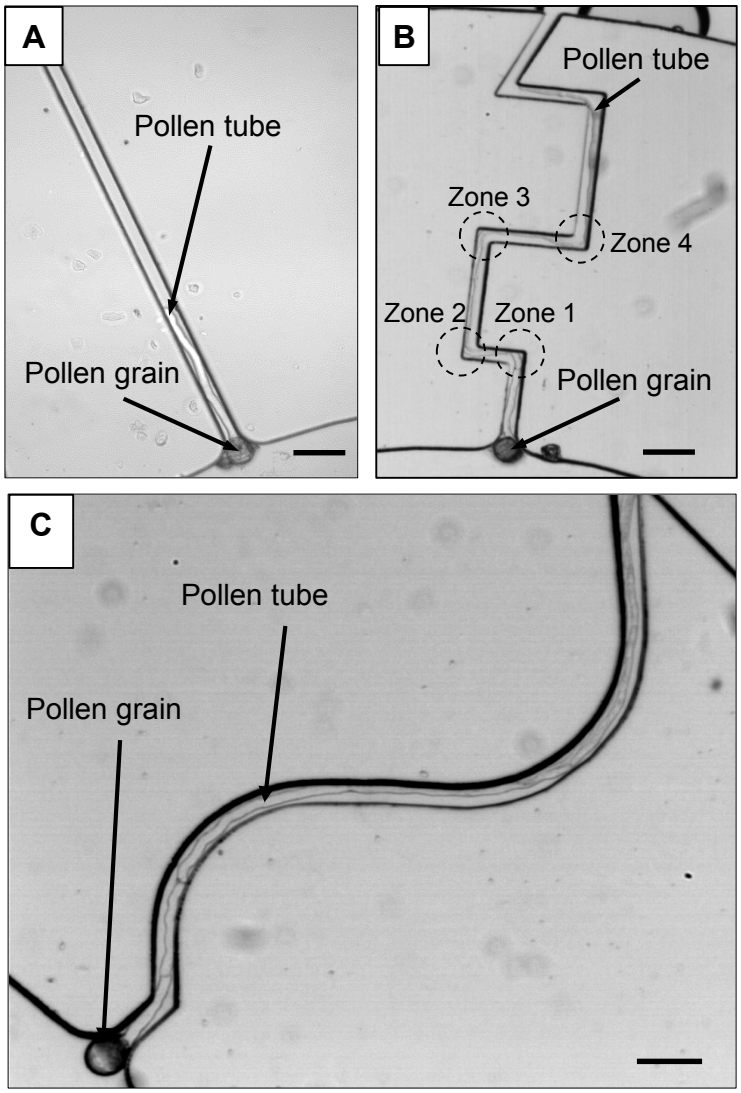


**Figure 3.7** Growth of pollen tubes through (A) straight microchannel (B) serpentine-shaped microchannel (C) curved microchannel. Scale bar =100 μm.

In order to measure the pollen tube growth rate within the microfluidic chip, time-lapse imaging was used. Figure 3.8 shows growth length versus time for pollen tubes growing inside straight, curved and serpentine-shaped microchannels. In the case of straight microchannel, Pollen tube was growing through the microchannel with the average growth rate of 14.4 μm/min which is consistent with the average growth rate reported for *Camellia*

pollen tubes in *in vitro* plate assays (about 12 µm/min) (F. Bou Daher & A. Geitmann, 2011).

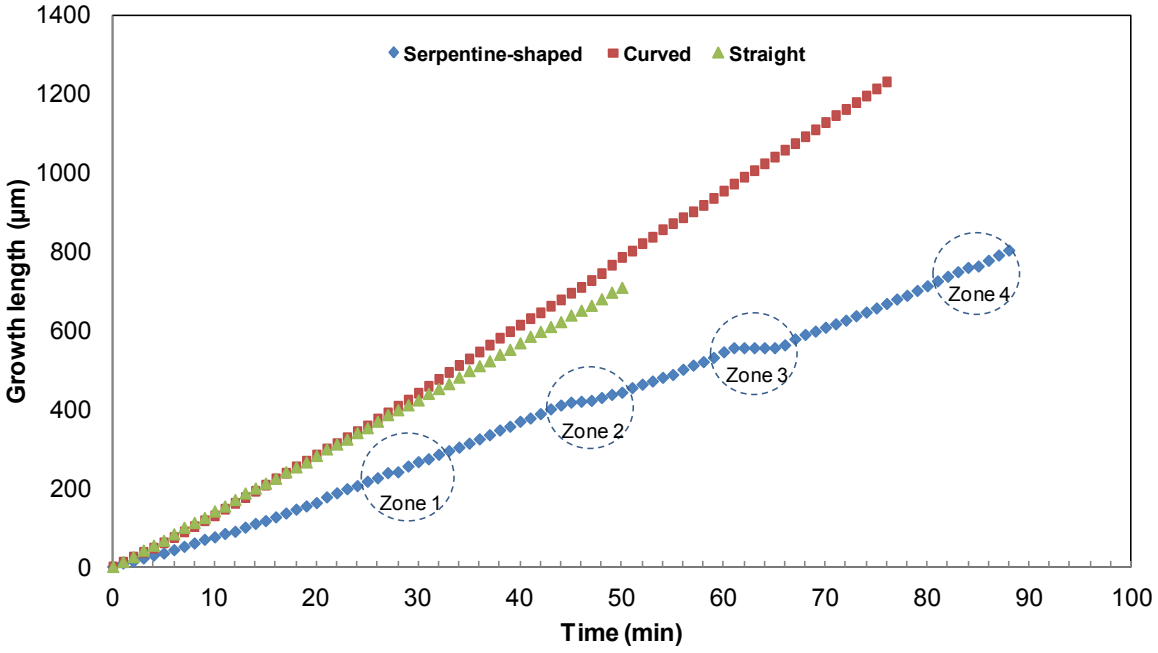


**Figure 3. 8** Pollen tube length versus time for a pollen tube growing inside straight, curved and serpentine-shaped microchannels. Zones 1 to 4 represent the locations at which the pollen tube encountered the microchannel wall and was forced to change its growth direction to follow the direction imposed by the channel wall.

The graph also illustrates that growth through the straight microchannel proceeds at very uniform average speed, and without significant increase or decrease over the measured distance (short term oscillations that typically occur in pollen tubes are neglected in the present assay as the temporal resolution was chosen to be lower than the typical period of oscillations). This is crucial as it shows that the precise location of any testing device to be included in future implementations is not critical in terms of *a priori* pollen tube behavior. For the curved microchnnel, the pollen tube shown here grew with the average growth rate of 16.2 µm/min and without substantial changes over the measured distances. On the other

hand, for the pollen tube growing through the serpentine-shaped microchannel, the average growth rate was 9.1 μm/min, and the growth rate changed considerably when the pollen tube encountered the microchannel wall and was forced to change its growth direction to follow the direction imposed by the channel wall (Figure 3.8). It is noted that depending on the collision angle between the pollen tube and the microchannel wall, the pollen tube growth rate decreased dramatically (82%, 68% and 66% decrease in Zones 1, 2, and 4 respectively) and could temporarily drop to zero (zone 3).

## 3.5 Summary and conclusion

A microfluidic device with an improved knot shaped distributor design is presented to enable single cell trapping of pollen grains at the entrances of the circularly arranged microchannels. Numerical and experimental testing were employed to compare different geometrical design features in terms of the trapping efficiency at the microchannel entrances, and regarding the uniformity of growth conditions within the serially arranged microchannels. Experimental validation proved the accuracy of the numerical predictions. The growth behavior of pollen tubes was characterized along different geometrical shapes of microchannels. The proposed microfluidic device can easily be modified to accommodate various experimental assays on pollen tubes and the concept of this method has a potential to be adapted for use with other tip growing cells such as fungal hyphae and filamentous yeast.

# Chapter 4

## Influence of Microenvironment Geometry on Cell Behavior

### 4.1 LOCto study the effect of the geometry of the microchannels on pollen tube growth

In future applications of the TipChip various types of sensor and micromechanical elements would be integrated within the microchannels which inevitably necessitate changing the dimensions of the microchannels which might influence the pollen tube growth. Therefore, it is essential to comprehensively investigate the effect of geometry of the microchannels on pollen tubes growth. In the present chapter we systematically addressed the potential concern of the effect of microfluidic network geometry on pollen tube growth. The content of this work is about to be submitted to the *Microfluidics and Nanofluidics* Journal.

**Abstract**

Understanding the effect of the geometry of the microenvironment on cells both in situ and in vitro is an important issue in the field of cell biology. Using microsystems technology, microchannels culture system with different geometries can be fabricated making possible studies of the effect of microchannel geometry on cell behavior. Here we present a microfluidic based Lab-on-a-chip platform to study the effect of the geometry of the microchannels on pollen tube growth. The device was fabricated using replica molding technique on Polydimethylsiloxane (PDMS) platform and comprises of a network of micro fluidic channels with varying widths and depths. We compare the growth rates of pollen tube, in traditional plate assays to those in microfluidic channels, and investigate the

relationship between microchannel geometry and cell growth rate. We observed that pollen tubes can grow inside the microchannels with comparable growth rates to those in traditional plate assay. Furthermore, it was observed that varying width did not significantly affect pollen tube growth rate, but varying depth did. In channels with varying width, the growth rate of *Camellia* pollen tubes remained very constant. On the other hand, an increase in microchannel depth from 80 μm to 160 μm, caused an increase of the pollen tube growth rate by up to 50%.Finite element analysis is exploited to model the effect of microfluidic geometry on the growth behavior of pollen tube and to validate the experimental results. The numerical analysis confirm that the increase of channel depth causes the increase of growth rate of pollen tube, but not in linear fashion.

## 4.2Introduction

Over the past decade, microfluidic cell culture systems have been increasingly used in cell biology research because of their unique advantages over conventional cell culture methods including low cost, low reagent consumption, reduced response time, enabling control local cellular microenvironment and performing parallel process (El-Ali, Sorger, & Jensen, 2006; Gross, Kartalov, Scherer, & Weiner, 2007; Meyvantsson & Beebe, 2008; Wu, Huang, & Lee, 2010). Moreover, the dimensions of structural components of microfluidic cell culture platforms match those of the cells, thus creating a more in vivo-like growth microenvironment (Prokop et al., 2004). In conventional cell cultures, cells are typically in contact with or physically near other cells, a situation that exposes them to the ions, proteins and other substances released by the adjacent cells. In contrast, microfluidic-based cell culture can provide, if desired, an autonomously controlled microenvironment

without the effect of neighboring cells. This elimination of superposing chemical gradients can be pivotal for the analysis of single cell behavior.

There are basic differences between microfluidic cell culture and conventional cell culture platforms. In order to efficiently use the potential of the microfluidic based cell culture platforms in the cell biology research, understanding the effect of the physical characteristics of these platforms on cell behavior is pivotal (Meyvantsson & Beebe, 2008; G. M. Walker, Zeringue, & Beebe, 2004; Young & Beebe, 2010). Accurate characterization of the microfluidic based cell cultures enables us to realize which macroscale assumptions are applicable when we are using micro-scale platforms.

Attempts have been made to understand the differences between behaviors of cells cultured in micro and macro scale culture platforms (Nikkhah, Strobl, & Agah, 2009; S Raty, Davis, Beebe, Rodriguez-Zas, & Wheeler, 2001; Stephanie Raty et al., 2004; G. Walker, Ozers, & Beebe, 2002). Raty et al. (S Raty et al., 2001) showed that the proliferation rate of mouse embryos cultured within microfluidic channels is faster than those cultured in a conventional culture system. By contrast, Walker et al. noted a reduced growth rate for Spodoptera frugiperda (Sf9) cells cultured inside PDMS based microfluidic channels (G. Walker et al., 2002) compared to conventional culture flasks. These significant discrepancies between results obtained for culture of different cells in micro and macro scale cell cultures, show the necessity of performing comprehensive studies to investigate the effect of the physical and geometrical properties of the microenvironment on cell behavior. Moreover, the knowledge obtained from these studies helps us to design effective and more reliable microfluidic cell cultures which more accurately mimic the in vivo cell microenvironment in vitro.

Among the physical characteristics of the cell culture environment, geometry of the microfluidic network is an important design parameter that has the potential to significantly affect cell behavior. Microfluidic cell cultures have therefore been developed to systematically assess the effect of microchannel geometry on cell behavior (Goyal & Nam, 2011; Mahoney, Chen, Tan, & Mark Saltzman, 2005; Nikkhah, Strobl, & Agah, 2007; Nikkhah et al., 2009; G. Walker et al., 2002; H. Yu, I. Meyvantsson, I. A. Shkel, & D. J. Beebe, 2005). The growth rate of HS68 normal human foreskin fibroblast cells was found to be reduced at increaseing microchamber depth (Nikkhah et al., 2007). Whereas channel width had no effect on the rate of insect cell proliferation (G. Walker et al., 2002). Fall armyworm ovarian cells (Sf9) grown under no flow condition experienced no changes to proliferation rate at altered microchannel width and length, but was increased with increasing microchannels height (Hongmei Yu et al., 2005). The authors speculate that the accumulation of the secreted factors within the limited space of the diffusion dominant microchannels under now flow conditions is the cause for the dimension dependence of cell proliferation rate.

PC12 cells were cultured in microfluidic channels fabricated using photolithographic technique to investigate the effect of microchannels width on neurite growth (Mahoney et al., 2005).The results showed that similar number of neurites were extended parallel to the channel walls from the PC12 cells in both narrow (20-30 μm) and wide channels (40-60 μm). However, only in wide microchannels neurites elongated in the direction perpendicular to the channel walls. Moreover, no statistically variations between the neurites length grown in microchannels with different widths were reported by the author.

Therefore, the results indicated that culturing PC12 cells within microfluidic channels with various widths affected the growth orientation of the neurites emerging from the cells.

Another group of researcher cultured hippocampal neurons from E-18 rat within varying dimensions microchannels to study the influence of microchannel geometry on neural maturation (Goyal & Nam, 2011). It was observed that neuron maturation in channels with smaller dimensions were faster than that of in bigger channels. However the authors indicated that there is an optimum size for the channel which if the dimensions are decreased more than that, the limited space of the microchannel cause accumulation of the cellular wastes and exhausted nutrients which reduces the neurons maturation rate.

In a previous study we showed that microfluidic based cell culture can be used as an alternative method to conventional in vitro bulk assays for pollen tube studies (C. Agudelo, Sanati, et al., 2012). We proved that pollen tubes can grow within microfluidic based platforms with comparable growth rate to that of in conventional plate assays. Recently we developed the TipChip a modular microfluidic based platform for studying individual pollen tubes (C. G. Agudelo et al., 2013). In the TipChip, pollen grains are trapped at the entrances of the microchannels and pollen tubes are guided to grow through individual microchannels whose sizes are slightly bigger than the diameter of the pollen tube. We modified the TipChip platform to achieve uniform distribution of pollen grains within the microfluidic platform and to have reproducible and identical growth conditions for all the trapped pollen grains (Ghanbari, Sanati, Agudelo, Packirisamy, & Geitmann, 2013). Modular design of the TipChip enabled us to use it for measuring Young's modulus of the pollen tube wall (Sanati Nezhad, Naghavi, Packirisamy, Bhat, & Geitmann, 2013b), and

for the quantification of penetrative force exerted by elongating pollen tubes (Sanati Nezhad, Naghavi, Packirisamy, Bhat, & Geitmann, 2013a).

In most of aforementioned applications of the TipChip, pollen tubes were surrounded by a limited amount of the culture medium within the microchannels. Therefore, they have access only to the limited amounts of nutrients and oxygen which may potentially have negative effects on pollen tube growth. However, in future applications of the TipChip different kinds of sensor and mechanical obstacles would be embedded within the microchannels which inevitably necessitate changing the dimensions of the microchannels which might influence the pollen tube growth.

For all these reasons, it is essential to comprehensively investigate the effect of geometry of the microchannels on pollen tubes growth. Here we systematically addressed the potential concern of the effect of microfluidic network geometry on pollen tube growth. Monitoring the growth rate of pollen tubes passing through the variously sized channel portions enabled us to assess the effect of changes in the widths and depths of the microchannel on the pollen tube growth profile.

## 4.3 Materials and methods

### 4.3.1 Microfluidic device fabrication

The PDMS was utilized for the fabrication of the microfluidic chip due to its high gas permeability, biocompatibility, low cost and ease of fabrication. Moreover, PDMS is transparent and allows optical access to the pollen tubes growing in the microchannels. The microfluidic chip consisted of two thick PDMS layers (~3mm), fabricated by replica molding technique (Xia & Whitesides, 1998). In the device employed to study the effect of

microchannel widths on pollen tube growth, only one of these layers included microfluidic channel features and the other one was utilized to create an enclosed microfluidic network. Whereas in the micro device utilized to study the effect of microchannel depth on pollen tube growth rate, both layers contained micro features. To fabricate the mold, standard photolithography process was utilized. Briefly, SU-8 2075 (MicroChem Corp., MA, USA)was spin coated onto a 4 inche silicon wafer, soft backed and exposed through a glass mask employing UV Double-sided Mask Aligner (Quintel Corp., CA). After post exposure bake and development, the positive pattern of the microfluidic network was obtained. Then, a mixture of curing agent and PDMS prepolymer (Sylgard 184, Dow Corning Corp., Midland, USA) at a weight ratio of 1:10 was cast against the SU-8/Silicone mold, degassed in the desiccator and cured for 4 hours at 60° C. The PDMS replica was then peeled off from the mold and the inlet and outlets were punched before bonding two PDMS layer using oxygen plasma treatment method (Harrick Plasma PDC-001).

### 4.3.2 Pollen Culture

*Camellia japonica* pollen was collected from a plant growing in Montreal Botanical Garden, preserved by dehydrating on silica gel for 2 h and stored at −20°C until use. Prior to each experiment, pollen was rehydrated in a humid chamber for at least 0.5 hour without direct contact with liquid water. Pollen grains were suspended in a liquid growth medium contained the following components: 2.54 mM of $Ca(NO_3)_2 \cdot 4H_2O$, 1.62 mM of $H_3BO_3$, 1 mM of $KNO_3$, 0.8 of mM $MgSO_4 \cdot 7H_2O$ and 8% sucrose (w/v). Once the pollen grains started to germinate, the pollen suspension was introduced into the microfluidic chip.

### 4.3.3 Observation and analysis

Observation of growing pollen tubes in microfluidic channels were carried out by an inverted microscope (Nikon TE2000) equipped with a CCD camera(Roper fx). ImagePro software (Media Cybernetics) and ImageJ 1.440 (National Institutes of Health, http://rsb.info.nih.gov/ij) softwares were used for data acquisition and analysis.

## 4.4 Results and Discussion

### 4.4.1 Design of microfluidic device

The presented microfluidic device was designed to enable manipulating and trapping of pollen grains suspended in a growth medium and to facilitate the investigation of the effect of microchannel geometry on pollen tube growth. There are different considerations for geometrical designing of the microfluidic network such as pollen grain and pollen tube size and architecture, growth rate, and compatibility with the type of desired microscopy method. The microfluidic network consists of an inlet, for injection of the pollen grains suspension, a main microfluidic chamber to give access to the growth microchannels, two sets of growth microchannels on the both sides of the main chamber and three outlets to evacuate liquid growth medium from the main chamber and from the ends of the microchannels (Figure 4.1).

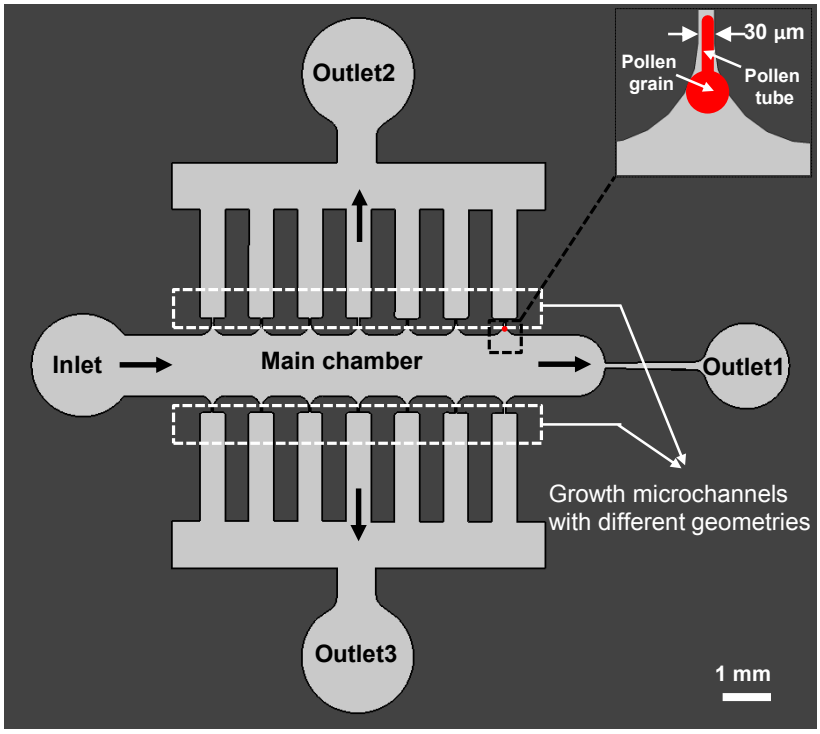


**Figure 4.1**Schematic showing the overall design of the microfluidic network and magnified view of a pollen grain trapped at the entrance of a growth microchannel. To promote trapping of pollen grains, the entrance of the growth microchannel is designed as a curved notch. Two identical sets of growth microchannels with different geometries were incorporated on the both sides (top and bottom) of the main chamber for redundancy.

Outlet 1 is large enough to also evacuate any excess pollen grains from the main chamber. To study the effect of geometry of the microchannels on pollen growth behavior, pollen grains are supposed to be trapped at the entrances of the growth microchannels through which the pollen tubes are guided to elongate (inset of Figure 4.1). Outlets 2 and 3 enable positioning of the pollen grains at the entrances of the growth microchannels using medium flow. Four different geometries for the growth microchannel were considered, 1) a microchannel with four different widths (W1 to W4) and constant depth (D) over the total

length (Figure 4.2A), 2) a microchannel with constant width (W) and depth (D) over the total length (Figure 4.2B) 3) a microchannel with constant width (W) but two different depths (D1 and D2) (Figure 4.2C) 4) a microchannel with varying width (W1 to W3) and depth (D1 and D2) (Figure 4.2D). It should be mentioned that a microchannel with constant dimensions serves as reference to ensure that possible changes in pollen tube growth rate are not related to various stages of pollen tube maturation (Figure 4.2B).

Considering the range of 50-60 μm for the diameter of *Camellia japonica* pollen grains, the height of the main microfluidic chamber was set to be 80 μm to allow the grains to be transported freely by the medium fluid flow within the microfludic network. In order to trap pollen grains at the entrance of the growth microchannels and facilitate the growth of pollen tube along the growth microchannels, the width of channel was set to be 30 μm, smaller than the diameter of pollen grains and larger than the diameter of the tube (which is in the range of 13-20 μm). To promote trapping of pollen grains, the entrances of the growth microchannels are designed as a curved notch (inset of Figure 4.1).

### 4.4.2 Effect of microchannel width on pollen tube growth rate

In order to investigate the influence of the microchannel width on pollen tube growth rate, four different microchannel widths (75, 200, 400 and 540 μm) were tested while keeping depth constant (80 μm) (Figure 4.). Parallel growth microchannels with constant width and depth (75 μm and 80 μm respectively) over the length of 450 μm were designed and fabricated as a reference to ascertain that temporal variations in pollen tube growth rate are not as a result of different stages of pollen tube maturation (see close-up inFigure 4.3).

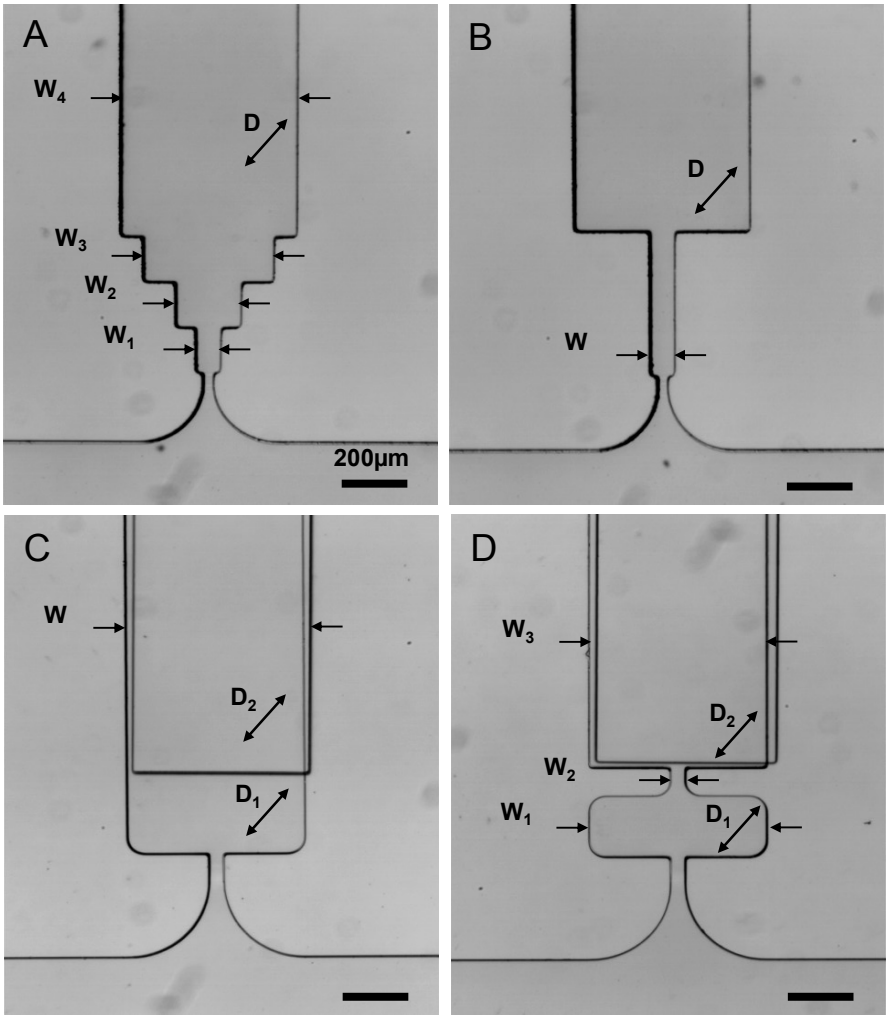


**Figure 4.2** (A) Micrograph of a microchannel with four different widths ($W_1$ to $W_4$) and constant depth (D) over the total length. (B) Micrograph of a microchannel with constant width (W) and depth (D) over the total length. (C) Micrograph of a microchannel with constant width (W) but two different depths ($D_1$ and $D_2$) over the total length. (D) Micrograph of a microchannel with varying width ($W_1$ to $W_3$) and depth ($D_1$ and $D_2$).

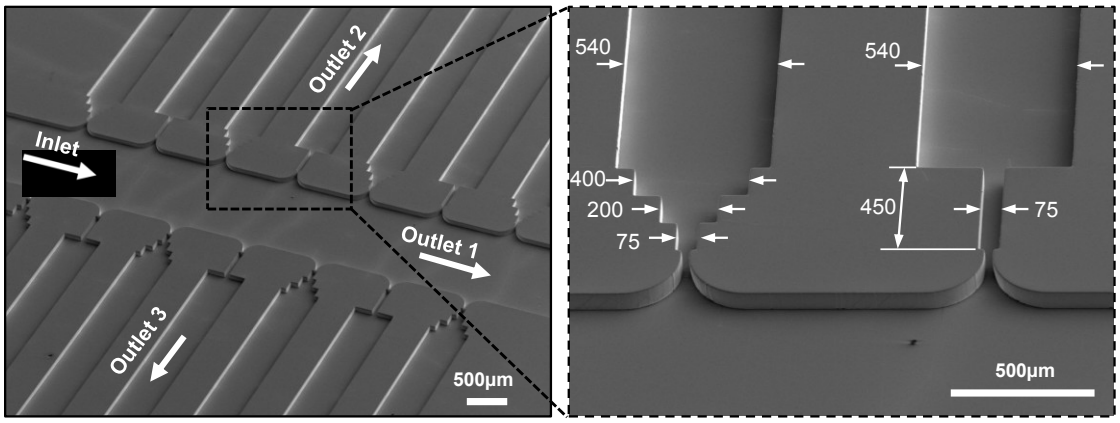


**Figure 4.3** Scanning electron micrograph of the microfluidic networks before bonding and close-up view of the microchannels. Parallel growth microchannel with constant width and depth (75 µm and 80 µm, respectively) over the length of 450 µm used as a reference to ascertain that possible changes in pollen tube growth rate are not as a result of different stages of pollen tube maturation. All numbers are dimensions in micrometers.

Then, the device was tested by injecting a suspension of *Camellia* pollen grains through the inlet using a syringe pump. The schematic diagram and photograph of the experimental setup are shown in Figure 4.4.Pollen grains were transported by medium fluid flow through the main chamber and trapped at the entrances of the growth microchannels. The injection velocity to ensure stable positioning of pollen grains at the entrances of the growth microchannels while preventing bursting of pollen grains was found to be about 0.01 m/s ( Sanati Nezhad, Ghanbari, Agudelo, Naghavi, et al., 2013). Since we wanted to study the effect of microchannel geometry on pollen tube growth rate under no flow conditions, once the pollen grains were trapped at the microchannel entrances, the injection of medium flow was stopped. Figure 4.5Aand Figure 4.5B show pollen tubes growing inside microchannels with varying and constant width respectively. In order to measure the pollen tube growth

rate within the microchannel with different geometries, the growth behavior of individual tubes (n=3) was monitored using time-lapse imaging. The results for sample pollen tubes are illustrated in Figure 4.6A and Figure 4.6B.

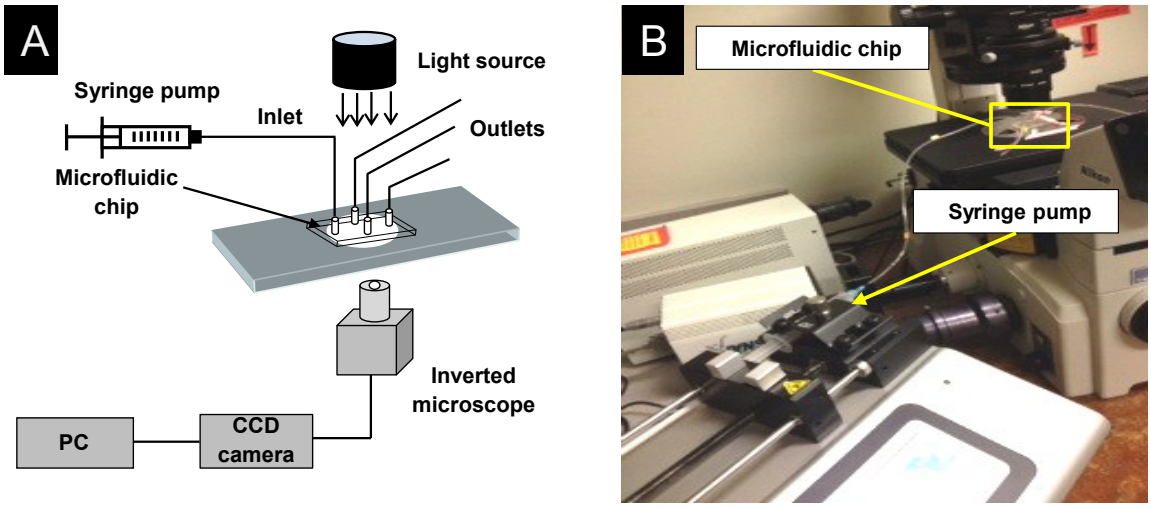


**Figure 4.4**The schematic diagram (A) and photograph (B) of the experimental setup.

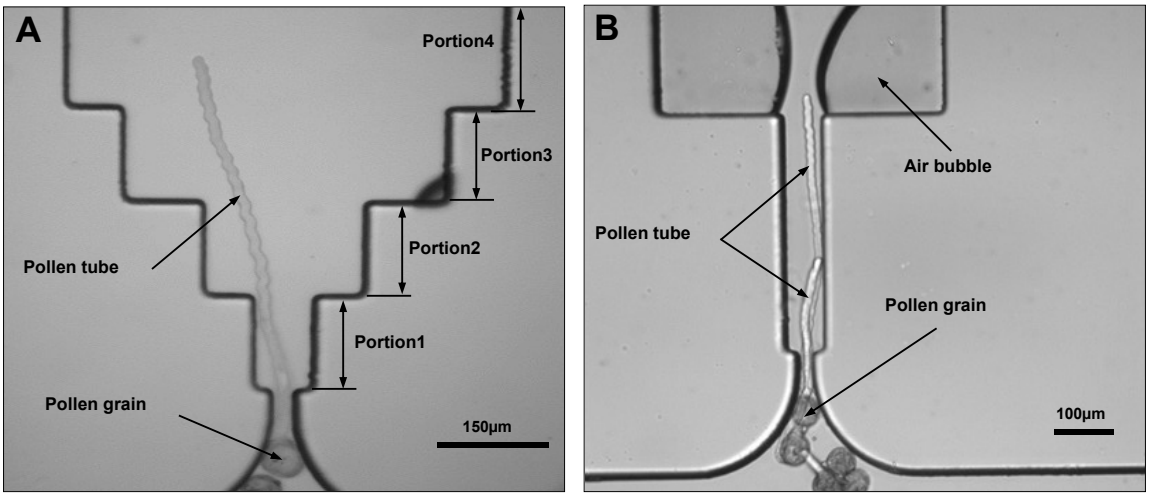

**Figure 4.5** (A) Micrograph showing a pollen tube growing inside the different portions of a microchannel with varying width. (B) Micrograph showing pollen tubes growing inside a microchannel with constant width and depth.

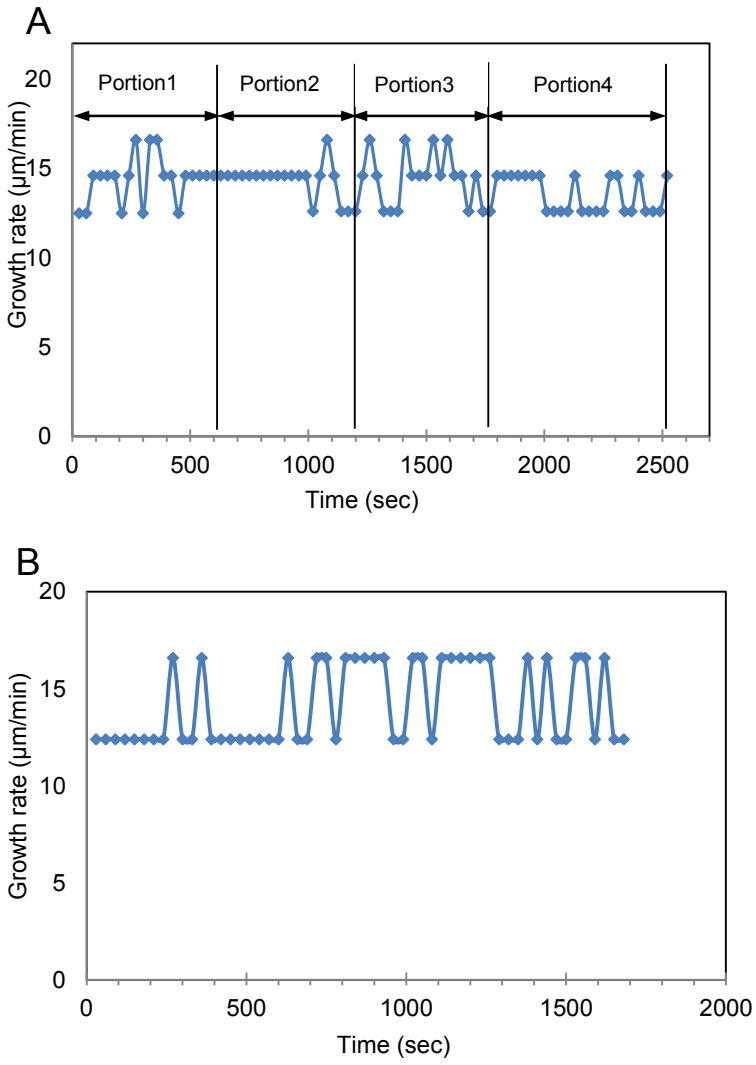


**Figure 4.6** (A) Pollen tube growth rate vs. time graph for a pollen tube growing inside a microchannel with varying width. (B) Pollen tube growth rate vs. time graph for a pollen tube growing inside a microchannel with constant width and depth.

These results clearly show that pollen tube grew inside the channel having constant width and depth at growth rate approximately 12 to 16 µm/min with temporal variation of ±2

μm/min vs. the average growth rate of the tube (14 μm/min). This growth rate is consistent with the average growth rate reported in the literature for *Camellia* pollen tubes in conventional *in vitro* plate assays (about 12 μm/min) (Firas Bou Daher & Anja Geitmann, 2011). In the case of microchannel with varying widths, changing the width from 75 μm to 540 μm in different parts of the microchannels did not cause any significant changes in pollen tube growth rate. Therefore, pollen tube growth rate is not sensitive to changes in microchannel width which is consistent with results obtained so far for insect cells using microchannel culture systems (Hongmei Yu et al., 2005).

### 4.4.3 Effect of microchannel depth on pollen tube growth rate

To study the effect of microchannel depth on pollen tube growth behavior, two different depths (80 and 160 μm) at constant width of 540 μm were tested (Figure 4.7A). The growth rate of pollen tubes growing inside the channel were monitored using time-lapse imaging (Figure 4.7B). The results clearly show that the initial growth rate at a depth 80 μm was 10 μm/min and it increased significantly to an average of 15 μm/min once the pollen tube entered the deeper portion of the channel (160 μm). This 50% increase in the average growth rate shows that pollen tubes are more sensitive to depth than those in-plane.

### 4.4.4 Combined effect of microchannel width and depth

In order to investigate the effect of both width and depth of the microchannel when combined, the overall design shown inFigure 4.8 and Figure 4.2D is employed. Portion 1 of the microchannel has a width of 540 μm and depth of 80 μm (close-up inFigure 4.8). In

Portion 2, the width is decreased to 40 um while keeping the same depth as in Portion 1. In Portion 3, both width and depth of the microchannels are increased to 540 μm and 160 μm, respectively. Monitoring the growth rate of pollen tubes passing different portions of the microchannel (Figure 4.9) confirmed the earlier results. When pollen tube transitions from the Portion 1 to Portion 2, no significant change in pollen tube growth rate was observed. On the other hand, an increase in microchannel depth from 80 μm to 160 μm upon transition to Portion 3, caused an increase of the pollen tube growth rate by up to 50% (Figure 4.10).We assume that this variation might be related to influence of heat generated from the microscope light on diffusion flux of ions into the pollen tube happening in the z-direction.

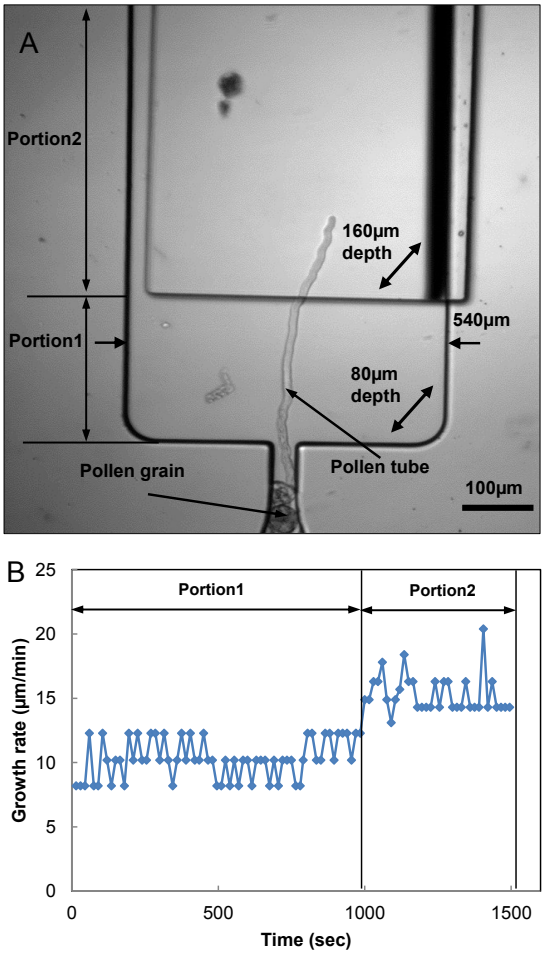


**Figure 4.7** (A) Micrograph showing a pollen tube growing inside a microchannel with two different depths (80 and 160 µm) and constant width of 540 µm over the total length. (B) Pollen tube growth rate vs. time graph for a pollen tube growing inside a microchannel two different depths and constant width.

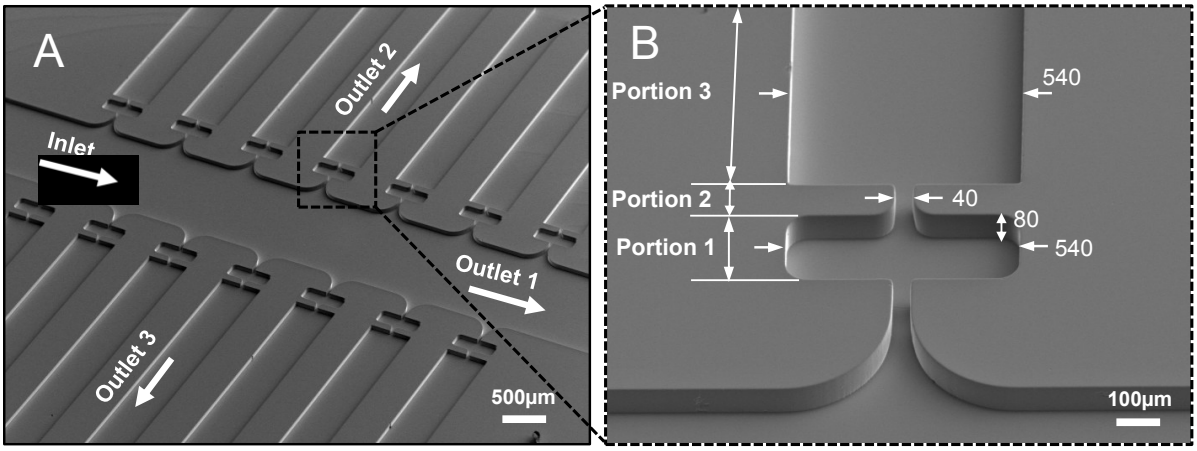


**Figure 4.8**(A) Scanning electron micrograph of the device used to study the effect of changing width and depth on pollen tube growth rate in the same chip and (B) close-up view of the microchannels. All numbers are dimensions in micrometers.

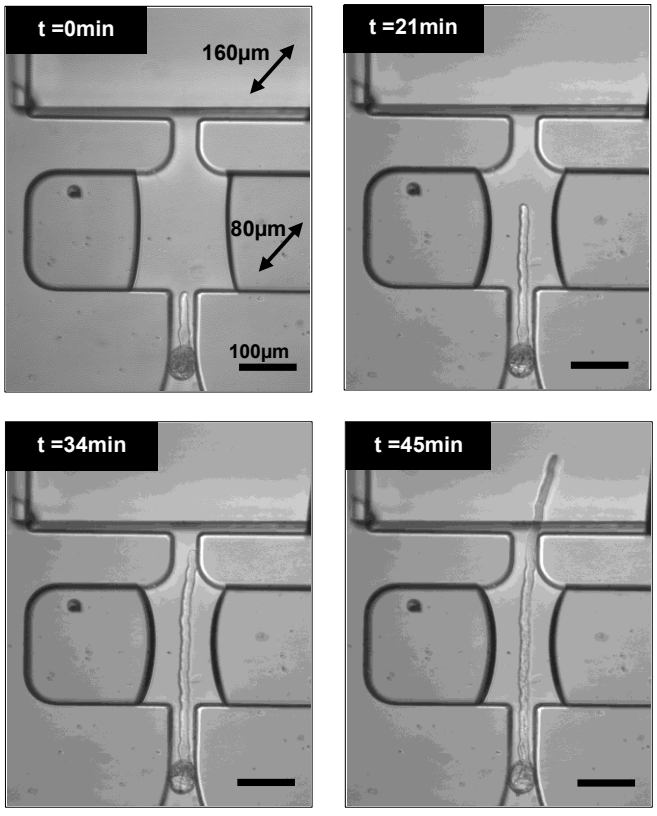

**Figure 4.9**Time lapse images of the pollen tube traversing the variously sized channel portions.

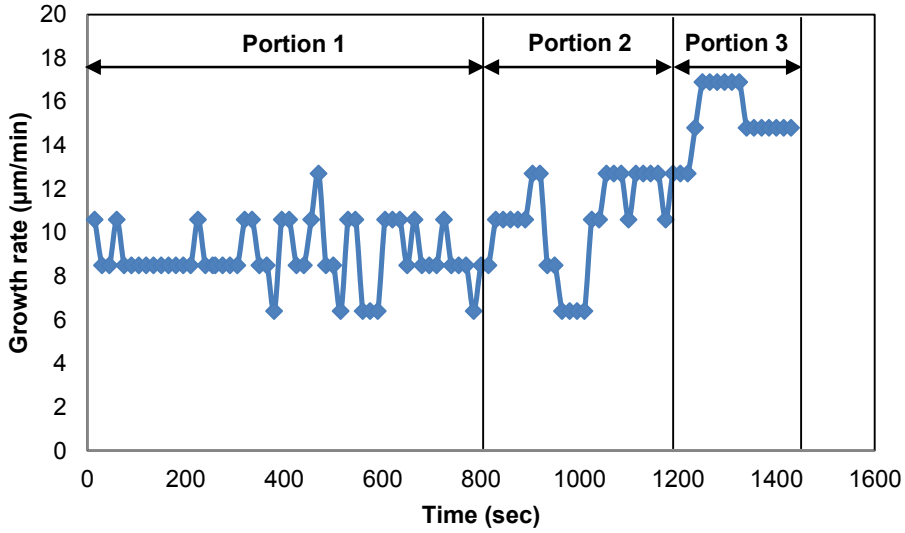


**Figure 4.10**Pollen tube growth rate vs. time graph for a pollen tube growing inside a microchannel with varying width and depth.

## 4.5 Numerical analysis: The effect of channel depth on growth rate

In order to find out how the heat generated from the microscope light influences the endocytosis and consequently the growth rate of pollen tube at different channel depth, numerical analysis is employed to model the diffusion flux of ions into the pollen tube. The comparison of ion flux into the tube when it grows at different channel depths will be able to show the effect of channel depth and the light source on pollen tube growth.

A 2D model is employed with the same dimensions as the fabricated microdevice. The model consists of a cross section of microchannel including a rectangular channel with a circlewith diameter D = 16 μminside as the cross section of pollen tube. In the first design (Design A, Figure 4.11A) the depth of microchannel is 160 μm while in the second design (Design B, Figure 4.11B), the channel has the depth of 80 μm. However in both designs,

the width of microchannel is equal to 540 μm. The centerline of pollen tube in both designs is located 40 μm above the bottom surface of the microchannel which is consistent with the location of pollen tube in the experimental testsas the pollen tube tend to be closer to the bottom surface. In this condition, the center-line of pollen tube is 120 μm away from the top surface in first design, while in the second design, this distance is 40 μm (Figure 4.11).The presented model is good enough to qualitatively compare the effect of heat generated from the microscope light on diffusion flux of ions into the pollen tube growing in microchannels with different designs. However, for quantitative studies, the model needs to be elaborated further.

To assess the effect of channel depth on the concentration gradient and diffusion flux into the pollen tube in presence of microscopic light energy, COMSOL Multiphysics3.5software isapplied to numerically solve the governing heat transfer equation and convection–diffusion transport equation. The heat transfer equation in 2D is given in Equation 4.1.

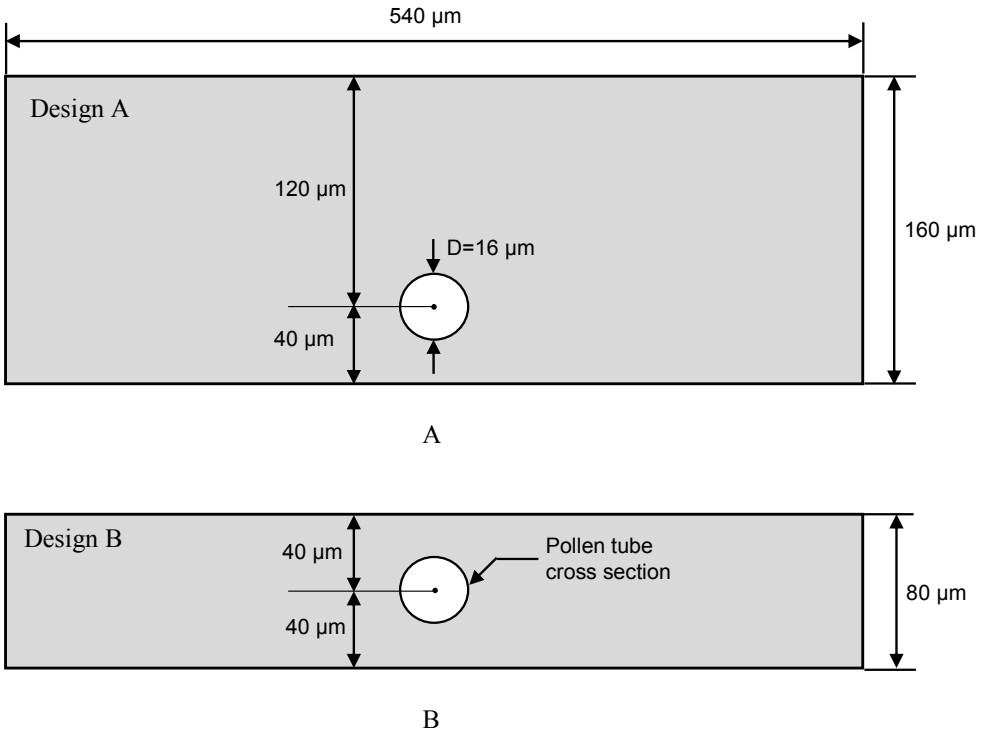


**Figure 4.11** The schematic of the design for use in numerical analysis, A) Design A: the channel depth=160 µm, channel width=540 µm, b) Design B: the channel depth=80 µm, channel width=540 µm.

$$\rho C_p \frac{\partial T}{\partial t} + \nabla . (-k \nabla T) = Q \quad (4.1)$$

where ρ is the density, $C_p$ is the specific heat capacity, T denotes the temperature, k is the thermal conductivity tensor, and Q is the heat source. The medium is chosen as water, hence the thermal conductivity is 0.58 (W/m.k), density is 1000 kg/m$^3$and the specific heat capacity is 4200 J/kg.k. Figure 4.12 shows the boundary conditions chosen to solve the governing heat transfer equation and convection–diffusion transport equation.

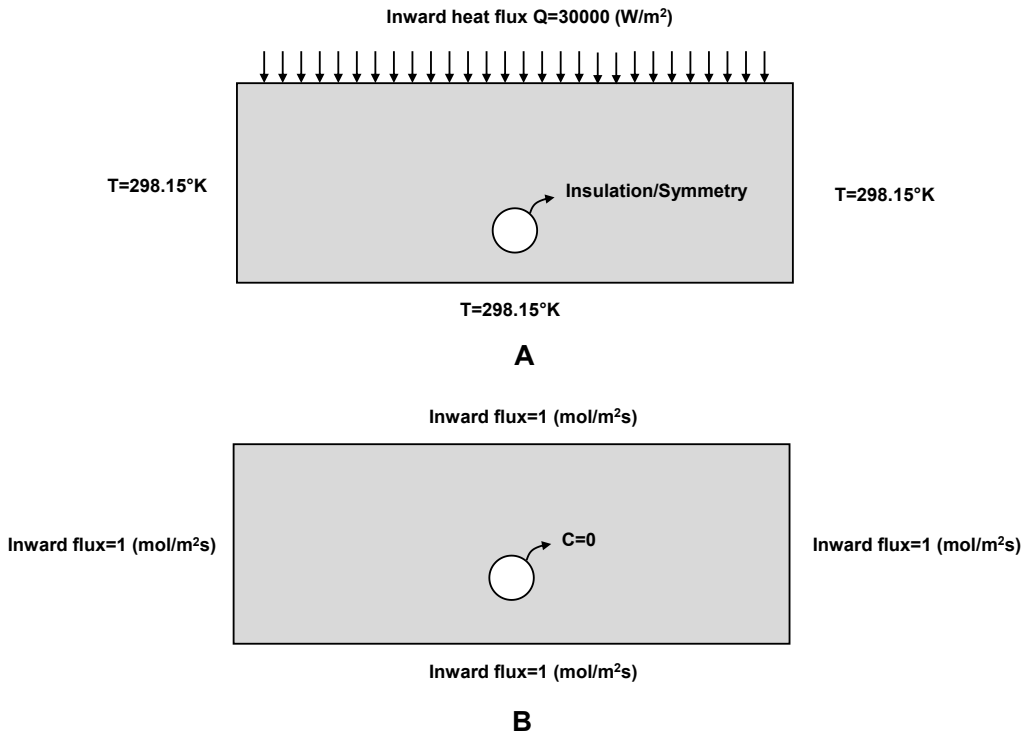


**Figure 4.12**The boundary conditions chosen in COMSOL Multiphysicsto solve (A) heat transfer equation (B) convection–diffusion transport equation.

The ambient temperature is chosen for the microchannel sides as well as the bottom surface of channel (T= 298.15°K). The influence of light source is modeled as a heat source on the top surface of microchannel as Q. To simplify analysis of the presented model, it is assumed that all the microscope light is absorbed by the effective top surface of the liquid inside the microchannel and converted to heat. Knowing the power of 12W for 12V light source on the top surface of microchannel, the inward heat flux of 30000 $W/m^2$

is defined for the top surface over effective top surface (4 $cm^2$). The heat transfer system is assumed to be steady state as shown in Equation 4.2.

$$\frac{\partial T}{\partial t} = 0 \qquad (4.2)$$

The results of temperature distribution predicted on microchannel cross section exposed to heat source at the top surface of the channel is shown in Figure 4.13 for both Designs A and B. The results shows that the light source over effective exposed surface can create temperature increase of about 7.5°C in Design A and 4.3°Cin Design B.

Once the temperature distribution is established, the convection–diffusion transport equation is solved to assess the diffusive flux into the cell. The convection–diffusion transport equation is shown as following (F. Wang et al., 2008).

W

$$\frac{\partial C}{\partial t} + (u.\nabla).C = D\nabla^2 C \qquad (4\text{-}3)$$

h

ere u is the velocity vector, and C and D are the concentration and diffusivity of the reagent within the medium. The system is assumed to be steady state as $\frac{\partial C}{\partial t}$=0.

Within a narrow temperature range from 10 to 20°C, the temperature dependence of the diffusion coefficient in a liquid is assumed to be linear and defined as Equation 4.4(Hirschfelder, Curtiss, & Bird, 1954; Sherwood, Pigford, & Wilke, 1975).

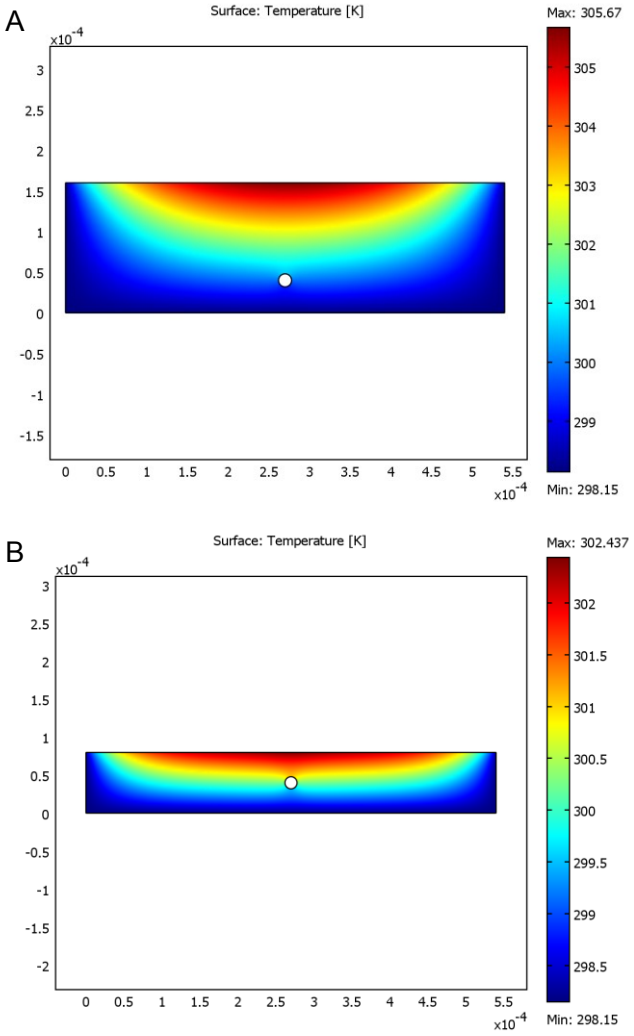

**Figure 4.13** The temperature distribution around pollen tube when it is exposed to light source of microscope, for A) Design A, B) Design B.

$$D = D_{298}[1 + \alpha(T - 298)] \quad (4.4)$$

Where $D_{298}$is the diffusion coefficient at T = 298°K, $\alpha = 20{\eta_{298}}^{1/2}\rho^{-1/3}$; $\eta_{298}$, the solvent viscosity at T = 298°K, Ns/m; ρ, the solvent density, g/cm$^3$. As the boundary condition for convection–diffusion transport equation, the pollen tube is considered as isolated environment which regulates its ion flux using semi-permeable membrane. Hence, a stable concentration is assumed for pollen tube boundary (assume C=0). In other words, due to the difference of osmotic pressure between inside and outside of pollen tube, the liquid tends to enter the cell to balance the osmotic pressure. The liquid carries the ions into the cells which is modeled as ion diffusion into the cells. Since the medium and ions enter the pollen tube, the medium at the channel walls is refreshed with new medium existing in the microchannel and the microfluidic network. Hence, the boundary condition of inward liquid flux is assumed on the microchannel walls to satisfy the convection-diffusion equation.

The results of concentration gradient at the cross section of microchannel for Design B is seen in Figure 4.14. As shown in Figure 4.14A, when the inward heat flux is zero, the concentration gradient is symmetric around the pollen tube. But, in presence of heat flux imposed at the top surface of microchannel (Figure 4.14B), the concentration gradient is

not symmetric in vertical direction with respect to the pollen tube centerline which has higher diffusivity in regions with higher temperature.

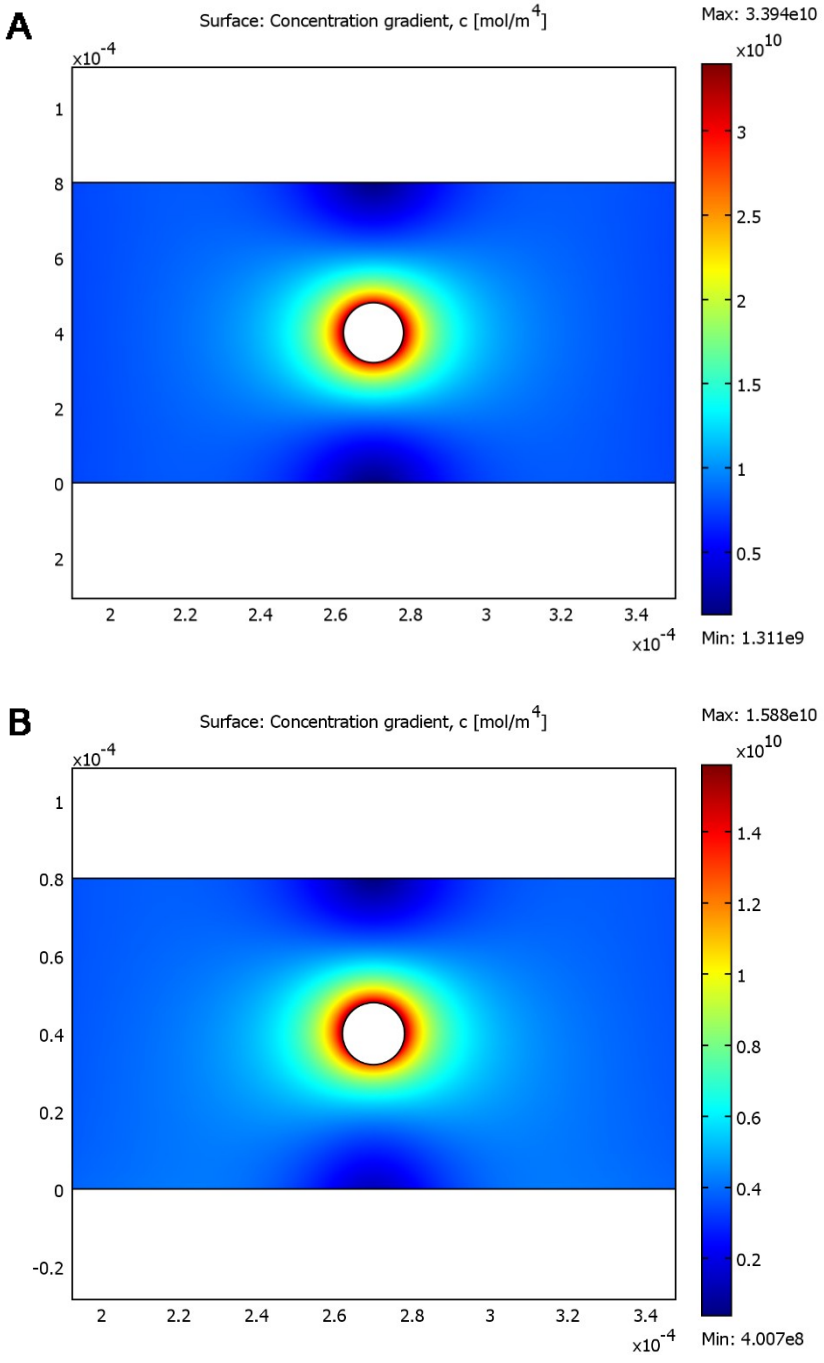

**Figure 4.14** The concentration gradient on channel cross section for Design B in (A) absence and(B)presense of heat flux

The diffusive flux is then defined as shown in Equation 4.5.

$$F = D(T)\frac{\partial C}{\partial y} \tag{4.5}$$

Where D is the diffusion coefficient and F is the diffusion influx (mol/kg.s). When there is no heat influx at the top surface (Q=0 in Equation 4.1), D is constant all over the cross section area and the diffusive flux is proportional to the concentration gradient (Equation 4.5). However in presence of heat influx at the top surface, diffusion coefficient is calculated from equation 4.3 and is dependent on the temperature distribution. It means that the diffusive flux (F) is not linearly proportional to gradient concentration asboth diffusion coefficient (D(T)) and gradient concentration can alter the diffusive flux (Equation 4.5). Figure 4.15 shows the distribution of diffusive flux in absence and presence of heat source (Q) for Design B. While the flux is symmetric in Figure 4.15A similar to Figure 4.14A, the comparison of Figure4.14B and Figure 4.15B shows how the diffusive flux is influenced from both gradient concentration and diffusion coefficient. In other words, the effect of temperature-dependent diffusion coefficient on variation of diffusive flux around pollen tube is depicted in Figure 4.15Bin comparison with results in Figure 4.14B.

For the design with 160 μm channel depth (Design A) in absence of heat source, the parameters of concentration gradient and diffusive flux over channel cross section are seen

in Figure 4.16. Since the pollen tube is not suspended at the center of microchannel in Design A, these two parameters are not symmetric in vertical direction respect to the pollen tube centerline. Correspondingly, in presence of heat source, similar asymmetric condition is seen in Figure 4.17, however the diffusive flux around pollen tube in Figure 4.17B is more than the flux in Figure 4.16B.

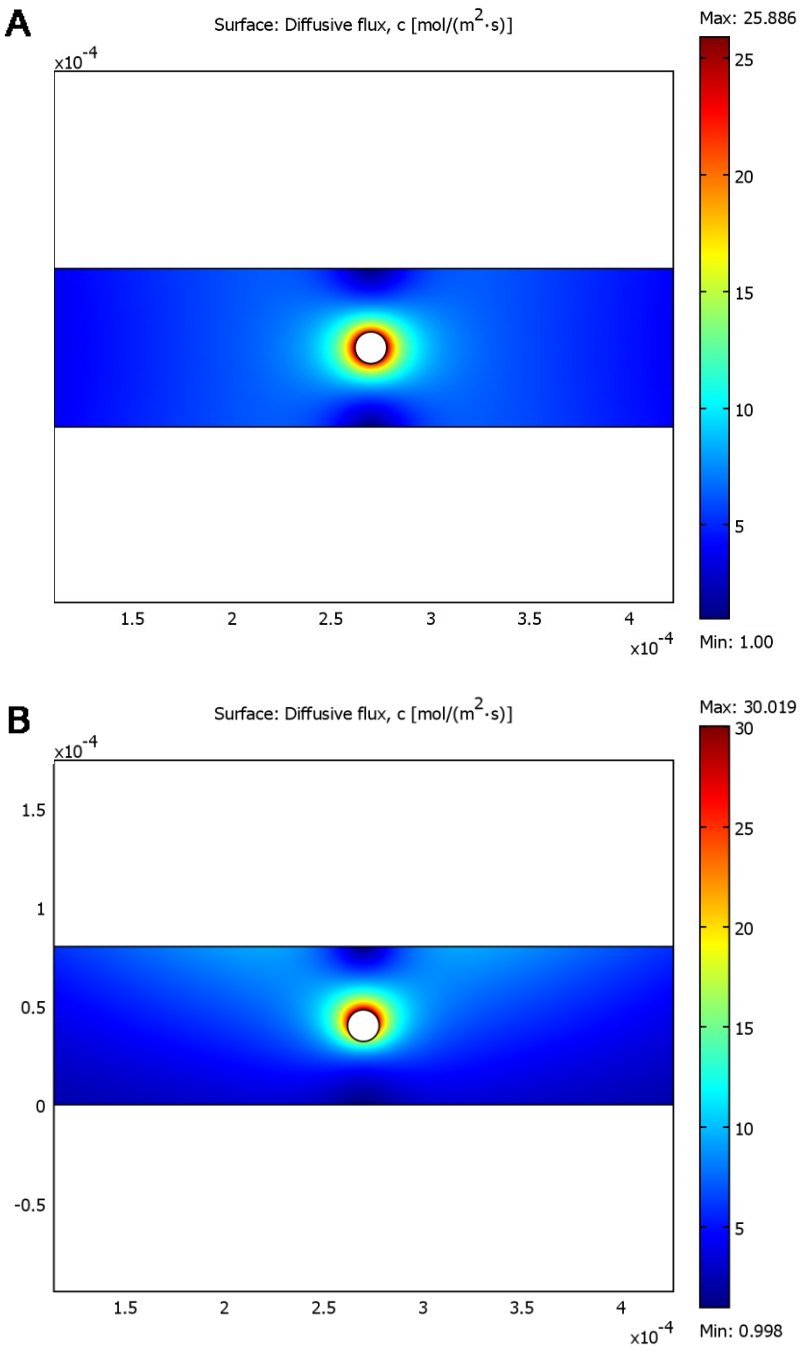


**Figure 4.15** The distribution of diffusive flux in (A) absence and (B) presence of heat source (Q) for Design B.

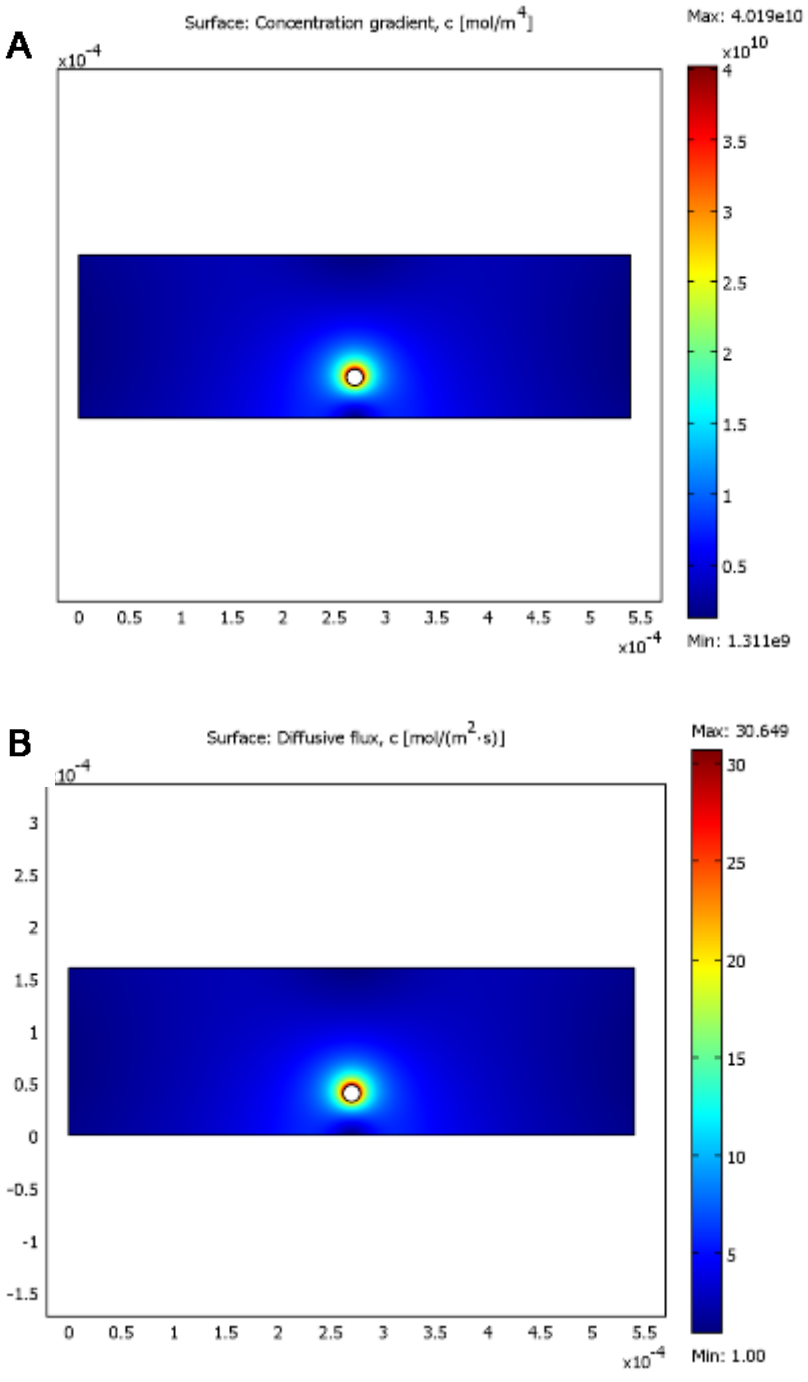


**Figure 4.16**(A) concentration gradient and (B) diffusive flux on channel cross section for Design Ain absence of light source

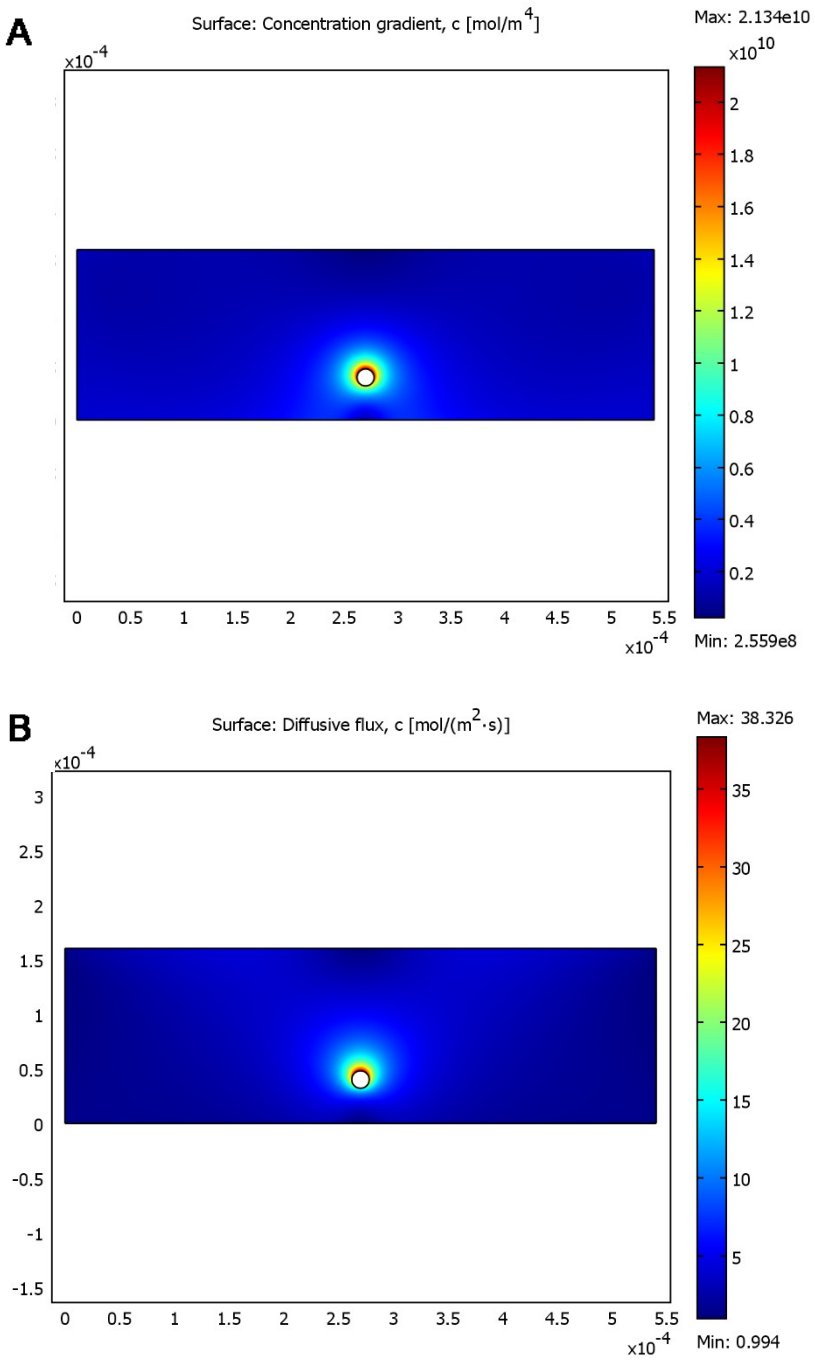


**Figure 4.17**(A) concentration gradient and (B) diffusive flux on channel cross section for Design A in presence of light source

Since we are not able to experimentally record the growth of pollen tube in absence of light source, we can only compare the experimental results from variation of growth rate at different channel depths with the corresponding theoretical data in presence of light source. Hence, the theoretical results in absence of light source are only reported as the control experiments showing the effect of temperature dependent diffusivity.

We integrate the diffusive flux from Figure 4.17B and Figure 4.15B over the pollen tube surrounding circumferential in order to calculate the overall normal diffusive flux ($F_T$) into the cell(Figure 4.18). The results are shown in Table 4.1.

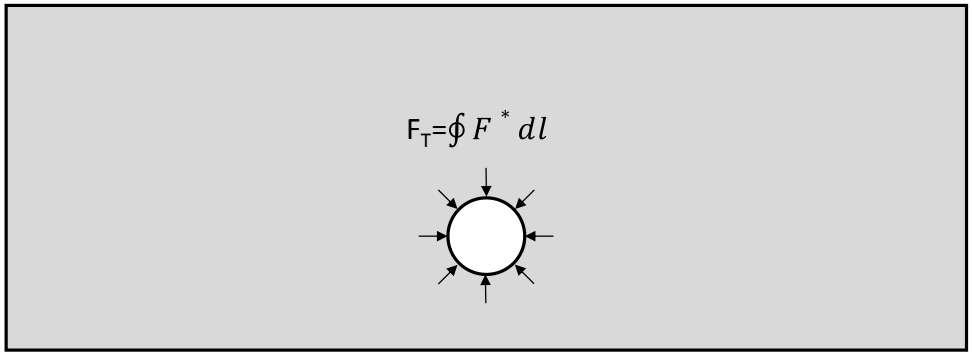


* F is normal diffusive flux per unit length.

**Figure 4.18**Diffusion of ions into the pollen tube

Table 4.1 The amounts of overall normal diffusive fluxes into the cell under heating from top.

| Design | $F_T$(mol/m.s) |
|---|---|
| A | 0.0014 |
| B | 0.0012 |

The results showed that the total normal diffusive flux in Design B is 0.0012 mol/m.s and for Design A is 0.0014 mol/m.s. This represents 16% increase on the flux into the cells. Since the regulatory mechanism of the growth for pollen tube is a complex process and is not linearly related to the influx, we cannot expect identical rate of rise on growth rate, however we can at least conclude that this ion influx has been interpreted as positive signal by the regulatory mechanism of the growth to increase the growth rate by 50% in Design A compared to Design B.

## 4.6 Conclusion and Summary

We present a microfluidic based lab-on-a-chip platform to study the effect of geometry of in vitro microenvironment on pollen tube growth behavior. We found that changing the width of the microchannel does not have a significant effect on the average pollen tube growth rate. On the other hand, a two-fold increase of the microchannel depth caused a more than 50% increase in pollen tube growth rate. In future applications of microfluidics device for pollen tubes studies, different microsensors might be embedded along the microchannel length which will necessitate changing in the width of the microchannels. Therefore, this fact that varying the width of the microchannels has minor or no effects on pollen tube growth under 'no flow' conditions is crucial for all further application of microfluidics devices for pollen tube studies. Otherwise, it will be difficult to draw conclusion from the experiments done using microfluidic devices. The numerical analysis was exploited to model the effect of microfluidic geometry on the growth of pollen tube. Using Comsol Multiphysics 3.5, the heat transfer and diffusion equations were solved for different geometries of microfluidic network to find out how the depth of growth

microchannel can influence the growth rate of pollen tube. The numerical results showed the rise of 16% in the diffusive flux of ions into the pollen tube when the depth of microchannel changes from 80 μm to 160 μm. This is consistent with the experimental results which is the increase of growth rate by raise of microchannel depth. Due to nonlinear dependence of growth rate to the diffusive flux, the rate of increase in the growth rate obtained from experimental data is not proportional to the rate of increase in diffusive flux, but the results of numerical analysis on the geometrical influence of microfluidic network shows the potential of this method toward a more accurate modeling of the pollen tube growth in microfluidic environment.

Our findings are novel in terms of pollen biology, and we believe understanding the effect of geometry of growth microenvironment on pollen tube growth profile will empower researchers to design more effective and reliable in vitro growth environment models for pollen tube analysis.

# Chapter 5

## PDMS microcantilever-based flow sensor integration for lab-on-a-chip

### 5.1 Development of horizontal PDMS microcantilever for flow sensing application

A high aspect ratio PDMS microcantilever is promising since it may provide sensors with higher sensitivity and improved linear response for LOC applications. Therefore, in the present chapter a novel and practical method for the fabrication of a horizontal high aspect ratio PDMS microcantilever integrated into a microfluidic device is developed and the cantilever is employed as a flow meter. The content of this chapter has been published in *IEEE Sensors Journal, Vol. 13, NO. 2, 2012 with* my contribution as the second author. In the results section, only my contribution to this work is presented.

**Abstract**

In this chapter, a simple practical method is presented to fabricate a high aspect ratio horizontal PDMS microcantilever-based flow sensor integrated into a microfluidic device. Multilayer soft lithography process is developed to fabricate thin PDMS layer involving the PDMS microcantilever and the microfluidics network. A three layer fabrication technique is explored for the integration of micro flow meter. The upper and lower PDMS layers are bonded to the thin layer to release the microcantilever for free deflection. The dynamic range of flow rates detectable using the flow sensor is assessed by experimental

method. Limited by the accuracy of the 1.76 μm resolution of the image acquisition method, the present setup allows for flow rates as low as 35 μl/min to be detected. This is equal to 0.8 μN resolution in equivalent force at the tip. This flow meter can be integrated into any type of microfluidic-based Lab-on-a-chip in which flow measurement is crucial such as flow cytometry and particle separation applications.

## 5.2Introduction

Application of microfluidic technology on lab-on-a-chip for biological and chemical processes has tremendous potential. Chemical analysis, mixing, bio-sensing, and particle separation are just a few examples of these applications. Among those, particle sorting/separation (Cho, Chen, Tsai, Godin, & Lo, 2010) and cytometry (Chandrasekaran & Packirisamy, 2009) are extremely sensitive to the flow rate within the microfluidic network. Therefore, flow meters integrated within a lab-on-a-chip to enable real time monitoring of the flow rate significantly improve the functionality of such a device.

Various flow meters have been reported in the literature by employing micro-electro-mechanical systems (MEMS) to miniaturize the flow sensor and to integrate it within the microfluidic device in order to monitor locally the flow rate (Dijkstra et al., 2007; Y.-H. Wang, Lee, & Chiang, 2007). Although these flow sensors have impressive performance, they usually involve complex fabrication including multi-step layer patterning which requires expensive facilities (Hossain, Packirisamy, & Rakheja, 2010; Quist, Chand, Ramachandran, Cohen, & Lal, 2006). Silicon or SU8 have mostly been used as a micro-mechanical element in the form of a microcantilever to sense the flow drag force. Since these materials have high elastic modulus, the deflection of the mechanical element is too

small and has to be detected by employing advanced detection methods such as optical or electrical (Balaban et al., 2001; Lien & Vollmer, 2007). Integration of optical or electrical components and their calibration is often elaborate and hence limits the application of these sensors for general lab. In addition, living cells are sensitive to electrical fields and the use of electrical detection methods has the potential to cause artifacts that make the interpretation of studies difficult (Kuoni, Holzherr, Boillat, & de Rooij, 2003). Similarly, thermal flow sensors have the potential to change the medium temperature (Ashauer et al., 1999; Rasmussen, Mavriplis, Zaghloul, Mikulchenko, & Mayaram, 2001; Terao, Akutsu, & Tanaka, 2007) and are therefore equally unsuitable for certain applications despite their simple readout system.

Besides conventional materials such as silicon or SU8(I. Lin et al., 2008), Polydimethylsiloxane (PDMS) is a favorable alternative material due to its low elasticity modulus (ranging between 0.5 MPa to 2 MPa depending upon the ratio of curing agent)(Lötters, Olthuis, Veltink, & Bergveld, 1997). It simplifies the detection system by measuring the deflection of the microcantilever's tip using vision based optical microscopy due to its large deflection in the range of few micrometers(Greminger & Nelson, 2004). Other PDMS attributes such as good biocompatibility, optical transparency, low chemical reactivity and non-toxicity in a microfluidic environment are also important factors in cell analysis(Pinto et al., 2010). The fabrication of a PDMS chip is also cost effective, making it suitable for disposable uses in biological applications.

Few vertical PDMS microcantilevers have been presented in the literature to measure the force within microfluidic devices. Sasoglu et al. (Sasoglu, Bohl, & Layton, 2007)used vertical PDMS microbeams to sense micro-scale cell forces. Liu et al. (X. Liu, Kim,

Zhang, & Sun, 2009) employed a visual algorithm for tracking the PDMS beam displacements to measure forces in the range of a few nanoNewton. Tan et al.(J. L. Tan et al., 2003)applied pillar structures while visually inspecting their deflection. Since fabrication limits the length of vertical cantilevers, they typically have a low aspect ratio which limits the range of forces that can be measured accurately. A high aspect ratio PDMS microcantilever is promising since it may provide flow meters with higher sensitivity and improved linear response for LOC applications.

In order to deduce flow drag force from microcantilever deflection, it is necessary to know the mechanical stiffness of the beam. Several experiments have been carried out to measure the Young's modulus of PDMS for bulk and thin PDMS layers. Depending upon the cantilever length, the small deflection beam theory for beam aspect ratios greater than 10 (Y. Zhang, Lo, Taylor, & Yang, 2006) or large deflection beam theory (Timoshenko & Gere, 1972) have been used to determine beam stiffness. In addition, the Mooney–Rivlin (MR) constitutive model (T. K. Kim, Kim, & Jeong, 2011), the hyperelastic model (Nunes, 2011) and finite element analysis have been used in order to consider the nonlinear properties of PDMS (Xiang & LaVan, 2007).

In this chapter, a high aspect ratio PDMS micro-cantilever-based flow sensor is presented. The micro-cantilever is integrated into a microfluidic device and fabricated using multilayer soft lithography. The microcantilever and the microchannels network are embedded into a thin PDMS layer. The flow sensor is made of PDMS material identical to the material of the microfluidic network in order to avoid any difficulties in bonding non-similar multi-layers. A three layer fabrication technique is used for the integration of the micro flow sensor. A thin middle layer is sandwiched between two other PDMS layers in

order to release the microcantilever and to seal the microfluidic device. The performance of the flow sensor is tested by introducing various flow rates into the microfluidic device and measuring the deflection of the cantilever's tip using an optical microscope. The elasticity modulus of the cantilever is measured using a precision balance method developed in house to measure the sensitivity of the microcantilever to the flow drag force. Based on the elastic modulus of the cantilever and the deflection, the drag force applied on the cantilever is determined.

Due to the high aspect ratio of the cantilever (>10), the calibration of the cantilever is simple and the effect of shear force on the deflection can be ignored. In addition, since the cantilever deflection is in the range of few micrometers, it can be measured effectively using vision based optical microscopy and it does not require advanced detection methods such as AFM or integrated optical or electrical systems. In spite of the off-line measuring method, the proposed flow sensor can be integrated into any kind of microfluidic-based LOC to accurately measure the local flow rate. As the sensor does not introduce any potentially disturbing signal, it is particularly useful for applications in which external electrical or thermal signals at the point of care should be avoided.

## 5.3 Sensor design

The proposed flow sensor can be integrated with LOC in two different ways to measure the flow rate such as monolithic integration and hybrid integration. For microfluidic-based LOC devices fabricated by multilayer PDMS fabrication technique such as multilayer micromixers, the flow sensor can be monolithically integrated into the design as shown in

Figure 5.1a. If the desired LOC is not a multilayer PDMS device, the flow sensor can be hybrid integrated as a stand-alone unit as shown in Figure 5.1b.

The 3D schematic of the flow sensor is shown in Figure 5.2a. The flow enters the device through the inlet, faces the microcantilever and then exits towards the outlet. Since the microcantilever is free, the flow induces the loading to the microcantilever and deflects it. The flow induced loading causes the cantilever's deflection (Figure 5.2b). The high aspect ratio PDMS microcantilever is suspended within the microfluidic device and is sandwiched between the bottom and top thick PDMS layers (Figure 5.2c). As the microcantilever deflects within the horizontal plane, the deflection is readily detected using vision based optical microscopy.

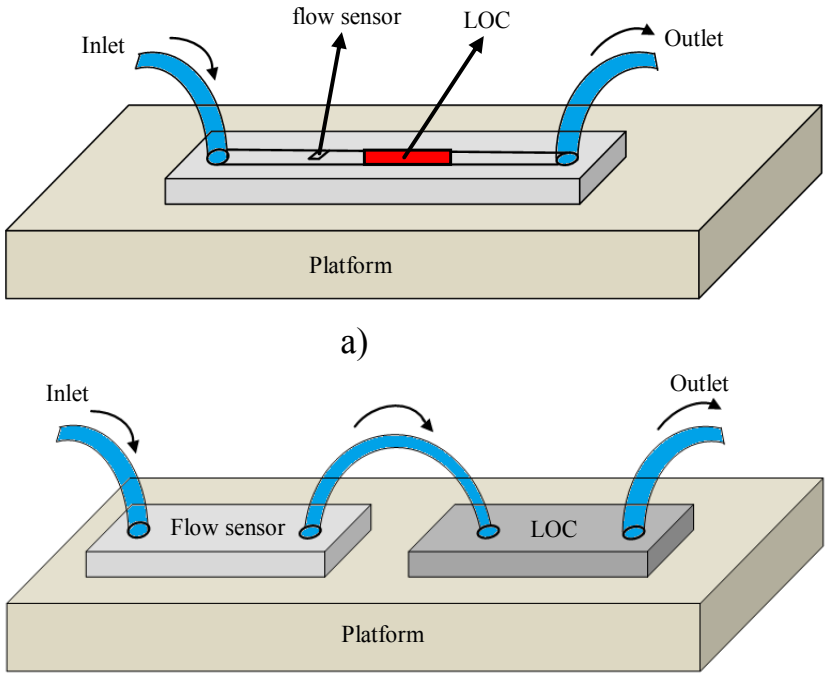


**Figure 5.1** Two different setups for integrating the flow sensor in a LOC device. (a) monolithic integration (b) hybrid integration

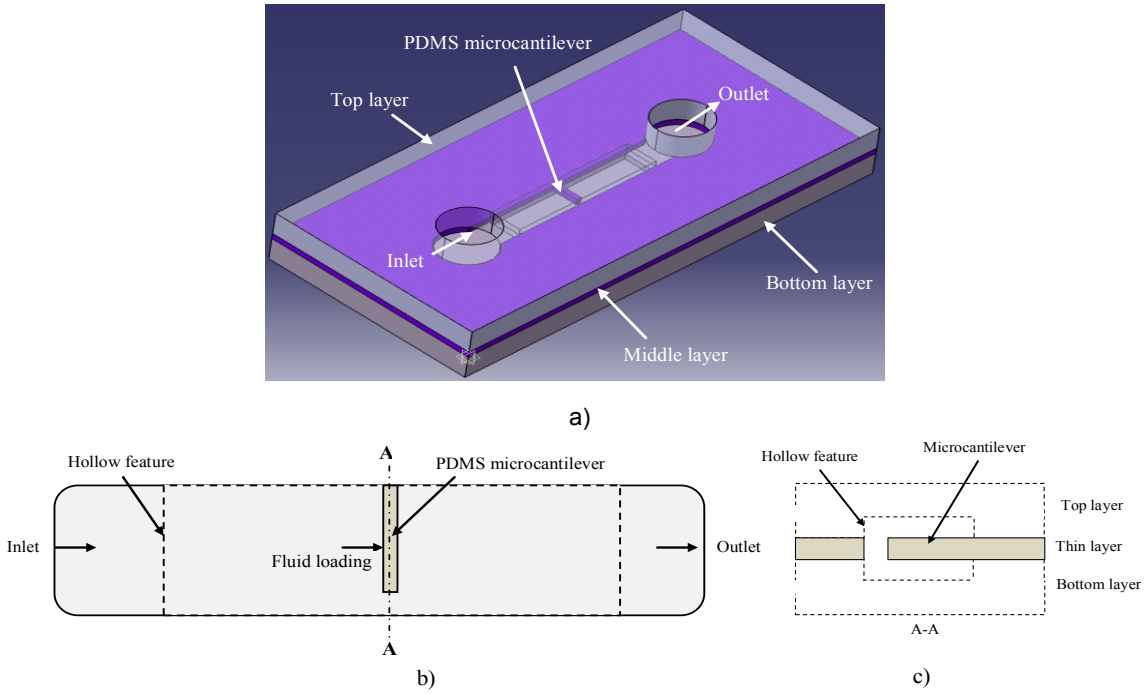


**Figure 5.2** Schematic of the PDMS microcantilever-based flow sensor a) 3D schematic of the design, b) top view, c) Cross section

## 5.4Fabrication of integrated PDMS microcantilever within a microchannel

The fabrication process of the integrated PDMS microcantilever within the microfluidic network is detailed in Figure 5.3. A 4-inch silicon wafer is cleaned with acetone and DI water, the surface is blow-dried with pure nitrogen, followed by baking for 5 min at 200°C to dehydrate the surface (Figure 5.3a). A SU8 mold is made using a standard photolithographic technique. The negative photoresist SU8 (MicroChem Corp.) is spin coated at 1500 rpm for 1 min to reach the thickness of 80 µm (Figure 5.3b). The SU-8 is next soft-baked for 3 min at 65 ºC and for 7 min at 95ºC in a hotplate. The resist is then cooled down at room temperature and exposed to UV light for 30s using a photo mask (Figure 5.3c). Post-exposure bake step (PEB) is then carried out, baking the resist for 3 min

at 65 ºC and for 6 min at 95 ºC in order to cross-link the SU-8. The SU-8 layer is then developed to obtain the SU8 mold (Figure 5.3d).

In order to employ flexible microstructures for bio-sensing, a multi-layer technique is developed. The microfluidic device involves a middle thin layer and two more top and bottom PDMS layers sealing the middle layer. The thickness of the middle layer is critical as it determines the thickness and hence the stiffness of the microcantilever. To fabricate the thin middle layer, a mixture of PDMS prepolymer (Sylgard 184 Dow Corning) with a curing agent at a volume ratio of 10:1 is poured into the silanized SU8 mold and placed in a vacuum chamber for degasification. A plastic sheet is then carefully placed on the PDMS to avoid introducing any bubble underneath. It is then loaded with a clamp to remove the extra PDMS (Figure 5.3e). By applying pressure, the plastic film comes into physical contact with the mold features and the PDMS is removed from the contact area. Next, the whole setup is kept in an oven to cure the PDMS for 2 hours at 60$^{o}$C. After curing, the thin layer is peeled off from the mold (Figure 5.3f). Similarly, top and bottom PDMS layers are fabricated by pouring PDMS onto the mold, curing in the oven, and then peeling off from the mold. The resulting thin middle layer and bottom layer are then subjected to plasma treatment (30s at 30W, Harrick Plasma PDC-001) and bonded using microscope alignment (Figure 5.3g). Last, the plastic layer is peeled from the package and the top PDMS layer is placed on top (Figure 5.3h). The alignment is done manually under the microscope, achieving an accuracy of less than 10 μm.

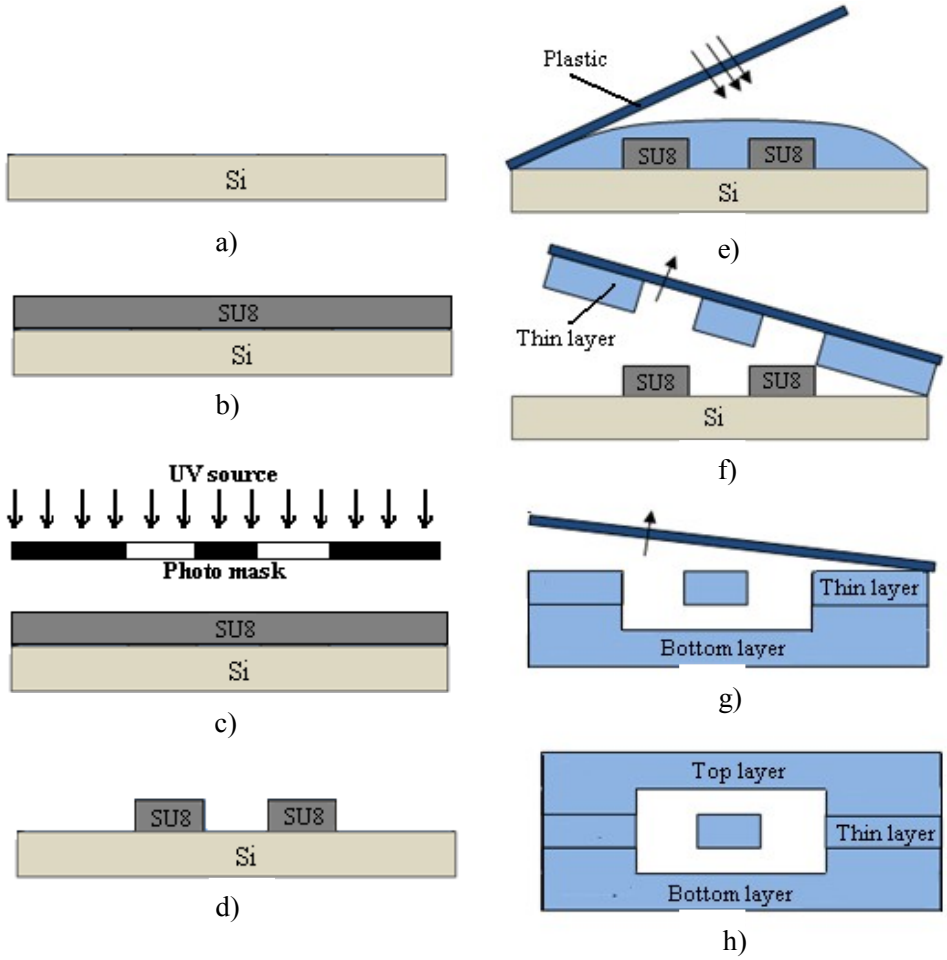


**Figure 5.3** Fabrication process of a multi-layer PDMS device, a) cleaning, b) SU8 coating, c) UV exposure, d) SU8 exposure to light, e) thin layer PDMS loading, f) thin layer is peeled off, g) thin and bottom layer bonding, h) top layer bonding

The PDMS squeezed between the plastic film and the mold tends to cover the mold features with a very thin blocking film in the range of a few micrometers, leaving a residual PDMS layer (Figure 5.4a,b).

Various methods have been presented to remove this residual PDMS layer such as squeezing the thin layer (Anderson et al., 2000), blowing the PDMS residue away (Kang, Um, & Park, 2009) and rupturing the residue by a sharp needle (Kloter, Schmid, Wolf, Michel, & Juncker, 2004). Although the sharp needle or blowing method might be useful

for fabrication of conventional thin PDMS layers, when a high aspect ratio microcantilever is embedded within the thin PDMS layer, these methods will lead to rupture of the microcantilever. The squeezing method seems more applicable for an integrated PDMS microcantilever and has been used in this report to remove the blocking PDMS layer using the clamp method. Figure 5.4c shows the top view image of the fabricated PDMS microcantilever. The cross section of the cantilever with blocking PDMS layer attached is seen in Figure 5.4d. By applying sufficient clamping force on the thin PDMS layer, the blocking layer is removed and only two small residues are left at the bottom edge of the cantilever which does not have significant effect on its performance (Figure 5.4e).

## 5.5Flow sensor testing

To be able to use the microcantilever in quantitative manner, the exact stiffness needs to be determined to allow for calibration. A precision balance method is employed to measure the force on the tip and hence the stiffness of PDMS microcantilever (700 μm length, 70 μm width, 80 μm thickness). We will explain the precision balance method in detail in Chapter 6. To assess the performance of the PDMS micro-cantilever suspended within the microfluidic channel, it was subjected to fluid flow. It was observed that the microcantilever often stuck to the microchannel floor or ceiling during fabrication in plasma bonding, most likely due to the large area of the structure (700 μm length by 70 μm width). In order to overcome stiction, the size of the microcantilever was modified to reduce its surface area. The new microcantilever has a length of 510 μm and a width of 40 μm. The thickness is maintained at 80 μm in order to avoid any change on the elastic modulus due to thickness alteration. By keeping the microcantilever's width less than its

height, the bending of the structure towards the top or bottom is minimized whereas the bending in the horizontal plane along the actual flow direction is promoted.

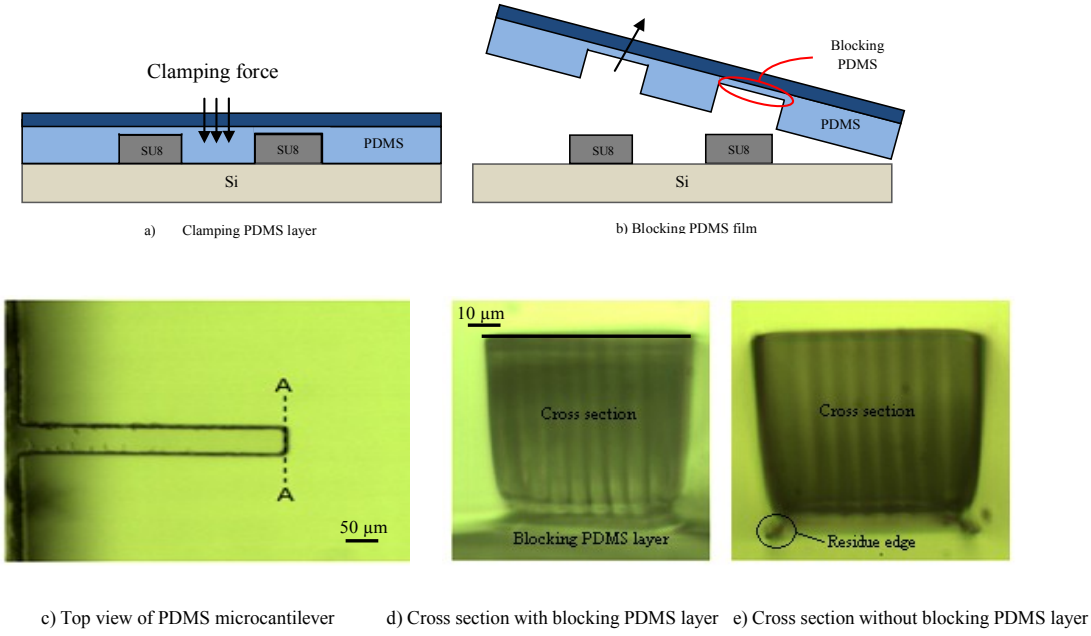


**Figure 5.4**Blocking PDMS film as challenge in fabricating thin PDMS layer a) Squeezing the thin layer, b) blocking PDMS film, c) PDMS microcantilever d) Cross section of PDMS microcantilever with blocking layer, e) Cross section of fully released PDMS microcantilever without blocking layer

Figure 5.5a shows the schematic of experimental testing of flow sensor. Water with a density of $\rho = 1000$ kg/m$^3$ and dynamic viscosity $\eta = 0.001$ Pa·s is injected into the microdevice through the inlet using a syringe pump with various flow rates while the cantilever deflection is monitored through the optical microscope (Figure 5.5b). The PDMS microdevice fabricated with PDMS multilayer technique consists of a thin PDMS layer with integrated microcantilever and microfluidics network sealed by two other top and bottom PDMS layers as shown in Figure 5.5c. The flow introduced into the chip

through the inlet, induces the loading force on the microcantilever to bend it and is transferred out toward the outlet. The inlet microchannel has a width of 840 µm and a depth of 80 µm which is equal to the thickness of thin PDMS layer. The microfluidic chip has a depth of 240 µm at the location of the flow sensor since there are hollow features above and below the microcantilever in order for it to be free. The deflection of the modified micro-cantilever is shown in Figure 5.5d.

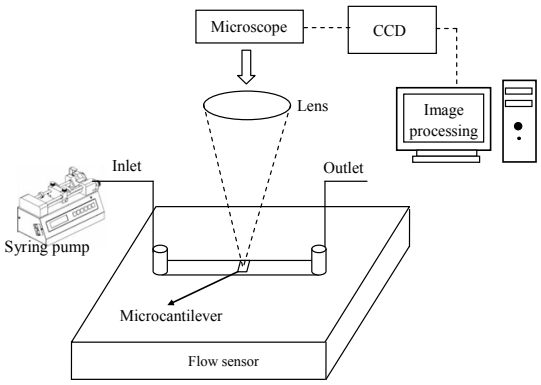


a)

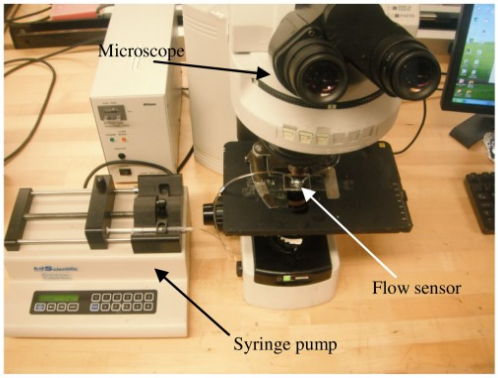


b)

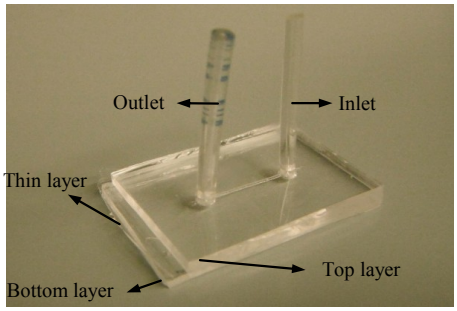


c)

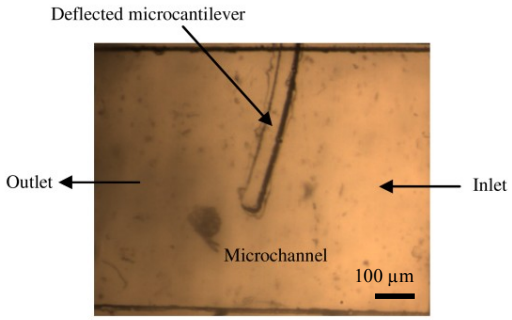


d)

Figure 5.5a) Schematic of experimental setup for the fluid flow test of the PDMS microcantilever, b) Experimental setup, c) Fabricated microdevice, d) Deflected cantilever under fluid flow

## 5.5 Conclusion

A high aspect ratio PDMS microcantilever-based flow sensor has been fabricated using a multilayer PDMS fabrication process. The stiffness of the cantilever has been found by a precision balance setup and the elastic modulus is estimated by linear beam theory. The performance of the flow sensor has been tested by introducing different flow rates into the microfluidic device and monitoring the cantilever response to the fluid force using optical microscopy method. The practical flow range of 0-600 µl/min was achieved for operation with water. The sensitivity of the proposed flow sensor can be increased either by modifying the dimension of the microcantilever or by employing higher resolution optical objectives.

# Chapter 6

# Flexure Integrated Lab-on-a-chip (FlexChip) on Polymer for Biomechanical Study of Growth Behavior of Tip Growing Cells of Camellia Pollen Tubes

## 6.1 Mechanical interaction of pollen tube with PDMS flexural microstructure

In this chapter, growth force and growth behavior of *camellia* pollen tube is quantified through deliberated biomechanical interaction of elongating pollen tube with PDMS flexural microstructure. Furthermore, the effect of the interaction with mechanical obstacles on the pollen tube's growth dynamics is also assessed and quantified. The content of this work is about to submitted to the *Journal of Nature Methods*.

**Abstract**

In this chapter, a microfluidic lab-on-a-chip device integrated with flexural structure is designed and fabricated on polymer platform to quantify the invasive growth force of tip growing plant cell, namely, pollen tube using interaction with PDMS (Polydimethylsiloxane) flexural microstructures. A mixture of *Camellia* pollen suspension is injected into the lab-on-a-chip platform and pollen grains are trapped at the entrances of the growth microchannels using fluid assisted trapping mechanism. Then, pollen tube starts to grow through microchannels that guide the elongating tip growing cells, namely pollen tubes, so that the growing cells collide with the flexible microstructures that are monolithically integrated within the microfluidic chip. The PDMS microstructure is designed such that it is flexible enough not to inhibit pollen tube growth after the interaction and also it enables quantification of the instant growth force of the pollen tubes

during the interaction. The invasive growth force of growing pollen tubular cells is estimated by Finite Element Analysis (FEA) using the deflection of the flexible microstructure created by interaction with cellular growth and mechanical properties of the PDMS material. A maximum growth force of 1.56 μN is estimated for the pollen tube just before bursting. Since the accuracy of the measurement is limited by the 0.2μm resolution of the image taken by optical microscopy,the minimum force that can be detected using the present setup is 10 nN asestimated by FE simulation. Furthermore, the effect of the mechanical obstacle on the dynamic growth behavior of pollen tube was assessed through the shift in the peak frequency characterizing the oscillatory behavior of pollen tube growth rate. This interaction caused a reduction in the oscillation frequency by 70-75% due to interaction with PDMS microstructure as observed in many experiments.

## 6.2 Introduction

Pollen tubes are the carriers of the sperm cells in the flowering plants. They are formed upon germination of pollen grains on a receptive stigma. During the germination process, a pollen grain absorbs fluid secreted by the mature stigma and forms a tubular protrusion (Figure 6.1A). This tube grows through the pistil toward the ovule to deliver the sperm cells to the egg cell resulting in fertilization and seed formation. Each pollen tube carries two sperm cells inside its *cytoplasm*. When the pollen tube enters the ovule through the micropyle, an opening in the outer layers of the ovule, it bursts and the two sperm cells are released. One of them fertilizes the female *gamete* and produces the embryo. The other one fuses with the central cell and forms the endosperm tissue which is responsible for providing nutrients for the embryo during its growth (Anja Geitmann & Ravishankar Palanivelu, 2007). During its way through the pistillar tissues, the pollen tube softens these

tissues by secreting cell wall degrading enzymes or by inducing cell death. However, in addition to these chemically based efforts, the pollen tube needs to generate a considerable physical force to invade different tissues including stigmatic and stylar tissues in its path (Olivier Gossot & Anja Geitmann, 2007).

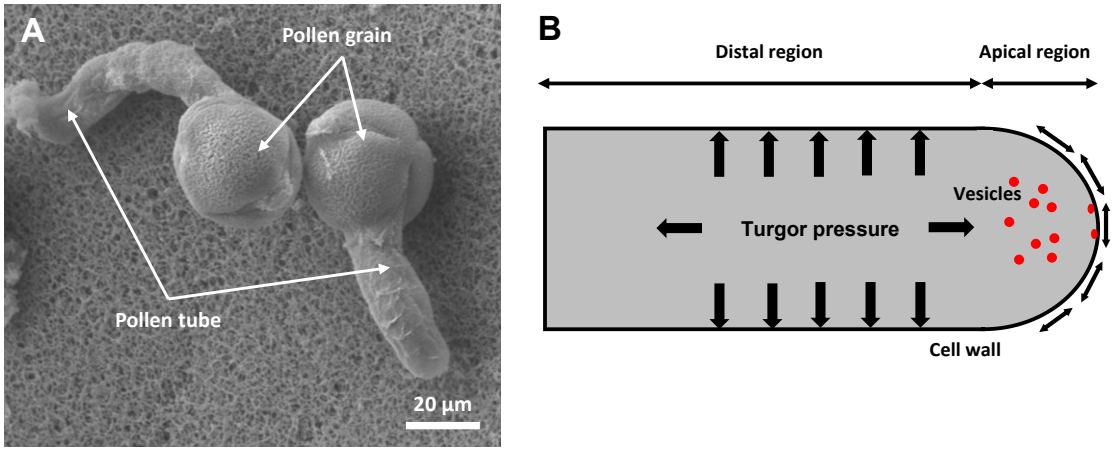


Figure 6.1 (A) Scanning electron micrograph of Camellia pollen tubes germinated in vitro from pollen grains. Scale bar = 10 µm. (B) Schematic representation of the tip growth*morphogenesis*.

In most plant cells, growth happens over large areas of the cellular surface and involves the stretching of the existing cell wall as well as assembly of new wall material. In pollen tubes on the other hand, this expansion of the cell surface is spatially confined to the cell apex (Figure 6.1B). This tip growth morphogenesis is typical for selected cell types in plants, fungi and animals cells including *root hairs*, fungal *hyphae*, and nerve cells (Youssef Chebli & Anja Geitmann, 2007). While many of factors governing pollen tube growth have been recognized, their exact role and precise interactions have not been fully elucidated yet. In particular, the role of turgor pressure in pollen tube growth is a matter of intense

discussion (J. H. Kroeger et al., 2011; Lawrence J Winship et al., 2010; Zonia, 2010; Zonia et al., 2006). A group of researchers believes that turgor pressure is driving force for pollen tube growth (M. A. Messerli et al., 2000a; Plyushch et al., 1995). Messerli et al. (M. A. Messerli et al., 2000a) presented the evidence of increase in growth rate by sharp decrease on osmolarity of the medium. They introduced turgor pressure as the main regulator of the pollen tube growth. Results obtained by Zerzour et al. (R. Zerzour et al., 2009) showed that although changes on turgor pressure through osmolarity variation affects the pollen tube growth rate, turgor pressure is not the main regulator of the pollen tube growth rate. Pierson et al. (Pierson et al., 1996) had previously shown that the increase on the level of osmolarity in the culture medium inhibits pollen tube growth suggesting that turgor pressure is essential for cell elongation. Benkert et al. (Benkert et al., 1997) quantitatively measured turgor pressure using a pressure probe, but they could not find any direct relation between turgor pressure and the growth rate oscillations in lily pollen tubes. From numerical point of view, the effect of turgor pressure on the growth rate of the pollen tube was numerically modeled by Fayant et al (Fayant et al., 2010). These simulations showed that higher turgor would be expected to cause higher instantaneous deformation of the cell wall but time-dependent behavior was not taken into consideration in that model.

The role of the turgor pressure in cell growth is not undisputed (Franklin M Harold, Ruth L Harold, & Nicholas P Money, 1995). In some species of fungal hyphae growth without any noticeable turgor pressure seems to be possible. Davis et al. (Davis, Burlak, & Money, 2000) even showed that some species of hyphae grow faster with zero or at least very low value of turgor pressure. Also, the growth rate of pollen tubes growing in a gel type medium is comparable with the rate of growth in liquid medium (Tomos, 1988). This

suggests that invasive force is not due to an increase in turgor pressure, but it is due to cell wall relaxation. It is a phenomenon in which the material strength of the cell wall reduces due to enzymatic reaction at the apex with increasing of water influx leading to cell growth (Parre & Geitmann, 2005).

Clearly both the cell wall mechanical properties and the turgor pressure influence cell growth and can be considered as the fundamental parameters that drive and regulate this process. The effect of other factors involved in cell growth such as intracellular ions can be interpreted as the regulator of turgor pressure or the cell wall material properties. The clue is that many of the underlying events such as vesicle trafficking, actin microfilament polymerization, and apical ion flux oscillate with the same pulsating frequency period of growth rate, but usually with different phases (Chebli & Geitmann, 2007; Feijo et al., 2001). Schopfer et al. (Schopfer, 2006) introduced a kind of interplay between turgor pressure and cell wall material. Cell wall was presented as a viscoelastic composite with stress relaxation property which is activated at a specific time depending on the value of stretching. Schopfer argued that in the next studies, both the turgor pressure and cell wall relaxation have to be considered as the regulators of growth. Later, Zerzour et al (R. Zerzour et al., 2009) argued that all growth regulators within the cell ultimately have to take action on one of the two main regulators of the growth including, cell wall softening or turgor pressure.

The turgor pressure has been measured through direct or indirect methods. In the direct measurement, the sensor is a pressure probe presented by Green (Green, 1968) and developed by Hüsken et al. (Hüsken, Steudle, & Zimmermann, 1978) which was used to estimate the turgor pressure in the range of 0.1 to 0.6 MPa for algae. Lew (Lew, 2005)

employed pressure-probe system for hyphal cell and found values of 0.4-0.5 MPa for the turgor pressure. Benkert et al. (Benkert et al., 1997) used the pressure probe to determine turgor pressure for plant cells and it has been estimated to be 0.1 to 0.4 MPa for lily pollen tubes. In an indirect technique, the cell is exposed to different known values of medium concentration. The method is based on determining the concentration at which the cell collapses. Howard et al (Howard & Valent, 1996) used this technique to measure the turgor pressure to be 0.8 MPa for fungal hyphae. However this pressure was the maximum turgor pressure at the tip of hyphae. To measure the cell wall mechanical properties, different strategies have been used. Micro-manipulation of cell wall using micro-indentation has been used on the growing cells by Parre et al. (Elodie Parre & Anja Geitmann, 2005) and Zerzour et al (R. Zerzour et al., 2009). This method used a glass stylus actuated by a horizontal beam. By monitoring the cell wall deflection and measuring the reaction force applied to glass stylus, the mechanical strength of the wall is compared between different parts of the cell. It showed that stiffness at the apex of pollen tube is significantly lower than stiffness at the shank part of the cell (Elodie Parre & Anja Geitmann, 2005). Vogler et al. (Vogler et al., 2013) used cellular force microscopy (CFM) in combination with Finite element modeling (FEM) to estimate the Young's modulus of elasticity of the growing lily pollen tube. This automated method is similar to microindentation technique and provided a first experimental approximation of the Young's modulus of elasticity for the pollen tube cell wall. Sanati Nezhad et al. (Amir Sanati Nezhad, Mahsa Naghavi, Muthukumaran Packirisamy, Rama Bhat, & Anja Geitmann, 2013) presented a novel microfluidic based experimental platform to quantitatively determine the Young's modulus of the pollen tube cell wall. They used fluid flow passing through a micro chamber to apply bending force

perpendicular to individual pollen tubes guided to grow into a microchannel. The Young's modulus of the cell wall material was calculated based on the measured flexural rigidity of the cell using finite element analysis. Another technique refers to the bio-chemistry side to identify the material components of cell apex and to determine the gradient of materials components at the tip as well as at the shank (Anja Geitmann, 1999; Holdaway-Clarke et al., 2003).

In order to study the interplay of turgor pressure and cell wall mechanical properties, development of new measurment techniques capable of detecting the interplay is essential to understand the polar cell growth. Mechanical sensing is an effective method that has recently been used to measure the growth force as one of the parameters for studying the growth of tip growing cells. Money (Nicholas P Money, 2004) practically estimated the invasive force of hyphae by positioning a strain gauge perpendicular to the direction of growth at the apex as approximately 1.4 μN. The applied pressure by hyphae to the strain gauge was estimated (0.07 MPa) by dividing the estimated force by the contact area with the strain gauge (20 $\mu m^2$). Money (N. Money, 2007) argued that there is a difference between the value of turgor pressure and the pressure that hyphae exert against the mechanical barrier. The difference is because of the resistance of cell wall against the internal pressure. It was tried to formulate the force applied on the obstacle by considering the interplay role of both turgor pressure and the cell wall material properties. By controlling the material properties of the tube wall, the hyphae have the capability to transfer the force against the barrier between zero to a maximum value.

The large size of silicon beam used as the strain gauge (100 μm thickness and 10 mm width) compared to the size of the cell (10 μm) depicts the complexity of employing this

method for the invasive force detection. Moreover, the silicon beam is not sensitive enough to be able to detect any possible fluctuations in cell invasive force. Since the pollen tube easily changes its growth direction when facing a flat, perpendicular mechanical obstacle, using the strain gauge method is not applicable for quantifying invasive growth force of pollen tubes. To address deficiencies associated with employing strain gauge method in pollen tube studies, Sanati Nezhad et al. (Amir Sanati Nezhad, Mahsa Naghavi, Muthukumaran Packirisamy, Rama Bhat, & Anja Geitmann, 2013) used microsystems technology to develop a PDMS-based lab-on-chip-platform which enabled quantification of dilating force of growing pollen tube. They consider a microchannel including a series of micro gaps through which the pollen tubes must squeeze to continue its elongation. The presented micro-gap structure limits the growth directions along the initial direction and prevents reorientation of the growth. Using FEM analysis, the dilating force exerted by elongating pollen tube was quantified based on the deformation of the gaps. The maximum dilating force of 14.7 μN was reported by the authors. Using this platform we can only estimate the force that pollen tube exerts normal to the laterally placed gap. Moreover, quantification of the possible fluctuation of the growth force at very tip of the tube was not possible using micro gap structures. Therefore, developing a reliable and precise technique to measure the invasive growth force in the direction of the unidirectional growth and its variations at the tip of pollen tube is very important as it can help in the understanding of the interplay between the turgor pressure and the mechanical properties of the cell wall.

In this chapter, we developed a PDMS based lab-on-a-chip platform that enables quantification of invasive growth force of a growing pollen tube at the tube apex. A mixture of *Camellia* pollen suspension is injected into the lab-on-a-chip platform and

pollen grains are trapped at the entrances of the growth microchannels. Then, pollen tube starts to grow through microchannels which are meant to guide the elongating pollen tubes towards micromechanical elements monolithically integrated within the microfluidic chip. In order to compel growing pollen tube to apply its maximum force to the micromechanical elements and prevent in plane reorientation of the tube after facing the sensing elements, a notch with the size in the range of pollen tube tip is created in the micromechanical sensing element. When the pollen tube tip trapped at the curved notch of the sensing elements, it exerts the invasive growth force onto the micromechanical element leading to its deflection. The deflection of the micromechanical element and mechanical properties of the polydimethylsiloxane (PDMS) enables us to quantify the invasive growth force of growing pollen tubes using FEM simulations.

## 6.3 Materials and methods

### 6.3.1 Pollen Culture

Camellia japonica pollen was collected from a plant growing in Montreal Botanical Garden, preserved by dehydrating on silica gel for 2 h and stored at −20°C until use. Prior to each experiment, pollen was rehydrated in a humid chamber for at least 0.5 hourwithout direct contact with liquid water. Pollen grains were suspended in a liquid growth medium contained the following components: 2.54 mM of $Ca(NO_3)_2 \cdot 4H_2O$, 1.62 mM of $H_3BO_3$, 1 mM of $KNO_3$, 0.8 of mM $MgSO_4 \cdot 7H_2O$ and 8% sucrose (w/v). Once the pollen grains started to germinate, the pollen suspension was introduced into the microfluidic chip.

### 6.3.2 Observation and analysis

Observation of growing pollen tubes in microfluidic channels were carried out using an inverted microscope (Nikon TE2000) equipped with a CCD camera(Roper fx). ImagePro

software (Media Cybernetics) and ImageJ 1.440 (National Institutes of Health, http://rsb.info.nih.gov/ij) softwares were used for data acquisition and analysis.

## 6.4 Resultsand Discussion

### 6.4.1Design and Fabrication

In order to quantify the invasive growth force of an elongating pollen tube, we characterized the interaction of a growing pollen tube with a flexible microcantilever with calibrated bending properties. To this end a PDMS-based Lab-on-a-chip platform (Figure 6.2) was designed to harbor growing pollen tubes and to present the elongating apex of the cell with a monolithically integrated PDMS microcantilever on its growth direction. The microfluidic network consists of an inlet for injection of the pollen grain suspension, a distribution chamber to guide the pollen grains to the entrances of growth microchannels, and two identical growth microchannels (top and bottom) are incorporated for redundancy. Growth microchannels are meant to guide the elongating pollen tubes in such a way to ensure the interaction of the pollen tube with the microcantilever located at the end of the growth microchannels. The microcantilever is located approximately 500 μm from the microchannel entrance to enable quantification ofthe pollen tube growth force while it displays a stabilized growth profile at the time of interaction.

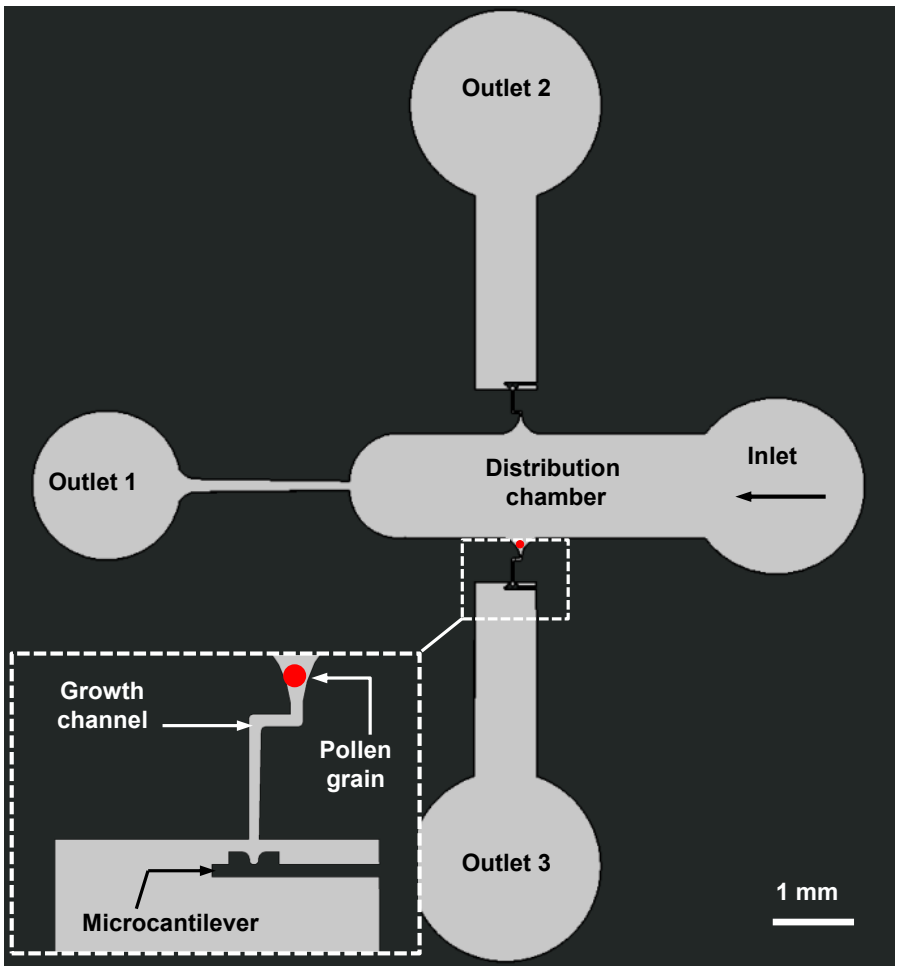


**Figure 6.2** Schematic showing the geometry of the microfluidic network and the monolithically integrated PDMS microcantilever. Magnified view shows a pollen grain trapped at the entrance of a growth microchannel.

In order to guide the pollen tubes into the microchannels, pollen grains have to be transported by laminar flow within the distribution channel and trapped at the entrances of the growth microchannels as shown in the inset of Figure 6.2. Three outlets pass medium from the distribution chamber and from the ends of the microchannels. The distribution chamber outlet (Outlet 1) is made large enough in order to also evacuate excess pollen

grains. Outlets 2 and 3 facilitate fluid flow through the microchannels to ensure the positioning of pollen grains at the entrances of the microchannels. Pollen grains of *Camellia japonica* have a typical diameter of 50-60 μm. Therefore, the depth of the entire microfluidic network is set to be 80 μm in order to allow the grains to be transported freely by the fluid flow, without allowing their stacking in vertical direction. In order to trap individual pollen grains at the entrances of the microchannels and to allow pollen tubes with a typical diameter of between 13-20 μm to enter these channels, the channel width ($W_C$) is set to 30 μm. The entrance of a microchannel is rounded with a radius of 210 μm to enhance trapping of pollen grains (Figure 6.3). The distance between the PDMS microcantilever and the exit of the growth microchannel has to be as small as possible, otherwise the growing pollen tube has enough space to change its growth direction and passes above or below the microcantilever without any interaction. Considering the limitations of the fabrication process, this distance (d) was set to be 30 μm in our design. To quantify the invasive growth force of a growing pollen tube, the pollen grain needs to be fixed in its location; otherwise the grain will be move backwards due to the reaction force of the microcantilever. This push back effect is prevented by inserting a kink consisting of two repeated 90° angles into the microchannel through which the pollen tube grows and that anchors its distal region (Figure 6.3). Since the pollen tube easily changes its growth direction when encountering a mechanical obstacle, we equipped the cnatilever with an appendix with Length $L_1$, width $W_1$ and including a curved notch with diameter ($D_1$) slightly bigger than the size of the average *Camellia* pollen tube diameter ($D_2$) to trap the pollen tube apex.

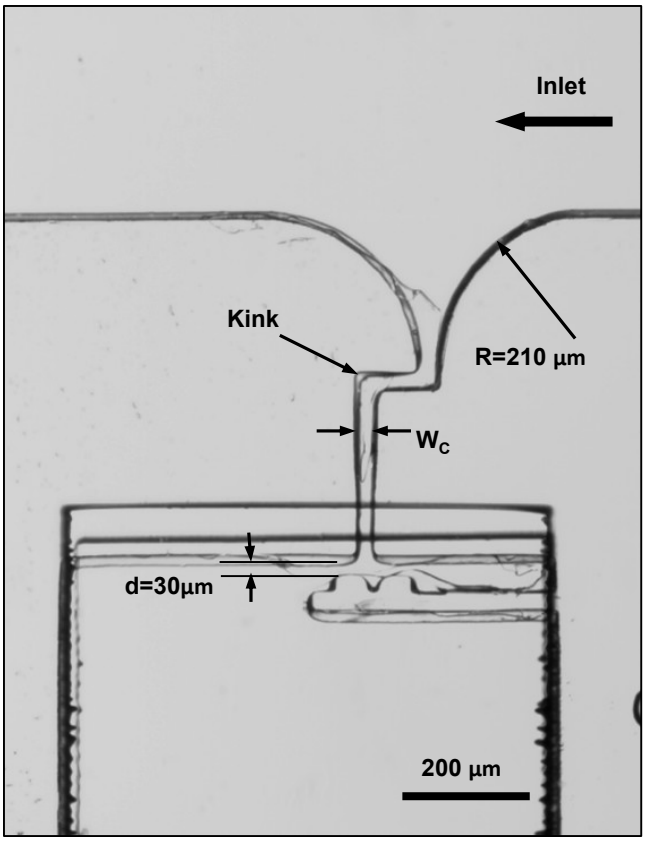


**Figure 6. 3** Brightfield micrograph showing the geometry of the microchannel and microcantilever. A kink is devised in the microchannel which prevents pollen grain backward displacement due to the reaction force applied to the tube, after the interaction of pollen tube and microcantilever.

This geometry prevents the pollen tube from in-plane reorientation and forces the cell to apply its maximum growth force to the PDMS microcantilever (Figure 6.4). When the expanding pollen tube hits the rounded corner ($R_1$ =17.5 µm) of the entrance of the notch, it is guided into the notch and this increases the chance of trapping the pollen tube apex at the intended location (point P). A pollen tube growing towards the micro cantilever hits the microcantilever at any position on the notch wall. To continue growing, the pollen tube must apply its growth force on the microcantileverleading to bending of the cantilever. The amount of deflection is proportional the growth force applied by the pollen tube to the

microcantilever. The interaction of pollen tube and PDMS microcantilever is experimentally characterized by the quantification of the cantilever deflection, and analyzing pollen tube dynamics growth pattern in terms of changing of the average growth rate and oscillation frequency before and during the contact with microcantilever.

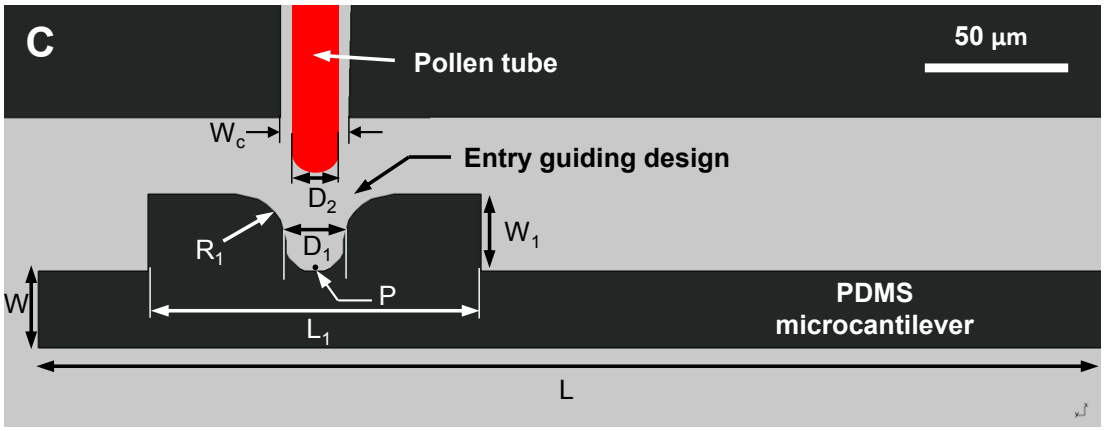


**Figure 6.4**Schematic showing the dimensions and geometry of the microcantilever. An appendix including a curved notch was considered in the architecture of the microcantilever which prevents pollen tube from in-plane reorientation and allows the tube to exert a pushing force against the microcantilever. The rounded corner of the notch entrance facilitates trapping of tube apex at the intended trapping point (P).

By considering a range of 1-15 µN for the pollen tube growth force (Nicholas P Money, 2004; Amir Sanati Nezhad et al., 2013), using FEM simulation length (L) and width (W) of the PDMS microcantilever were optimized to be 400 µm and 30 µm respectively. Two different criteria were considered in the determination of these dimensions. 1) The cantilever should be flexible enough to have visible deflection when it was hit by the pollen tube, and 2) The microcantilever aspect ratio (length/width) must be reasonable, otherwise we will experience snapping of the cantilever to the top or bottom layer during

the fabrication process. Finally, the length ($L_1$) and width ($W_1$) of the appendix and diameter of the curved notch ($D_1$) were selected as 120μm, 30 μm and 25 μm respectively in our design.

Multi-Layer soft lithography process is developed for monolithic integration of the PDMS microcantilever within the microfluidic networks. Microfluidic networks and flexible microcantilever are implemented in a thin PDMS structural middle layer (80 μm thick) sandwiched between top and bottom layer to create enclosed microfluidic networks. The bottom layer is a patterned thick PDMS layer containing cavities to release the microcantilever for free in-plane deflection. The top layer consists of a patterned thin PDMS layer (80 μm thick) bonded to an ultra thin glass slide (100 μm thick) contains cavities to release the microcantilever. The glass-PDMS top layer (180 μm thick) allows us to take high resolution picture with high magnification and also makes the LOC compatible with the confocal microscopy that might be used for fluorescence imaging in future experiments.

The schematic of the fabrication process is demonstrated in Figure 6.5A-I. First a photoresist layer is spin coated on the surface of a 4 inches silicon wafer (Figure 6.5A) and patterned using conventional lithography process (Figure 6.5B). Here we used SU8-2075 negative photoresist (MicroChem Corp). The thickness of the photoresist layer was set using spin coating at 80 μm. After fabrication of the SU-8/silicon mold, a mixture of curing agent and PDMS prepolymer (Sylgard 184 silicone elastomer, Dow Corning Corporation, Midland, USA) at a weight ratio of 1:10 was poured onto the SU-8/Silicone mold (Figure 6.5C). In order to remove excessive PDMS on the surface of SU-8 features, a knife edge was traversedabove the substrate surface while maintaining contact with the

top surface of the photoresist layer (Figure 6.5D). Usually a thin film of PDMS (less than 5µm thick) remains on the surface of photoresist region after this step. Then the mixture

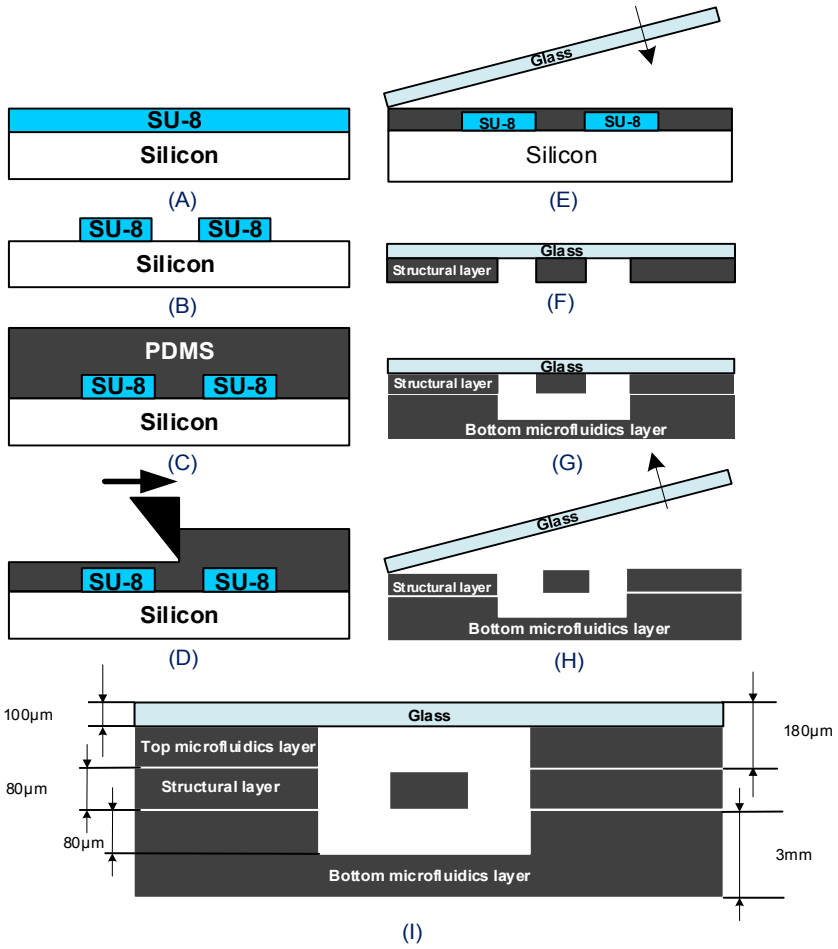


was completely degassed in the desicator to get rid of the bubbles. Afterward, a glass slide was placed on the surface of PDMS mixture (Figure 6.5E).

**Figure 6.5**Schematic of the multi-layer fabrication processes developed for the fabrication of LOC platform (Dimensions not to scale)

The glass slid should be lowered carefully onto the PDMS mixture to prevent introducing any air bubbles at the interface. In order to remove the remaining thin film PDMS layer on

the top of the SU-8 features, the glass slide was loaded using a clamp and then the whole setup was placed in an oven for 4 hours at 65º C for curing. After curing, using glass slide, the thin PDMS structural layer was peeled off from the mold (Figure 6.5F). In order to bond the thin PDMS structural layer with bottom microfluidics layer, which was fabricated by replica molding technique before, they were placed in a plasma cleaner (Harrick Plasma PDC-001) to perform oxygen plasma treatment for about 30 sec. After that, both the surfaces were placed face to face and aligned under a microscope (Figure 6.5G). Then, the glass slide was peeled off, and the patterned PDMS structural layer was bonded to the top surface of the thick bottom microfluidic layer (3mm thick) (Figure 6.5H). Afterward the inlet and outlets were punched in the bottom microfluidics layer. Finally, the top microfluidics layer which consists of a pattern tin PDMS layer (80 μm thick) on top of an ultra thin glass slide (100 μm thick) fabricated before using replica molding technique was bonded to the thin PDMS layer using oxygen plasma treatment (Figure 6.5I).

### 6.4.2Biomechanical interaction between pollen tube and microcantilever

The LOC was tested by injecting a mixture of *Camellia* pollen suspension through the inlet using a syringe pump. Pollen grains were transported by medium fluid flow through the distribution chamber and trapped at the entrances of the growth microchannels. The injection velocity to ensure stable positioning of pollen grains at the entrances of the growth microchannels while preventing bursting of pollen grains was found to be about 0.01 m/s. Since injection of medium fluid flow may lead to an overestimation of the pollen tube growth force, once the pollen grains were trapped at the microchannel entrances, the injection of medium flow was stopped. Then, pollen tube started to grow through the

microchannels, passed the kink devised in its direction to prevent push back effect and continued its growth towards the microcantilever (Figure 6.6).

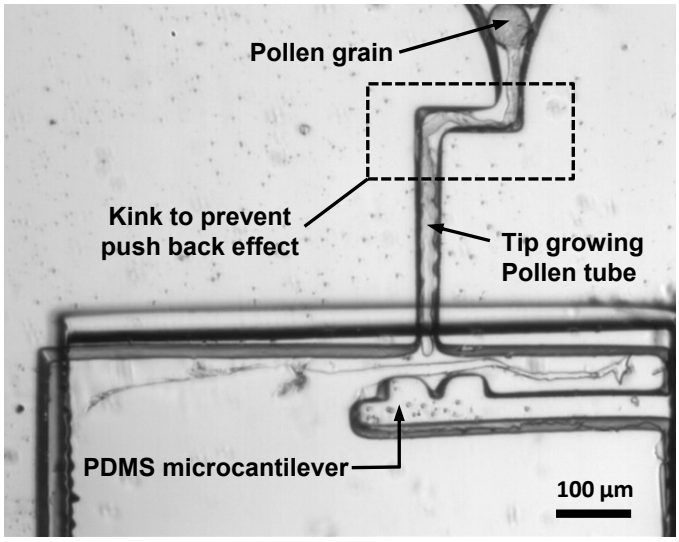


**Figure 6.6**Micrograph of a *Camellia* pollen tube growing through a kink in the microchannel towards the microcantilever.

The in-situ progress of bio-mechanical interaction between cantilever and pollen tube is depicted in images taken at various instant during growth as shown in Figure 6.7. Two different types of action were observed when pollen tubes interacted with the microcantilever: (i) **Complete trapping to burst:**As shown in Figure 6.7A the pollen tube touched the microcantilever at point A on the rounded corner (R1 =17.5 µm) of the notch entrance and pushed the cantilever to bend. As expected, the pollen tube tip was guided into the notch by the rounded corner of the notch entrance (Figure 6.7B). The pollen tube continued its growth toward the intended trap point while applying its growth force against the cantilever leading to its deflection (Figure 6.7C). At this point, the growth was stopped,

and after 6 minutes the tube resumed its growth and bent the cantilever further (Figure 6.7D). The pollen tube continued to its progress until it reached the point that the pollen tube growth force was not sufficient to displace the cantilever further (Figure 6.7E). The accurate comparison of the location of point B on the cantilever before and after the deflection through image analysis of Figure 6.7A and Figure 6.7E shows a maximum deflection of 58 μm for this point which corresponds to 118 μm of the cantilever tip (Point C) deflection.

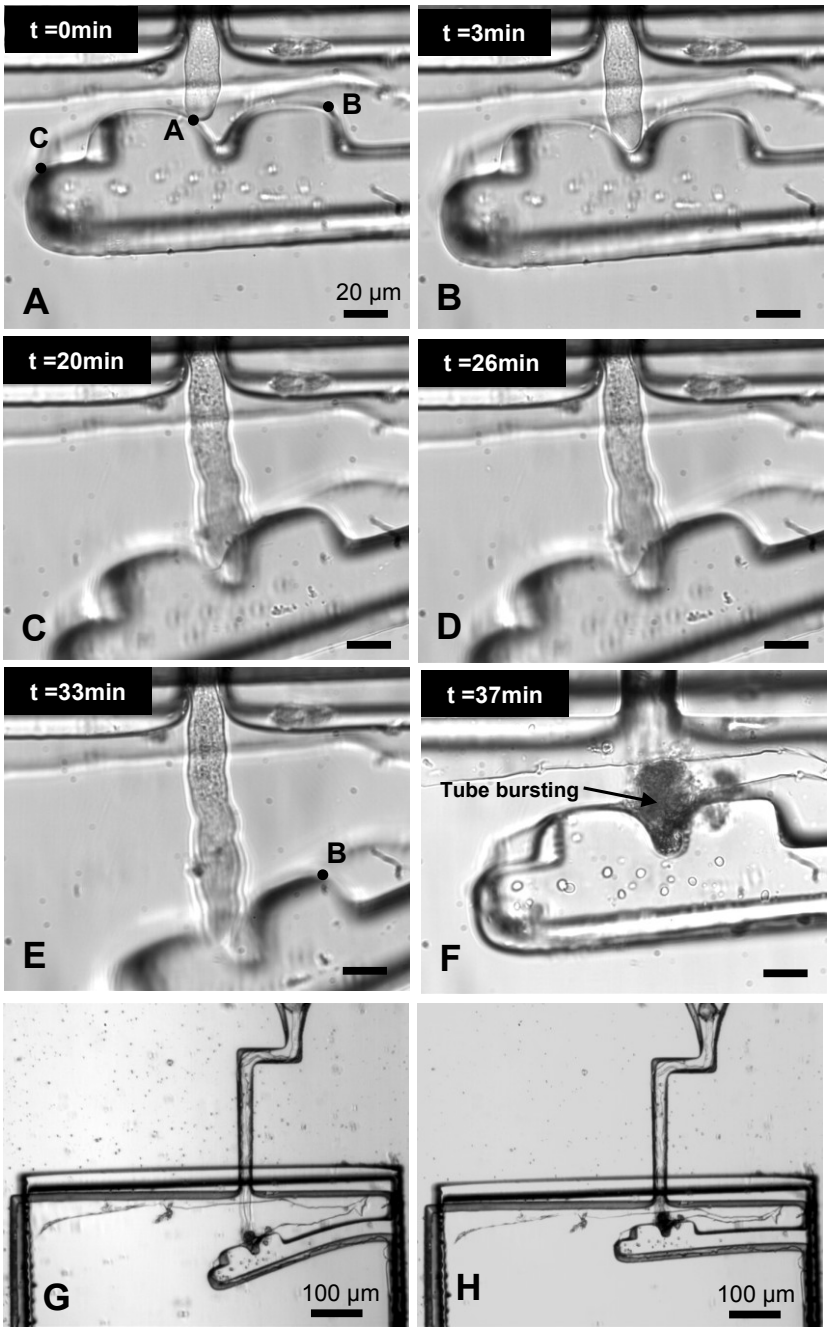


**Figure 6.7** Time lapse image series of the pollen tube behavior during interaction with the microcantilever. (A) The Pollen tube touch the microcantilever at point A on the rounded corner. (B) The pollen tube tip is guided into the notch by the rounded corner of the notch entrance. (C) The pollen tube continues its growth towards the intended trap point while

applying its growth force against the cantilever. (D) Pollen tube growth is stopped, and after 6 minutes the tube resumes its growth and bends the cantilever further. (E) The pollen tube continues its progress until it reaches the point at which the growth force is not sufficient to displace the cantilever further. A maximum deflection of 58 μm for point B is observed. (F) The pollen tube bursts and cantilever is gradually returning to its initial position. (G) A micrograph showing the whole cantilever at the moment of the pollen tube bursting before it returned to its initial position. (H) A micrograph showing the whole cantilever at the moment of pollen tube bursting after it returned to its initial position. (Scale bar in A applies to A-F).

At this point, the pollen tube growth was stopped and after 4 minutes the tube burst. After bursting, the pollen tube was not able to apply any force against the microcantilever, so the cantilever gradually returned to its initial position (Figure 6.7F). Figure 6.7G and Figure 6.7H show the whole cantilever at the moment of the pollen tube bursting, just before and after it completely returned to its initial position respectively.

(ii) **Slippery trapping:**The pollen tube hit the cantilever at point I (Figure 6.8A) and it was guided into the intended trapping position by the rounded corner (Figure 6.8B) while applying its growth force against the microcantilever. Then, the pollen tube tip slid along the notch wall toward the intended trapping point. At this point, the pollen tube lost its contact with the cantilever for just an instant and cantilever resiled until the pollen tube tip came in contact again with the trapping point on the microcantilever. When the tube tip came in contact again with the cantilever, it exerted its growth force against the cantilever and bent it more (Figure 6.8C). The pollen tube continued its growth until it reached the points at which its growth force was not sufficient to deflect the cantilever further. The accurate comparison of the location of point J on the cantilever before and after the deflection through image analysis of Figure 6.8A and Figure 6.8D shows a maximum

deflection of 67 µm for this point which corresponds to 137µm of the cantilever tip (Point C) deflection.

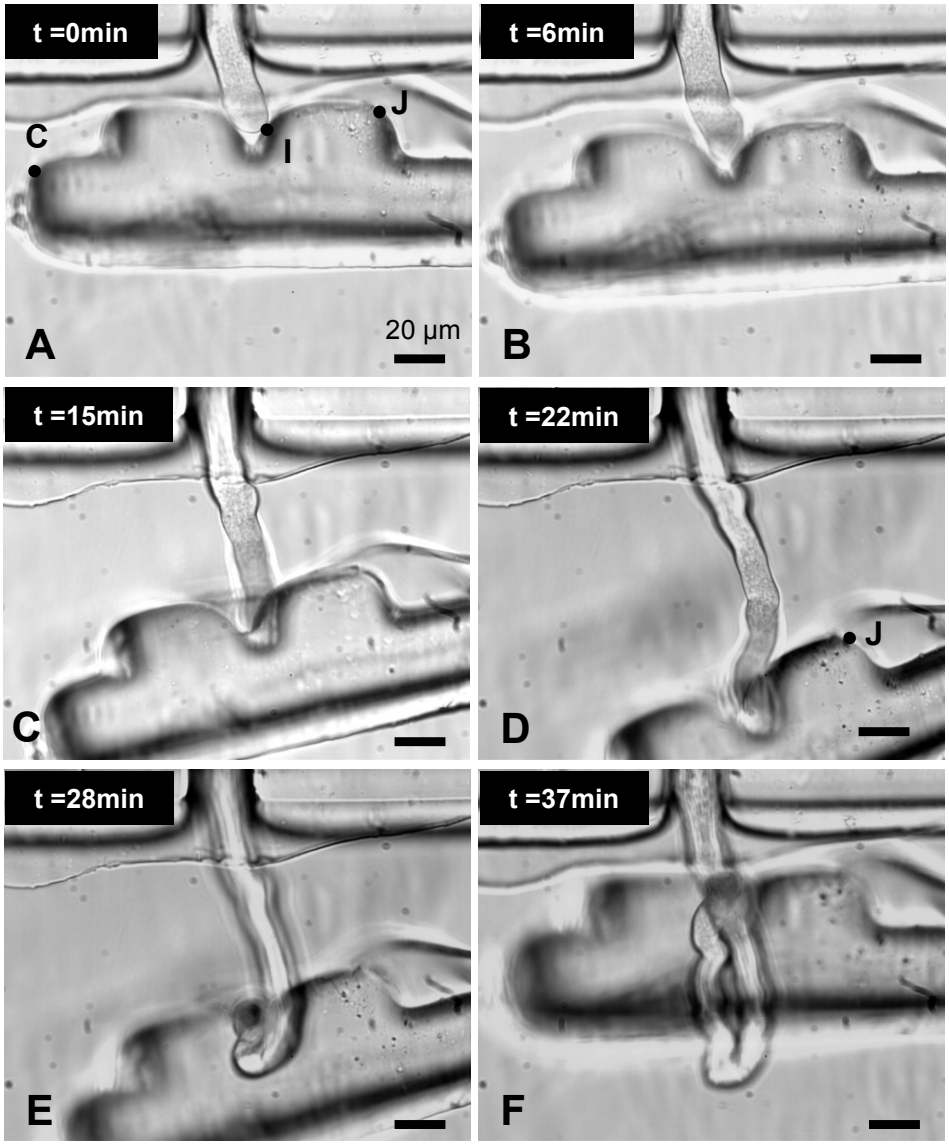


**Figure 6.8** Time lapse image series of the pollen tube behavior during interaction with the microcantilever. (A) The pollen tube hit the microcantilever at point I. (B) The pollen tube tip is guided into the notch by the rounded corner of the notch entrance. (C) The pollen tube loses its contact with the cantilever for just an instant and cantilever resiles until the

pollen tube tip comes in contact again with the microcantilever. When the tube tip come in contact again with the cantilever, it exerts its growth force against the cantilever and bends it more. (D) The pollen tube continues its growth until it reaches the point at which its growth force is not enough to deflect the cantilever further. A maximum deflection of 67 μm for point J is observed. Then, the tube starts to buckle under the reaction force applied to it by the cantilever. (E) the pollen tube turns back and starts to grow in the reverse direction (F) The pollen tube tip is not in contact with the cantilever in this position. Therefore, it is not able to apply enough growth force needed to keep the cantilever deflected anymore and the microcantilever gradually returns to its initial position. (Scale bar in A applies to A-F)

At this point the pollen tube first started to buckle under the reaction force applied to it by the cantilever (Figure 6.8D) and then turned back and started to grow in the reverse direction (Figure 6.8E). Since the pollen tube tip was not in contact with the cantilever in this position, it was not able to apply enough growth force needed to keep the cantilever deflected anymore, therefore the microcantilever gradually returned to its initial position (Figure 6.8F).

### 6.4.3 Effect of microcantilever as a mechanical stimulus on pollen tube dynamic growth behavior

In order to analyze the effect of interaction of pollen tube with the PDMS microcantilever, the dynamic growth pattern of pollen tube in the form of growth rate, growth length and oscillatory growth frequency before and during the contact with microcantilever were evaluated. As shown in Figure 6.9,before contact with the microcantilever (region BC), the normal growth rate of the pollen tube fluctuated between 4 μm/min and 19 μm/min with the average growth rate of 11.3 μm/min. During contact with the microcantilever (region DC), the pollen tube growth rate varied between 1.7 μm/min to 12.7 μm/min and the average growth rate was reduced by 44 % to 6.3 μm/min. The results of growth length

versus time before the contact and during the interaction with the microcantilever are also shown inFigure 6.9. During the interaction of pollen tube with the microcantilever the resistance of the microcantilever against pollen tube growth and as result the rate of the energy dissipation during the interaction increased. However, the results of growth length versus time show that the average growth rate remained stable despite the increasing resistance.

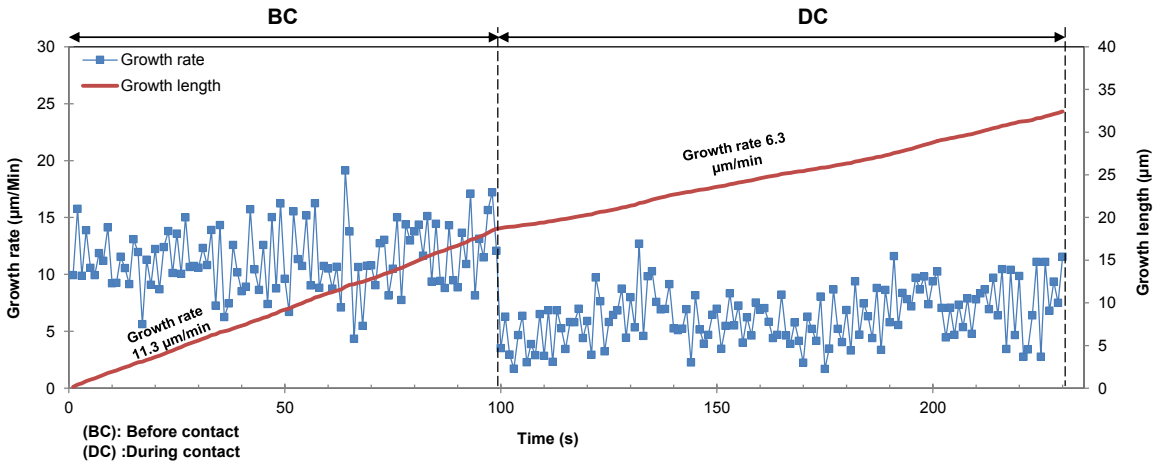


**Figure 6.9** Pollen tube growth rate before contact (BC) and during contact (DC) with the microcantilever. The mean growth rate is reduced by 44% from 11.3 µm/min to 6.3 µm/min after contact with the microcantilever. Pollen tube growth length before contact (BC) and during contact (AC) with the microcantilever is also shown.

In order to understand how the interaction between a pollen tube and a PDMS microcantilever can affect the oscillatory growth pattern of a growing pollen tube, the frequencies of the pollen tube growth rate before and during contact with the microcantilever were assessed. Since it is hard to recognize these frequencies just by evaluating the growth rate versus time signal, the time domain signal was transformed to

the frequency domain and the peak frequency of the oscillation was identified using Discrete Fourier Transform (DFT). For the calculation of the DFT, Fast Fourier Transform (FFT) algorithm was employed (R. Zerzour et al., 2009). Then, to obtain waveform analysis reflecting the power of each frequency component associated with the oscillatory growth, power spectral density (PSD) was employed. The FFT analysis of the growth rate signals for the two tested Camellia pollen tubes before interaction with the microcantilever show dominant peak frequencies at 40 mHz and 16 mHz, respectively (Figure 6.10A). All three PSD windowing functions (Kasier, Hamming and Chebyshev) revealed similar peak frequencies (Figure 6.10B ).

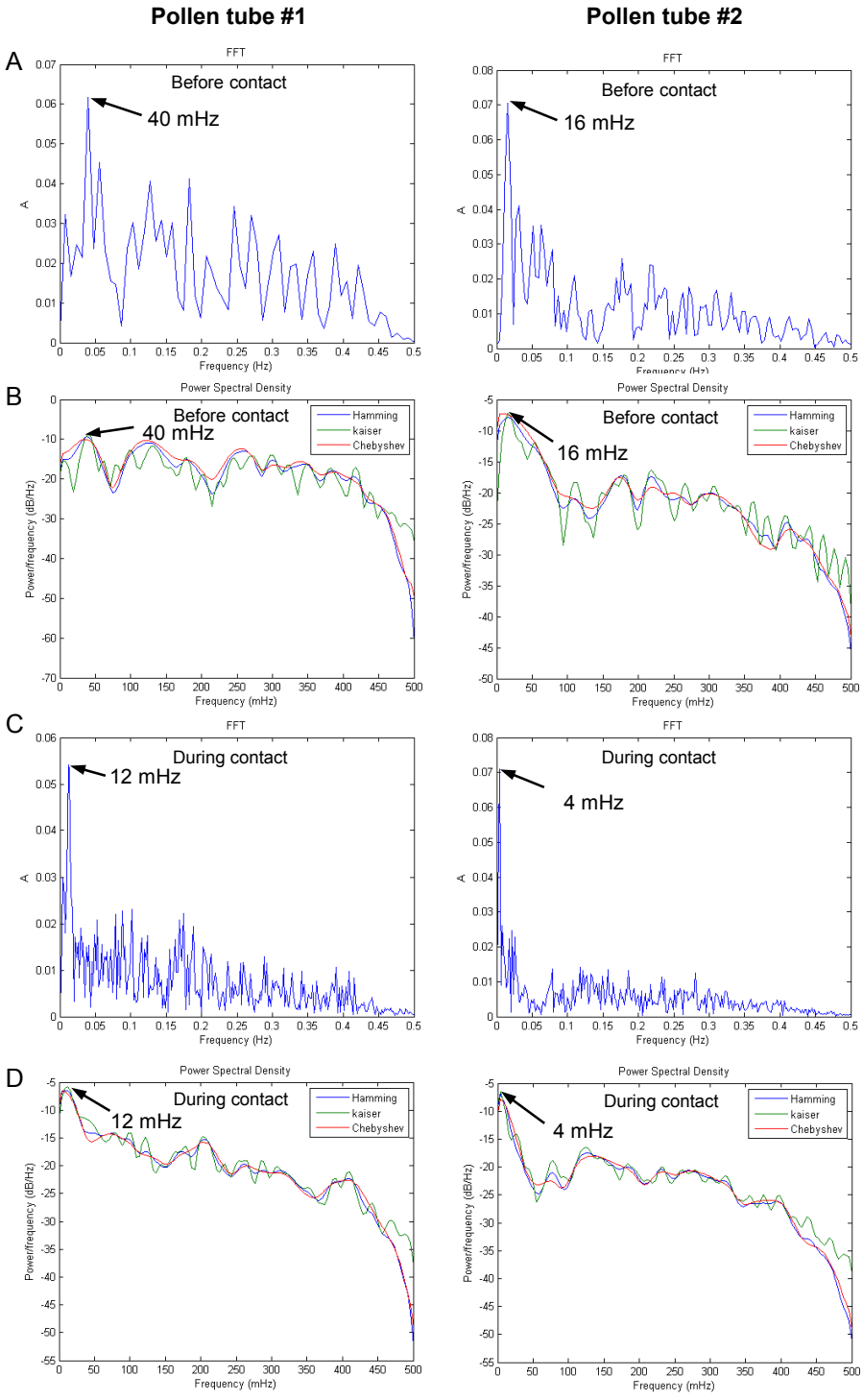


**Figure 6.10**(A) FFT analysis on time-series data of two sample *Camellia* pollen tubes growth rate (sample rate = 1s) before contact with the microcantilever. Peak frequencies are seen around f=40 mHz and f=16 mHz. (B) PSD analysis on time-series data of two sample *Camellia* pollen tubes growth rate before contact with the microcantilever. The

primary peak frequencies are detected at 40 mHz and 16 mHz. (C) FFT analysis on time-series data of the same *Camellia* pollen tubes growth rate (sample rate = 1s) during contact with the microcantilever. Peak frequencies are seen around f=12 mHz and f=4 mHz. (D) PSD analysis on time-series data of two sample *Camellia* pollen tubes growth rate during contact with the microcantilever. The primary peak frequencies are detected at 12 mHz and 4 mHz.

The FFT analysis of the growth rate signals of the tested pollen tubes during contact with the microcantilever show peak frequency of 12 mHz and 4 mHz for the pollen tubes number 1 and 2 respectively (Figure 6.10C), verified by the result obtained using PSD analysis (Figure 6.10D). This means that the oscillation frequency of the pollen tube growth rate was reduced by 70% for pollen tube 1 and 75% for pollen tube 2 caused by the mechanical stimulus due to interaction of the growing pollen tubes with the PDMS microcantilever.

### 6.4.4 Quantification of pollen tube invasive growth force using Finite element method (FEM) simulation

FEM was used to determine the pollen tube growth force based on the deflection of the microcantilever. Mechanical properties of the PDMS such as Young's modulus and Poisson ratio are important in the determination of the growth force exerted by pollen tube to the microcantilever using FEM. Since the Young's modulus of the thin PDMS layer is dependent on the thickness of the layer and the fabrication process (M. Liu, Sun, Sun, Bock, & Chen, 2009; ), to avoid errors caused by employing previously published data for the Young's modulus of PDMS, a precision balance method was employed to quantify the Young's modulus of PDMS from the microcantilever stiffness (A Sanati Nezhad, Mahmood Ghanbari, Carlos G Agudelo, Muthukumaran Packirisamy, et al., 2013). A

photograph and a schematic diagram of the setup are depicted in Figure 6.11A and Figure 6.11B respectively. In brief, a PDMS microcantilever was fabricated using the same method explained before in the fabrication process and bonded to another thick PDMS layer to give mechanical stability. Then, the microcantilever was mounted horizontally on a micro positioner (ULTRAlign™ Metric Linear 3 Axis Stag, with resolution of 1 μm). Since the sensitivity of the precision balance method was not sufficient to find the in-plane stiffness of the cantilever, we measured the cantilever stiffness in the normal direction. The PDMS beam is stiffer in that direction and can thus easily be detected using the precision balance setup. Since PDMS is an isotropic material, the elastic modulus calculated from the cantilever stiffness in the normal direction will be the same as that of in horizontal direction.

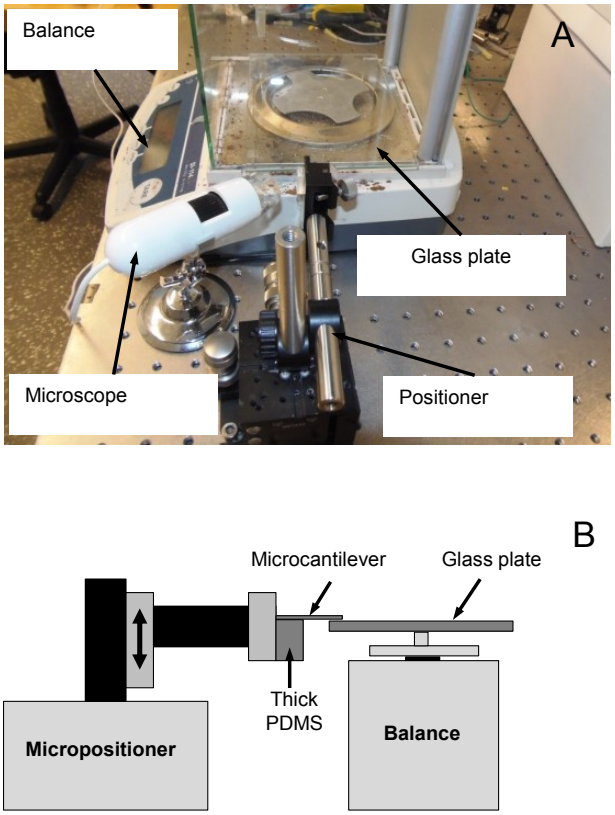


**Figure 6.11**The photograph (A) and schematic diagram (B) of the precision balance setup used for the characterization of the PDMS microcantilever.

The microcantilver was lowered gradually such that comes in contact with the glass plate placed on the balance at 200 µm away from the cantilever's support. The force applied by the microcantilever to the glass plate is directly transferred to the balance. The deflection of the cantilever was considered to be equal to the movement of the micro positioner. To quantify the stiffness of the microcantilever, the amount of force needed for the deflection (δ) of 15 µm, 30 µm, 45 µm, 60 µm of the microcantilever was measured. As shown inFigure 6.12, linear regression was used to estimate the average beam stiffness (K) of 0.35 µN/µm using the equation of F=Kδ from the data obtained in two different experiments.

Where F is bending force which is determined using the balance and δ is the corresponding deflection of the microcantilever.

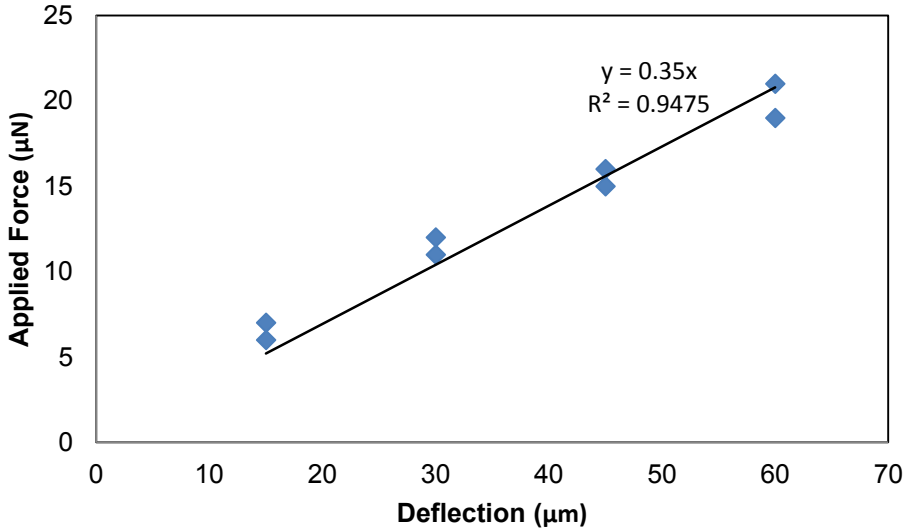


**Figure 6. 12**The force vs. deflection diagram of microcantilever for two different experiments. Linear regression is used to estimate the stiffness of 0.35 µN/µm for the microcantilever.

The force-deflection diagram of the microcantilever confirms the linear behavior of the PDMS microcantilever even for large deflection. The elastic modulus of PDMS (E) was then calculated from the deflection equation of the beam $K= (3EI/L^3)$ to be E= 750 kPa, where I and L are the moment of inertia and distance of the applied force from the cantilever support. This value is close to the value reported for the Young's modulus of thin PDMS layers (M. Liu, Sun, Sun, Bock, & Chen, 2009; A. Sanati Nezhad, et al., 2013).

In order to obtain an estimate of the force that pollen tubes exert on the PDMS microcantilever, using image analysis technique the deflection of the PDMS microcantilever at point J was measured for the two tested pollen tubes (Figure 6.13A). Stress strain relations are used to calculate what forces satisfy the measured deflections

resulted from the interaction between the pollen tube and the PDMS microcantilever. Assuming large deflections, the strain components are defined by the derivatives of deformation u, v, and w in 3D:

$$\varepsilon_x = \frac{\partial u}{\partial x} + \frac{1}{2}\left(\left(\frac{\partial u}{\partial x}\right)^2 + \left(\frac{\partial v}{\partial x}\right)^2 + \left(\frac{\partial w}{\partial x}\right)^2\right) \tag{6.1}$$

$$\varepsilon_y = \frac{\partial v}{\partial y} + \frac{1}{2}\left(\left(\frac{\partial u}{\partial y}\right)^2 + \left(\frac{\partial v}{\partial y}\right)^2 + \left(\frac{\partial w}{\partial y}\right)^2\right) \tag{6.2}$$

$$\varepsilon_z = \frac{\partial w}{\partial z} + \frac{1}{2}\left(\left(\frac{\partial u}{\partial z}\right)^2 + \left(\frac{\partial v}{\partial z}\right)^2 + \left(\frac{\partial w}{\partial z}\right)^2\right) \tag{6.3}$$

$$\varepsilon_{xy} = \frac{\partial u}{\partial y} + \frac{\partial v}{\partial x} + \frac{\partial u}{\partial x} * \frac{\partial u}{\partial y} + \frac{\partial v}{\partial x} * \frac{\partial v}{\partial y} + \frac{\partial w}{\partial x} * \frac{\partial w}{\partial y} \tag{6.4}$$

$$\varepsilon_{yz} = \frac{\partial v}{\partial z} + \frac{\partial w}{\partial y} + \frac{\partial u}{\partial y} * \frac{\partial u}{\partial z} + \frac{\partial v}{\partial y} * \frac{\partial v}{\partial z} + \frac{\partial w}{\partial y} * \frac{\partial w}{\partial z} \tag{6.5}$$

$$\varepsilon_{xy} = \frac{\partial w}{\partial x} + \frac{\partial u}{\partial z} + \frac{\partial u}{\partial z} * \frac{\partial u}{\partial x} + \frac{\partial v}{\partial z} * \frac{\partial v}{\partial x} + \frac{\partial w}{\partial z} * \frac{\partial w}{\partial x} \tag{6.6}$$

The symmetric stress tensor σ in a material is defined as:

$$\sigma = \begin{bmatrix} \sigma_x & \tau_{yx} & \tau_{xz} \\ \tau_{xy} & \sigma_y & \tau_{yz} \\ \tau_{zx} & \tau_{zy} & \sigma_z \end{bmatrix}, \quad \tau_{xy} = \tau_{yx} \ , \quad \tau_{xz} = \tau_{zx} \ , \quad \tau_{yz} = \tau_{zy} \tag{6.7}$$

where $\sigma_x$, $\sigma_y$, $\sigma_z$ are normal stresses and $\tau_{xy}$, $\tau_{yz}$, $\tau_{xz}$ , $\tau_{zx}$ , $\tau_{zy}$ , $\tau_{yx}$ are the shear stresses. The stress-strain relation is given by:

$$\sigma = \mathbf{D}\varepsilon \tag{6.8}$$

where D is the elasticity matrix. The inverse of elasticity matrix is defined by the 6-by-6 matrix as (Beer, 1974):

$$\mathbf{D}^{-1} = 1/E \begin{pmatrix} 1 & -\nu & -\nu & 0 & 0 & 0 \\ -\nu & 1 & -\nu & 0 & 0 & 0 \\ -\nu & -\nu & 1 & 0 & 0 & 0 \\ 0 & 0 & 0 & 2(1+\nu) & 0 & 0 \\ 0 & 0 & 0 & 0 & 2(1+\nu) & 0 \\ 0 & 0 & 0 & 0 & 0 & 2(1+\nu) \end{pmatrix} \quad (6.9)$$

where E is the modulus of elasticity and ν is the Poisson's ratio of PDMS material. The force equilibrium during the interaction is expressed in the global stress tensor as (Beer, 1974):

$$-\nabla.\sigma = \mathbf{F} \quad (6.10)$$

where **F** is the force applied to the microcantilever.We substituted the strain-displacement Equations (6.1) to (6.6) and stress-strain Equation (6.7) in the Equilibrium Equation (6.10), and the resulting equation for static analysis was solved through finite element analysis using COMSOL Multiphysics 3.5 software. We assume that pollen tube exerts a point force (F) at the contact angle of Θ with respect to the horizontal at the contact point (I) to the microcantielever (Figure 6.13B). The experimental results of the interaction of pollen tube and PDMS microcantlever showed that the contact angle and contact point are changing during the interaction (Figure 6.7 and Figure 6.8). Figure 6.13C shows different contact angles at regular intervals of one minute obtained using the image analysis of the progress of bio mechanical interaction. Coordinates of contact points for the two experiments are depicted in Figure 6.14A and Figure 6.14B.

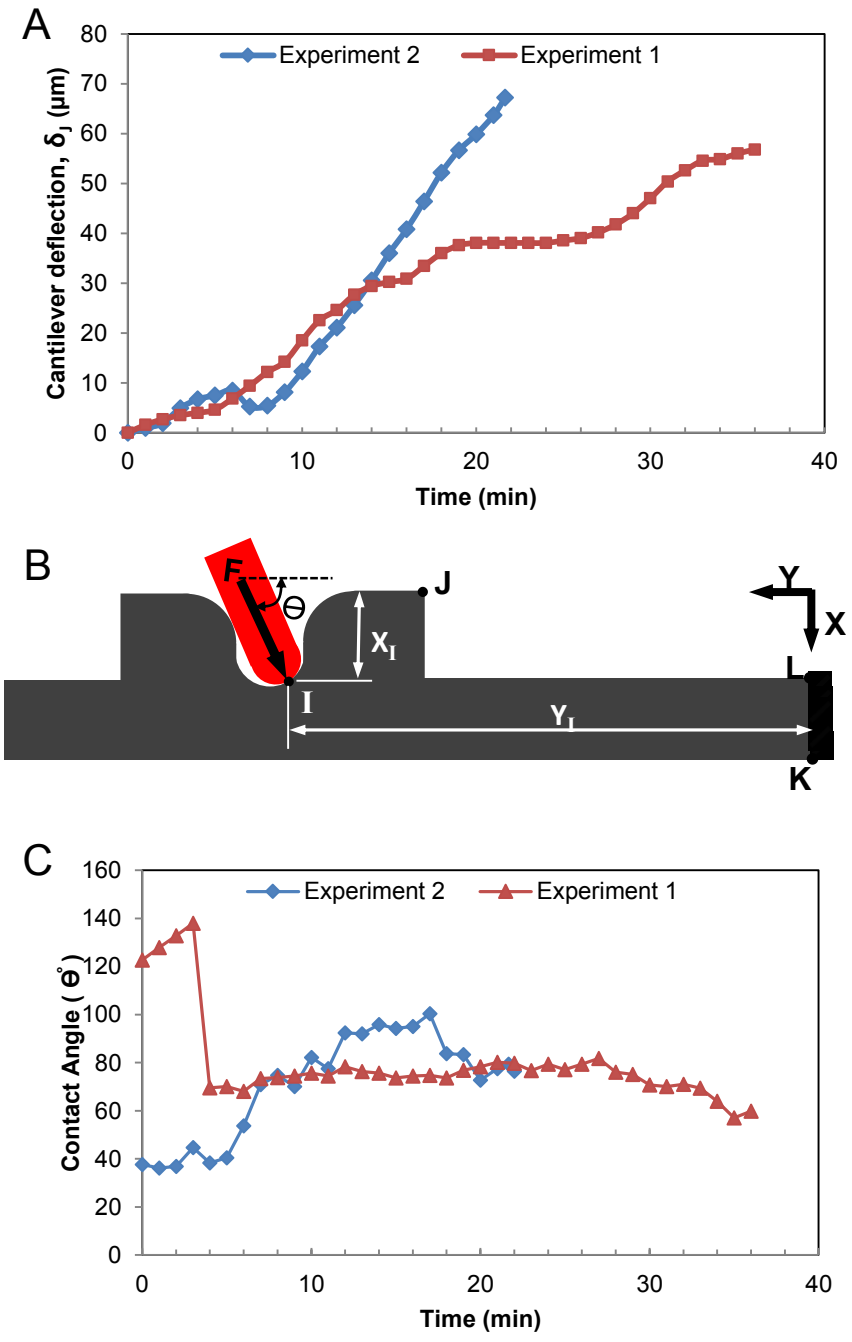


**Figure 6.13** (A) Cantilever deflection at point J versus time measured through image analysis technique for the two experimental interactions. (B) Simplified schematic view of the interaction between an elongating pollen tube and PDMS microcantilever. (C) Different contact angles (Θ) between the pollen tube and PDMS microcantilever at regular intervals of one minute obtained by image analyzing technique for the two experiments.

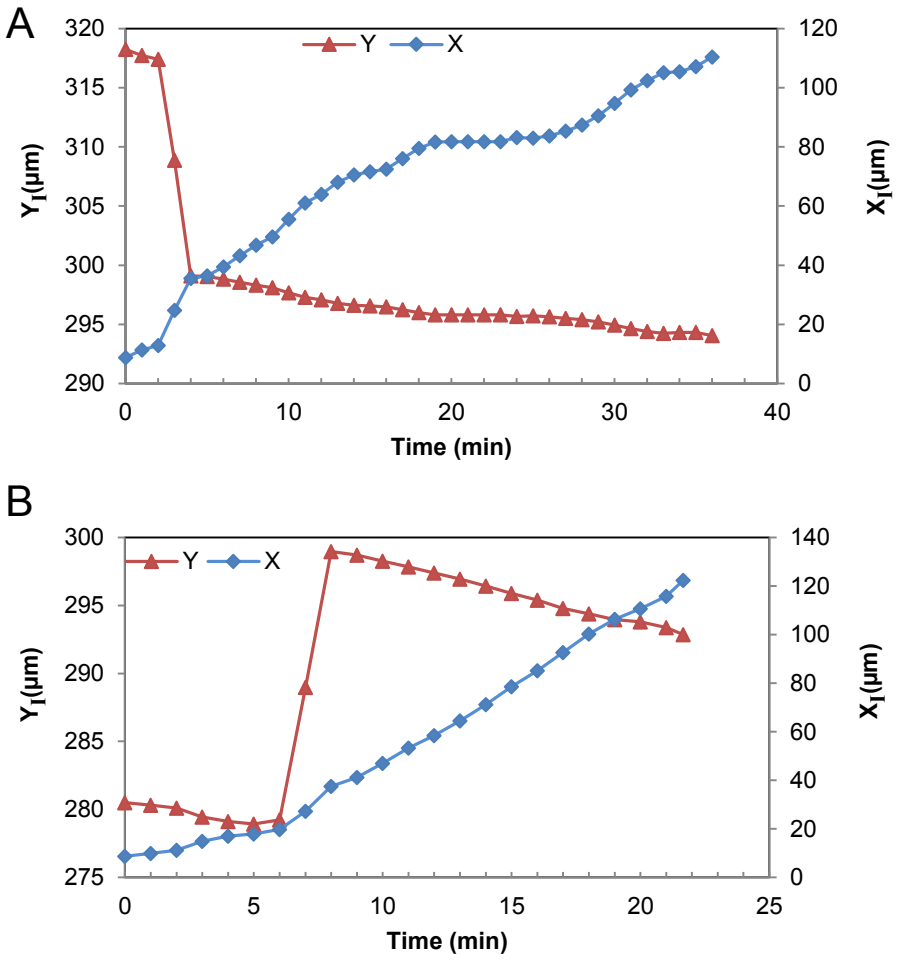


**Figure 6.14** Coordinates of contact points for the (A) first experiment (B**)** second experiment.

The microcantilever was modeled as 3D structure with the dimensions mentioned in the Design and Fabrication section (Figure 6.15). The Young's modulus of E=750 kPa estimated by the precision balance method and the Poisson's ratio of ν=0.45 were chosen for the PDMS material (A Sanati Nezhad, Mahmood Ghanbari, Carlos G Agudelo, Muthukumaran Packirisamy, et al., 2013). As the boundary condition for FEM analysis, the

bottom surface of the microcantilever (MNLK surface) was the fixed support. The geometry of the 3D microcantilever was meshed using quadratic Lagrange elements. A point force with angle Θ with respect to the horizontal direction was applied to the variable contact point of the pollen tube and PDMS microcantilever. To have an estimate of the pollen growth force during the interaction, the force corresponds to the measured deflection was obtained using FEM. The force versus time curves derived for the two experiments are shown in Figure 6.16A.

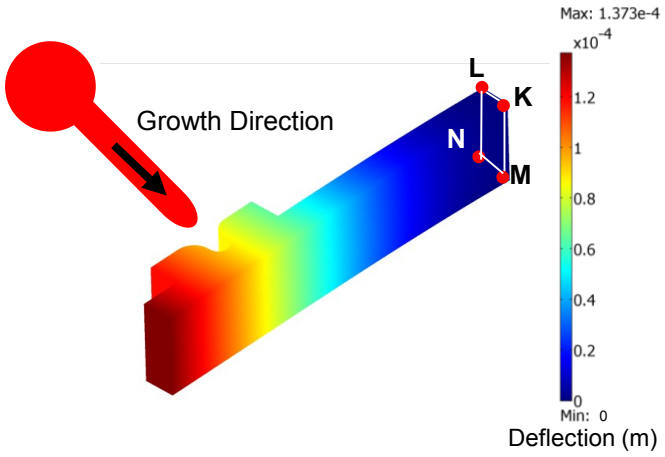


**Figure 6.15**3D view of microcantilever deflection at F= 1.53 µN, Θ=80˚ obtained using COMSOL Multiphysics 3.5 software. The color code represents the deflection of the PDMS microcantilever at the tip.

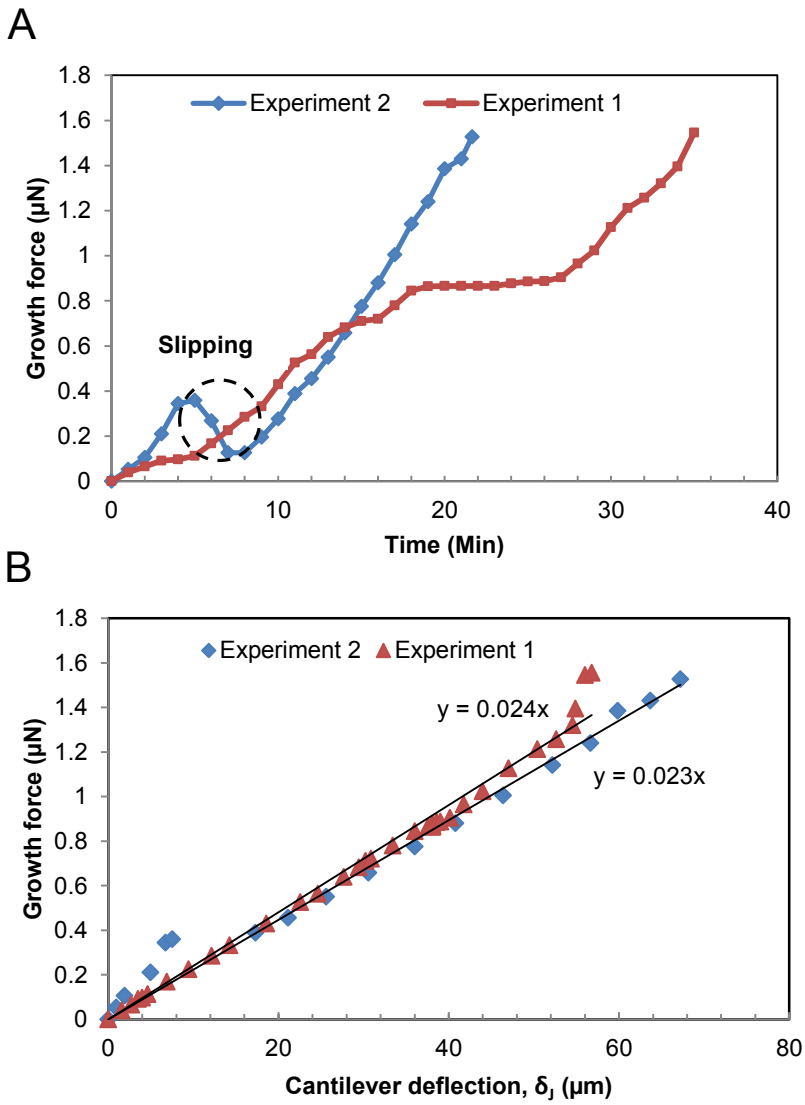


**Figure 6.16**(A) The force versus time curves estimated for the two experiments using 3D FEM simulation. In the case of experiment 2, At t=5min, the pollen tube started to changed its contact point with the microcantilever and slipped along the wall of the cantilever, so provide the space for the cantilever to go backward and as a result, the growth force was reduced in the zone illustrated by a dashed circle on the graph. The contacted points and contact angles between the pollen tube and the microcantilever were considered in the force calculations using FEM. (B) The force-deflection curves obtained using FEM analysis for the two experiments. Using linear regression and extrapolating F to zero cantilever deflection and then computing the slope of the line, the stiffness (K) of 0.023 and 0.024 µN/µm are estimated for PDMS micro cantilever in the two experiments.

Although, we expected the same curve for the deflection-time and force-time graphs, In the case of experiment 2, results show that during the time that the pollen tube was sliding

along the notch, these two curves did not follow each other completely. This may be because of the sharp changes in the contact angle and position of the contact point during that time. The force-deflection curve (Figure 6.16B) obtained using FEM analysis shows that a point force of 1.56 μN with angle of 60 degrees causes the deflection of 58 μm at point J which is equal to the maximum deflection measured for this point using image analysis. For the second experiment, a point force of 1.53 μN with angle of 79 degrees causes deflection of 67 μm at point J which is corresponded to the maximum deflection observed before pollen tube bursting. From the force-deflection curve (Figure 6.16B), using linear regression and extrapolating F to zero cantilever deflection and then computing the slope of the line, the stiffness (K) of 0.023 and 0.024 μN/μm obtained for the two different PDMS microcantilevers used in the first and second experiment respectively.

By estimating the area of the pollen tube apex in contact with the PDMS microcantilever, the effective pressure exerted by the elongating pollen tube onto PDMS microcantilever can be determined. Since the tube apex was obscured by the top edges of the notch wall, the area of contact of pollen tube with the microcantilever could not be visualized clearly when the pollen tube exerted the maximum growth force to the microcantilever. Therefore, the contact area was estimated form the moment that pollen tube touched the microcantilever and deflects it. We assume that pollen tube maintains this contact area with the micocantilever until the moment at which it applies the maximum force to the microcantilever. Experimental results showed that the pollen tube apex flattened slightly within a few seconds of contact with microcantilever. Therefore, contact area (A) was estimated with the formula $A=2\pi Rh$ (area of the flattened spherical cap) where R is the radius of pollen tube (8 μm in our experiment) and h is the flattened height (0.16 μm)

calculated using CAD software (Figure 6.17). By dividing the maximum force (1.53 μN) by the calculated contact area (8.2 $\mu m^2$) the maximum pressure exerted by elongating pollen tube was determined to be 0.19 MPa.

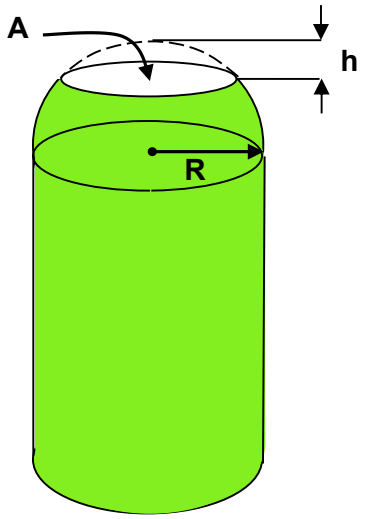


**Figure 6.17**Estimation of the contact area (A) between pollen tube apex and PDMS microcantilever after interaction using the area of the flattened spherical cap.

### 6.5 Discussion and conclusion

To quantify the invasive growth force of an elongating pollen tube, we presented growing pollen tubes with flexible PDMS microcantilevers. The PDMS microcantilever presented here includes a curved notch which prevents in-plane reorientation of pollen tube growth after interaction with the microcantilever. The PDMS microcantilever is flexible enough so that it does not inhibit pollen tube growth after the interaction and it enables quantification of instant growth force of the pollen tub during the interaction. The presented setup is sensitive enough to have the potential to be used for monitoring the fluctuations in force at

the pollen tube apex that might provide more insights into the exocytotic process in pollen tubes. The pollen tube invasive growth force measured through this method is around 1.5 μN which is comparable to the 1.4 μN reported for hyphal invasive growth force using strain gauge (Nicholas P Money, 2004). However, since the size of the fungal hypha is much smaller than camellia pollen tube, almost the same amount of force detected by the strain gauge translates into a much higher turgor pressure in the hypha. Any growth force exerted by elongating pollen tube against the microcantilever is generated by the internal turgor pressure. So the maximum pressure that could be determined from the invasive growth force could not exceed this pressure. We found out that a maximum pressure of 0.19 MPa is exerted on the PDMS microcantilever at the contact area, before the tube bursting occurred. The turgor pressure results in maximum elongation or growth of the wall when pollen tube is allowed to grow freely without any obstacle on it way. But, when the pollen tube encounters obstacle like microcantilever part of the turgor pressure is expended in bending of the cantilever in addition to contributing toward the wall growth. As a result, one could note that the growth rate and growth oscillating frequency reduce after the contact with the cantilever as shown in Figures 6.9 and 6.10. Hence, it becomes important to estimate the turgor pressure under the absence of any growth. In addition, the pressure has to be estimated just before bursting in order to obtain the full extent of turgor pressure. So, the turgor pressure was estimated when the cantilever was bent to maximum position just before bursting. It is also interesting to note that the pollen tube stopped growing for approximately 4 to 6 minutes before bursting. This bursting might be caused because of pollen tube attempts to exert greater force onto the cantilever by increasing the turgor pressure or softening the cell wall. Although there is no number for the turgor pressure of

Camellia pollen tube in the literature, the average turgor pressure reported in the literature for lily pollen tubes which has similar size to Camellia is 0.2 MPa (Benkert et al., 1997).

By analyzing the interaction of elongating pollen tube and serially arranged micro gaps laterally placed within the modified version of the TipChip platform, Sanati Nezhad et al. estimated a maximum turgor pressure of 0.15 MPa exerted on the gap wall by the Camellia pollen tube (Amir Sanati Nezhad et al., 2013a). Therefore the amount of effective pressure we have estimated from the invasive growth force exerted into the microcantilever in the direction of elongation is on the same order of magnitude but somewhat higher. This suggests that the compliance of the cell wall at very tip of the pollen tube is even higher than that at the flanks (Fayant et al., 2010), thus the amount of the turgor –induced pressure transmitted to the microcantilever is more than that transmitted to the miro gap. However, confirmation of this idea needs performing more experiments. We can perform our experiments by administration of different enzymes modulating the mechanical properties of the cell wall at the tube apex, to investigate the effect of this change on the ratio of the turgor-induced pressure that can be transmitted to the microcantilever. Moreover, by using various concentration of sugar in pollen tube growth medium we can change the internal turgor pressure. By investigating the effect of changing turgor pressure on the invasive growth force transmitted to the microcantilever, may contribute to answer outstanding questions in this field such as the controversy around the exact contribution of turgor pressure in the pollen tube growth (J. H. Kroeger et al., 2011; Lawrence J Winship et al., 2010; Zonia, 2010; Zonia et al., 2006).

Our detailed analysis of the pollen tube growth dynamic before and during the contact with microcantilever reveals that, pollen tube growth rate was reduced by 44% during the

contact with the microcantilever. This predicted reduction in the growth rate is probably caused by the force applied by the microcantilver onto the pollen tube tip.

Although the resistance of the microcantilever against elongating pollen tube and as a result the total energy required by advancing pollen tube to overcome this resistance continuously increases during the interaction, the growth rate remained stable over time. Therefore, this energy should be compensated for either by increasing the turgor pressure or by modulation of the cell wall compliance. Our observation did not allow us to discriminate between these two mechanisms. However, detailed analysis of the interaction of elongating pollen tube with serially arranged microgaps(Sanati Nezhad et al., 2013a)support the notion that softening the cell wall is the main mechanism employed by pollen tube to cope with increasing mechanical resistance of the sidewalls.

Moreover, our detailed analysis showed that the peak of oscillation frequency of pollen tube growth rate was reduced between 70-75% for the two tested pollen tubes after contact with the PDMS microcantilever. These changes can be considered as the response of pollen tube to the change in growth conditions due to the interaction with a mechanical obstacle (Feijo et al., 2001; M. A. Messerli, Créton, Jaffe, & Robinson, 2000b; M. A. Messerli & K. R. Robinson, 1998; Mark A Messerli & Kenneth R Robinson, 2003) and also to the change in boundary support conditions for the structure. One possible explanation for the oscillatory growth rate of the pollen tube is a disequilibrium in the force balance between turgor and cell wall strength, regulated by feedback mechanism through chemical signaling cascade (J. Feijó, 1999). Therefore, feedback is believed to be an important parameter involved in controlling pollen tube growth. Changes in oscillation frequency of the pollen tube growth rate resulting from interaction with mechanical obstacle could be a distinctive

signature of the underlying feedback. Therefore analyzing the growth dynamic enables us not only to quantitatively evaluate the effect of a mechanical stimulus on pollen tube functioning but also it can help us understand the feedback mechanism that have been used by pollen tube to regulate its normal growth.

# Chapter 7

## Conclusion and future work

### 1.1 Summary and Conclusion

The main objective of the present thesis was the development of an LOC platform to study morphogenesis of pollen tubes. To attain the objective, various LOC platforms including integrated micromechanical structures and microchannels with different geometries and dimensions, were designed fabricated and tested. These platforms were successful in providing an *ex-vivo* testing environment that physically resembles the *in vivo* growth conditions of the pollen tube and enabled more efficient experimentation on individual pollen tubes under precisely controlled and reproducible conditions. Furthermore, the platform allowed quantifying the invasive growth force of elongating pollen tube for the first time, through characterizing the micromechanical interaction of the pollen tube apex against a calibrated obstacle.

The TipChip, an experimental platform based on microfluidics technology, was developed to enable efficient and high-throughput execution of more sophisticated assays. The device allows positioning of pollen grains at the entrances of serially arranged microchannels equipped with microscopic experimental set-ups. The platform was modular to allow incorporation of various structural, micro-mechanical and chemical testing methods. The device is compatible with Nomarski optics and fluorescence microscopy. Using this platform, we were able to answer several outstanding questions on pollen tube growth. We established that, unlike root hairs and fungal hyphae, pollen tubes do not have a directional memory. The platform opens new avenues for more efficient experimentation and large-scale phenotyping of tip-growing cells under precisely controlled, reproducible conditions.

While performing successfully in preliminary tests, the TipChip had a number of limitations that made large scale experiments problematic. In order to provide reproducible and identical conditions, the fluid flow through all parallel microchannels would have to be similar, and each microchannel would have to be occupied by exactly one pollen grain. Both conditions were not met by the primary version of the TipChip and although functional, this limited the performance of the device at large scale. Most critically, differences in trapping efficiency between the microchannels led to the accumulation of several cells at the entrance of certain microchannels whereas others remained unoccupied. The accumulation of cells resulted in a narrowing of the passage and hence a change in the conditions regulating fluid flow through these microchannels.

To address the aforementioned issues associated with the TipChip, we made a significant modification to the primary design of the TipChip and presented a microfluidic device with an improved knot shaped distributor design which enabled single cell trapping of pollen grains at the entrances of the circularly arranged microchannels. Two different criteria were established to assess the cell trapping probability of each microchannel. Numerical and experimental testing were employed to compare different geometrical design features in terms of the trapping efficiency at the microchannel entrances, and regarding the uniformity of growth conditions within the serially arranged microchannels. The design was optimized based on trapping probability and uniformity of fluid flow conditions within the microchannels. Experimental validation proved the accuracy of the numerical predictions. The growth behavior of pollen tubes was characterized along different geometrical shapes of microchannels. Experimental results illustrated that in the case of straight and curved microchannel, pollen tube growth proceeded at very uniform average

speed and without significant increase or decrease over the measured distance. This is crucial as it shows that the precise location of any testing device to be included in future implementations is not critical in terms of *a priori* pollen tube behavior. On the other hand, for the pollen tube growing through the serpentine-shaped microchannel, the growth rate changed considerably when the pollen tube encountered the microchannel wall and was forced to change its growth direction to follow the direction imposed by the channel wall. It was noted that depending on the collision angle between the pollen tube and the microchannel wall, the pollen tube growth rate decreased dramatically and could temporarily drop to zero. The proposed microfluidic device can easily be modified to accommodate various experimental assays on pollen tubes and it has the potential to be adapted for use with other tip growing cells such as fungal hyphae and filamentous yeast.

In most of the TipChip applications, pollen tubes were surrounded by a limited amount of the culture medium within the microchannels. Therefore, they have access only to the limited amounts of nutrients and oxygen which may potentially have negative effects on pollen tube growth. However, in future applications of the TipChip different kinds of sensor and mechanical obstacles would be embedded within the microchannels which inevitably necessitate changing the dimensions of the microchannels which might influence the pollen tube growth. Thus, it is essential to comprehensively investigate the effect of geometry of the microchannels on pollen tubes growth. Here we systematically addressed the potential concern of the effect of microfluidic network geometry on pollen tube growth. Monitoring the growth rate of pollen tubes passing through the variously sized channel portions enabled us to assess the effect of changes in the widths and depths of the microchannel on the pollen tube growth profile. We found that changing the width

of the microchannel does not have a significant effect on the average pollen tube growth rate. On the other hand, a two-fold increase of the microchannel depth caused a more than 50% increase in pollen tube growth rate. This finding is novel in terms of pollen biology, and we believe understanding the effect of geometry of growth microenvironment on pollen tube growth profile will empower researchers to design more effective and reliable *in vitro* growth environment models for pollen tube analysis.

Measuring the cellular force using microfluidic devices has been done based on designs that include vertical PDMS microcantilevers (Sasoglu et al., 2007; J. L. Tan et al., 2003). However, since fabrication limits the length of vertical cantilevers, they typically have a low aspect ratio which limits the range of forces that can be measured accurately. A high aspect ratio PDMS microcantilever is promising since it may provide sensors with higher sensitivity and improved linear response for LOC applications. Therefore, we developed a practical method for the fabrication of a horizontal high aspect ratio PDMS microcantilever integrated into a microfluidic device and we used the cantilever as a flow meter. A three layer fabrication technique was explored for the integration of micro flow meter. The upper and lower PDMS layers were bonded to the thin layer to release the microcantilever for free deflection. The stiffness of the cantilever was found by a precision balance setup and the elastic modulus was estimated by linear beam theory. The performance of the flow sensor was tested by introducing different flow rates into the microfluidic device and monitoring the cantilever response to the fluid force using optical microscopy method. The dynamic range of flow rates detectable using the flow sensor was found by experimental method. Limited to the accuracy of 1.76 μm resolution of the image taken with optical microscopy, a minimum flow rate of 35 μl/min was detected by the flow meter which is

equal to 0.8 μN resolution in equivalent force at the tip. The sensitivity of the proposed flow sensor can be increased either by modifying the dimension of the microcantilever or by employing higher resolution optical objectives. This flow meter can be integrated into any type of microfluidic-based LOC in which flow measurement is crucial such as flow cytometry and particle separation applications.

Despite the importance of the invasive force in pollen tubes growth, no quantitative data on the growth force of pollen tubes are available up until now. Therefore, in order to quantify the invasive growth force of an elongating pollen tube, we characterized its interaction with a flexible microstructure with calibrated bending properties. To this end the FlexChip, a PDMS-based LOC platform, was designed to harbor growing pollen tubes and to present the elongating apex of the cell with a monolithically integrated PDMS microcantilever. The PDMS microcantilever was designed such that it was flexible enough not to inhibit pollen tube growth after the interaction and also enabled quantification of the instant growth force of the pollen tubes during the interaction. The growth force of growing pollen tubular cells was estimated by Finite Element Analysis (FEA) using the deflection of the microcantilever. The measured growth force through this method is around 1.5 μN which is comparable to the 1.4 μN reported for hyphal invasive growth force using strain gauge (Nicholas P Money, 2004).

Multi-layer soft lithography process was developed for monolithic integration of the PDMS microcantilever within the microfluidic networks. Microfluidic networks and flexible microcantilever are placed in a thin PDMS structural layer (80 μm thick) sandwiched between top and bottom layer to create enclosed microfluidic networks. The bottom layer is a patterned thick PDMS layer containing cavities to release the

microcantilever for free in-plane deflection. The top layer consists of a pattern thin PDMS layer (80 μm) on top of an ultra thin glass slide (100 μm thick) and contains cavities to release the microcantilever. Using a very thin top layer (180 μm thick) allowed us to take high resolution images and made the LOC compatible with confocal microscopy that might be used for fluorescence imaging in future experiments.

Monitoring the growth rate of an elongating pollen tube before and during contact with a microcantilever revealed that the growth rate was reduced by 44% during the contact with the microcantilever. This observed reduction in the growth rate is probably caused by the force applied by the microcantilver onto the pollen tube tip. We observed that although the resistance of the microcantilever against pollen tube growth and as result the rate of the energy dissipation during the interaction increased continuously, the growth rate remained stable over time. This finding confirmed the hypothesis of modulation of the cell wall compliance and in consequence, the rise in the amount of invasive force that could be transmitted to the microcantilever during the interaction.

In order to understand how the interaction between a pollen tube and a PDMS microcantilever can affect the oscillatory growth pattern of a growing pollen tube, the frequencies of the pollen tube growth rate before and during contact with the microcantilever were assessed. Since it is hard to recognize these frequencies just by evaluating the growth rate versus time signal, using Discrete Fourier Transform (DFT), the time domain signal was transformed to the frequency domain and the peak frequency of the oscillation was identified. For the calculation of the DFT, Fast Fourier Transform (FFT) algorithm was employed (R. Zerzour et al., 2009). Then, to obtain waveform analysis reflecting the power of each frequency component associated with the oscillatory

growth, power spectral density (PSD) was employed. The FFT analysis of the growth rate signals for the two tested *Camellia* pollen tubes before and during interaction with the microcantilever showed that the peak of oscillation frequency of pollen tube growth rate was reduced between 70-75% after contact with the PDMS microcantilever, verified by the result obtained using PSD analysis. These changes can be considered as the response of pollen tube to the change in growth conditions due to the interaction with a mechanical obstacle. Therefore analyzing the growth dynamic enables us not only to quantitatively evaluate the effect of a mechanical stimulus on pollen tube functioning but also it can help us to understand the feedback mechanism that have been used by pollen tube to regulate its normal growth.

Any growth force exerted by elongating pollen tube against the microcantilever is generated by the internal turgor pressure. So the maximum pressure that could be determined from the invasive growth force cannot exceed this pressure. We found out that a maximum pressure of 0.19 MPa is exerted on the PDMS microcantilever at the contact area, before the tube bursting occurred. This bursting might be caused because of pollen tube attempts to exert greater force onto the cantilever by increasing the turgor pressure or softening the cell wall. Although there is no number for the turgor pressure of *Camellia* pollen tube in the literature, the average turgor pressure reported in the literature for lily pollen tubes which has similar size to *Camellia* is 0.2 MPa (Benkert et al., 1997). Therefore, the amount of effective pressure we have determined from the invasive growth force is very close to the average turgor pressure reported for pollen tubes of similar size to *Camellia* in the literature. This suggests that the compliance of the cell wall at the pollen

tube tip is very high, thus almost all of the turgor pressure (95 %) is exerted against the PDMS microcantilever. However, confirmation of this idea warrants more experiments.

## 1.2 Future work

In the present thesis, several microfluidic based LOC platforms were employed to study biology of a kind of tip growing plant cell, namely the pollen tube. Although outstanding results were obtained through experimentations using the aforementioned platforms, there are still many unanswered questions regarding the biology of the pollen tube and other kinds of tip growing cells which requires performing further experiments or improve the current designs of the platforms. Here are some suggestions for future research:

a. The proposed TipChip platform was only tested with *Camellia* pollen tubes. In order to support the versatility of the TipChip, the platform can easily be modified to accommodate different experimental assays on other species of tip growing cells such as *Arabidopsis* pollen tubes, fungal hyphae and filamentous yeast.

b. It was suggested that pulsatile growth in pollen tubes may be caused by oscillations in turgor pressure. However, the resolutions of the existing turgor pressure measurement techniques were not enough to detect putative changes in turgor pressure of elongating pollen tubes. The dimensions of the integrated microcantilever within the FlexChip can be modified such as to make it sensitive enough to detect the possible changes in turgor pressure.

c. The presented FlexChip platform enabled quantification of the instant growth force of elongating pollen tubes and deduce the amount of turgor pressure transmitted to the PDMS microcantilever. Different enzymes modulating the mechanical properties of the cell wall can be applied at the tube apex to investigate the effect of this change on the ratio

of turgor-induced pressure that can be transmitted to the microcantilever. Insight from this research will improve our understanding of the contribution of the cell wall mechanical properties on pollen tube morphogenesis.

d. Pollen tube turgor pressure can be changed by using various concentration of sugar in the growth medium. Investigating the effect of changing turgor pressure on the invasive growth force transmitted to the microcantilever may contribute to answering outstanding questions in the field of pollen tube biology such as the controversy around the exact contribution of turgor pressure in the pollen tube growth (J. H. Kroeger et al., 2011; Lawrence J Winship et al., 2010; Zonia, 2010; Zonia et al., 2006).

e. In the present thesis image analysis was used to measure the deflection of the PDMS microcantilever due to interaction with the elongating pollen tube. Therefore, the amount of the minimum growth force that could be detected using FlexChip was related to the resolution of the images taken with optical microscopy. In the future application of the FlexChip, a simple optical detection system can be integrated within the platform to directly measure the growth force and also improve the detection limit.

f.FEM can be utilized to present a time dependent model for the growth and interaction of a growing pollen tube with flexible PDMS microcantilever. Comparing the experimental results obtained using FlexChip by those predicted by FEM may allow to estimate different parameters involved in pollen tube growth such as turgor pressure and mechanical properties of the cell wall.

## 7.3 Contributions of the present work

From the current thesis, the following articles have been published or submitted.

### 7.3.1 Journal papers

[1] **M. Ghanbari**, A. Sanati Nezhad, C.G. Agudelo, M. Packirisamy, A. Geitmann, "*Microfluidic positioning of pollen grains in lab-on-a-chip for single cell analysis"*,J. Biosci.Bioeng., (2013), http://dx.doi.org/10.1016/j.jbiosc.2013.10.001.

[2] C. G. Agudelo*, A. Sanati Nezhad*, **M. Ghanbari***, M. Naghavi, M. Packirisamy, A. Geitmann, "*TipChip- a modular, MEMS (micro-electro-mechanical systems) based platform for the investigation of tip growing cells*", The plant J, vol: 73, pp:1057-1068, 2013. [***equal contributions**].

[3] A. Sanati Nezhad, **Mahmood Ghanbari**, Carlos Agudelo, Muthukumaran Packirisamy, Rama B. Bhat, Anja Geitmann, "*PDMS microcantilever-based flow sensor integration for lab-on-chip*", IEEE sensors J, vol. 13, pp: 601-609, 2012.

[4] A. Sanati Nezhad, **M. Ghanbari**, C. G. Agudelo, M. Naghavi, M. Packirisamy, R. B. Bhat, A. Geitmann, "*Optimization of flow assisted entrapment of pollen grains in a microfluidic platform for tip growth analysis*", Biomedical Microdevices, 2013 DOI 10.1007/s10544-013-9802-8.

[5] C. G. Agudelo, A. Sanati Nezhad, **M. Ghanbari**, M. Packirisamy, A. Geitmann, "*A Microfluidic Platform for the Investigation of Elongation Growth in Pollen Tubes*", J. Micromechanics and Microengineering, vol. 22, 115009, 2012.

[6] **M. Ghanbari**, M.Packirisamy, A. Geitmann, "*Flexure Integrated Lab-on-a-chip (FlexChip) on Polymer for Biomechanical Study of Cellular Growth Force of Camellia Pollen Tip GrowingCells*", 2013 [To be submitted to Nature Methods].

[7] **M. Ghanbari,** M.Packirisamy, A. Geitmann, "*Influence of Microenvironment Geometry on Cell Behavior*", 2013 [To be submitted to Microfluidics and Nanofluidics].

### 7.3.2 Conferences and presentations

[1] **M. Ghanbari**, M. Packirisamy, A. Geitmann, "*A Microfluidic Platform for the Investigation of Directional Memory in Tip Growing*", Lab-on-a-Chip European Congress, Spain, 5th - 6th March, 2013.

[2] C. G. Agudelo,**A.** Sanati Nezhad, M. **Ghanbari**, Naghavi, M., Packirisamy, M., Geitmann, A. "*Combining live cell imaging and MEMS (microelectromechanical systems) technology*", Annual Meeting of Microscopical Society of Canada, British Columbia, Canada, June 19-21, 2013

[3] A. Sanati Nezhad, **M. Ghanbari**, C. Agudelo, M. Packirisamy, R.B. Bhat, "*A new PDMS microcantilever with integrated waveguide for biosensing application*", Photonic North 2012, Montreal, Canada.

[4] **M. Ghanbari,** M. Packirisamy, A. Sanati Nezhad, "*Finite Element Modeling of Novel MEMS Based Pressure/flow Sensor with Optical readout"* Photonic North 2011, Ottawa, Canada.

[5] A. Sanati Nezhad, **M.Ghanbari**, M. Packirisamy, R. B. Bha*t "Simulation of detecting PDMS microcantilever deflection using Integrated Optical fibers",* Photonic North 2011, Ottawa,Canada.

## References:


Agudelo, C., Sanati, A., Ghanbari, M., Packirisamy, M., & Geitmann, A. (2012). A microfluidic platform for the investigation of elongation growth in pollen tubes. *Journal of Micromechanics and Microengineering, 22*(11), 115009.

Agudelo, C. G., Sanati Nezhad, A., Ghanbari, M., Naghavi, M., Packirisamy, M., & Geitmann, A. (2013). TipChip: a modular, MEMS-based platform for experimentation and phenotyping of tip-growing cells. *The Plant Journal*.

Anderson, J. R., Chiu, D. T., Jackman, R. J., Cherniavskaya, O., McDonald, J. C., Wu, H., Whitesides, G. M. (2000). Fabrication of topologically complex three-dimensional microfluidic systems in PDMS by rapid prototyping. *Analytical Chemistry, 72*(14), 3158-3164.

Andersson, H., & Van den Berg, A. (2003). Microfluidic devices for cellomics: a review. *Sensors and Actuators B: Chemical, 92*(3), 315-325.

Ashauer, M., Glosch, H., Hedrich, F., Hey, N., Sandmaier, H., & Lang, W. (1999). Thermal flow sensor for liquids and gases based on combinations of two principles. *Sensors and Actuators A: Physical, 73*(1), 7-13.

Balaban, N. Q., Schwarz, U. S., Riveline, D., Goichberg, P., Tzur, G., Sabanay, I., Addadi, L. (2001). Force and focal adhesion assembly: a close relationship studied using elastic micropatterned substrates. *Nature cell biology, 3*(5), 466-472.

Bastmeyer, M., Deising, H. B., & Bechinger, C. (2002). Force exertion in fungal infection. *Annual review of biophysics and biomolecular structure, 31*(1), 321-341.

Beebe, D. J., Mensing, G. A., & Walker, G. M. (2002). Physics and applications of microfluidics in biology. *Annual review of biomedical engineering, 4*(1), 261-286.

Benkert, R., Obermeyer, G., & Bentrup, F.-W. (1997). The turgor pressure of growing lily pollen tubes. *Protoplasma, 198*(1-2), 1-8.

Bibikova, T. N., Zhigilei, A., & Gilroy, S. (1997). Root hair growth in Arabidopsis thaliana is directed by calcium and an endogenous polarity. *Planta, 203*(4), 495-505.

Birkbeck, A. L., Flynn, R. A., Ozkan, M., Song, D., Gross, M., & Esener, S. C. (2003). VCSEL arrays as micromanipulators in chip-based biosystems. *Biomedical microdevices, 5*(1), 47-54.

Blewett, J., Burrows, K., & Thomas, C. (2000). A micromanipulation method to measure the mechanical properties of single tomato suspension cells. *Biotechnology letters, 22*(23), 1877-1883.

Bou Daher, F., Chebli, Y., & Geitmann, A. (2008). Optimization of conditions for germination of cold-stored *Arabidopsis thaliana* pollen. *Plant Cell Reports, 28*, 347–357.

Bou Daher, F., & Geitmann, A. (2011). Actin is involved in pollen tube tropism through redefining the spatial targeting of secretory vesicles. *Traffic, 12*, 1537–1551

Brand, A., & Gow, N. A. R. (2008). Mechanisms of hypha orientation of fungi. *Current Opinion in Microbiology, 12*, 350-357.

Brush, L., & Money, N. P. (1999). Invasive Hyphal Growth in Wangiella dermatitidis Is Induced by Stab Inoculation and Shows Dependence upon Melanin Biosynthesis. *Fungal Genetics and Biology, 28*(3), 190-200.

Bubendorfer, A., Liu, X., & Ellis, A. (2007). Microfabrication of PDMS microchannels using SU-8/PMMA moldings and their sealing to polystyrene substrates. *Smart Materials and Structures, 16*, 367-371.

Carlson, R. H., Gabel, C. V., Chan, S. S., Austin, R. H., Brody, J. P., & Winkelman, J. W. (1997). Self-sorting of white blood cells in a lattice. *Physical review letters, 79*(11), 2149.

Chabert, M., & Viovy, J.-L. (2008). Microfluidic high-throughput encapsulation and hydrodynamic self-sorting of single cells. *Proceedings of the National Academy of Sciences, 105*(9), 3191-3196.

Chandrasekaran, A., & Packirisamy, M. (2009). *Integrated biophotonic Micro Total Analysis Systems for flow cytometry and particle detection.* Paper presented at the SPIE Photonics North.

Chang, W. C., Lee, L. P., & Liepmann, D. (2005). Biomimetic technique for adhesion-based collection and separation of cells in a microfluidic channel. *Lab Chip, 5*(1), 64-73.

Chebli, Y., & Geitmann, A. (2007). Mechanical principles governing pollen tube growth. *Functional Plant Science and Biotechnology, 1*(2), 232-245.

Cheung, A. Y., & Wu, H.-m. (2007). Structural and functional compartmentalization in pollen tubes. *Journal of Experimental Botany, 58*, 75-82.

Cheung, A. Y., & Wu, H.-m. (2008). Structural and signaling networks for the polar cell growth machinery in pollen tubes. *Annual Review in Plant Biology, 59*, 547-572.

Cheung, K., & Renaud, P. (2006). BioMEMS for medicine: On-chip cell characterization and implantable microelectrodes. *Solid State Electronics, 50*, 551-557.

Chiou, P. Y., Ohta, A. T., & Wu, M. C. (2005). Massively parallel manipulation of single cells and microparticles using optical images. *Nature, 436*(7049), 370-372.

Cho, S. H., Chen, C. H., Tsai, F. S., Godin, J. M., & Lo, Y.-H. (2010). Human mammalian cell sorting using a highly integrated micro-fabricated fluorescence-activated cell sorter (μFACS). *Lab on a Chip, 10*(12), 1567-1573.

Chung, J., Kim, Y. J., & Yoon, E. (2011). Highly-efficient single-cell capture in microfluidic array chips using differential hydrodynamic guiding structures. *Applied Physics Letters, 98*, 123701.

Cui, S., Liu, Y., Wang, W., Sun, Y., & Fan, Y. (2011). A microfluidic chip for highly efficient cell capturing and pairing. *Biomicrofluidics, 5*, 032003.

Davis, D. J., Burlak, C., & Money, N. P. (2000). Osmotic pressure of fungal compatible osmolytes. *Mycological Research, 104*(7), 800-804.

Di Carlo, D., Aghdam, N., & Lee, L. P. (2006). Single-cell enzyme concentrations, kinetics, and inhibition analysis using high-density hydrodynamic cell isolation arrays. *Analytical chemistry, 78*(14), 4925-4930.

Di Carlo, D., Wu, L. Y., & Lee, L. P. (2006). Dynamic single cell culture array. *Lab Chip, 6*(11), 1445-1449.

Dijkstra, M., De Boer, M., Berenschot, M., Lammerink, T., Wiegerink, R., & Elwenspoek, M. (2007). *Miniaturized flow sensor with planar integrated sensor structures on semicircular surface channels.* Paper presented at the Micro Electro Mechanical Systems, 2007. MEMS. IEEE 20th International Conference on.

El-Ali, J., Sorger, P. K., & Jensen, K. F. (2006). Cells on chips. *Nature, 442*(7101), 403-411.

Fayant, P., Girlanda, O., Chebli, Y., Aubin, C.-É., Villemure, I., & Geitmann, A. (2010). Finite element model of polar growth in pollen tubes. *The Plant Cell Online, 22*(8), 2579-2593.

Feijó, J. (1999). The Pollen Tube Oscillator: Towards a Molecular Mechanism of Tip Growth? *Fertilization in Higher Plants* (pp. 317-336): Springer.

Feijó, J. A., Malhó, R., & Obermeyer, G. (1995). Ion dynamics and its possible role during in vitro pollen germination and tube growth. *Protoplasma, 187*, 155-167.

Feijo, J. A., Sainhas, J., Holdaway-Clarke, T., Cordeiro, M. S., Kunkel, J. G., & Hepler, P. K. (2001). Cellular oscillations and the regulation of growth: the pollen tube paradigm. *Bioessays, 23*(1), 86-94.

Felekis, D., Muntwyler, S., Vogler, H., Beyeler, F., Grossniklaus, U., & Nelson, B. (2011). Quantifying growth mechanics of living, growing plant cells *in situ* using microrobotics. *Micro Nano Letters, 6*, 311-316.

Flynn, R. A., Birkbeck, A. L., Gross, M., Ozkan, M., Shao, B., Wang, M. M., & Esener, S. C. (2002). Parallel transport of biological cells using individually addressable VCSEL arrays as optical tweezers. *Sensors and Actuators B: Chemical, 87*(2), 239-243.

Furdui, V. I., & Harrison, D. J. (2004). Immunomagnetic T cell capture from blood for PCR analysis using microfluidic systems. *Lab Chip, 4*(6), 614-618.

Galbraith, C. G., & Sheetz, M. P. (1997). A micromachined device provides a new bend on fibroblast traction forces. *Proceedings of the National Academy of Sciences, 94*(17), 9114-9118.

Geitmann, A. (1999). The rheological properties of the pollen tube cell wall *Fertilization in Higher Plants* (pp. 283-302): Springer.

Geitmann, A. (2006). Experimental approaches used to quantify physical parameters at cellular and subcellular levels. *American Journal of Botany, 93*(10), 1380-1390.

Geitmann, A., & Dumais, J. (2009). Not-so-tip-growth. *Plant Signaling & Behavior, 4*, 136-138.

Geitmann, A., McConnaughey, W., Lang-Pauluzzi, I., Franklin-Tong, V. E., & Emons, A. M. C. (2004). Cytomechanical properties of *Papaver* pollen tubes are altered after self-incompatibility challenge. *Biophysical Journal, 86*, 3314-3323.

Geitmann, A., & Palanivelu, R. (2007). Fertilization requires communication: signal generation and perception during pollen tube guidance. *Floriculture and Ornamental Biotechnology, 1*(2), 77-89.

Geitmann, A., & Parre, E. (2004). The local cytomechanical properties of growing pollen tubes correspond to the axial distribution of structural cellular elements. *Sexual Plant Reproduction, 17*(1), 9-16.

Geitmann, A., & Steer, M. W. (2006). The architecture and properties of the pollen tube cell wall. In R. Malhó (Ed.), *The pollen tube: a cellular and molecular perspective, Plant Cell Monographs* (Vol. 3, pp. 177-200). Berlin Heidelberg: Springer Verlag.

Ghanbari, M., Sanati, A., Agudelo, C., Packirisamy, M., & Geitmann, A. (2013). Microfluidic positioning of pollen grains in LOC for single cell analysis. *Journal of Bioscience and Bioengineering*.

Giouroudi, I., Kosel, J., & Scheffer, C. (2008). BioMEMS in diagnostics: A review and recent developments. *Recent Patents on Engineering, 2*, 114-121.

Gossett, D. R., Weaver, W. M., Ahmed, N. S., & Di Carlo, D. (2011). Sequential Array Cytometry: Multi-Parameter Imaging with a Single Fluorescent Channel. *Annals of biomedical engineering, 39*(4), 1328-1334.

Gossot, O., & Geitmann, A. (2007). Pollen tube growth - Coping with mechanical obstacles involves the cytoskeleton. *Planta, 226*, 405-416.

Goyal, G., & Nam, Y. (2011). Neuronal micro-culture engineering by microchannel devices of cellular scale dimensions. *Biomedical Engineering Letters, 1*(2), 89-98.

Green, P. B. (1968). Growth physics in Nitella: a method for continuous in vivo analysis of extensibility based on a micro-manometer technique for turgor pressure. *Plant Physiology, 43*(8), 1169-1184.

Greminger, M. A., & Nelson, B. J. (2004). Vision-based force measurement. *Pattern Analysis and Machine Intelligence, IEEE Transactions on, 26*(3), 290-298.

Grodzinski, P., Yang, J., Liu, R., & Ward, M. (2003). A modular microfluidic system for cell pre-concentration and genetic sample preparation. *Biomedical microdevices, 5*(4), 303-310.

Gross, P. G., Kartalov, E. P., Scherer, A., & Weiner, L. P. (2007). Applications of microfluidics for neuronal studies. *Journal of the neurological sciences, 252*(2), 135-143.

Grossmann, G., Guo, W.-J., Ehrhardt, D. W., Frommer, W. B., Sit, R. V., Quake, S. R., & Meier, M. (2011). The RootChip: an integrated microfluidic chip for plant science. *The Plant Cell Online, 23*(12), 4234-4240.

Hanson, K., Filipponi, L., Lee, A., & Nicolau, D. (2005). *Negotiation of obstacles by fungi in micro-fabricated structures: to turn or not to turn?* Paper presented at the Microtechnology in Medicine and Biology, 2005. 3rd IEEE/EMBS Special Topic Conference on.

Hanson, K. L., Nicolau, D. V., Filipponi, L., Wang, L., & Lee, A. P. (2006). Fungi use efficient algorithms for the exploration of microfluidic networks. *small, 2*(10), 1212-1220.

Harold, F. M. (2002). Force and compliance: rethinking morphogenesis in walled cells. *Fungal Genetics and Biology, 37*(3), 271-282.

Harold, F. M., Harold, R. L., & Money, N. P. (1995). What forces drive cell wall expansion? *Canadian journal of botany, 73*(S1), 379-383.

Held, M., Edwards, C., & Nicolau, D. (2011). Probing the growth dynamics of *Neurospora crassa* with microfluidic structures. *Fungal Biology, 115*, 493-505.

Hepler, P. K., Vidali, L., & Cheung, A. Y. (2001). Polarized cell growth in higher plants. *Annual Review of Cell and Developmental Biology, 17*, 159-187.

Higashiyama, T., & Hamamura, Y. (2008). Gametophytic pollen tube guidance. *Sexual Plant Reproduction, 21*, 17-26.

Hirschfelder, J. O., Curtiss, C. F., & Bird, R. B. (1954). *Molecular theory of gases and liquids* (Vol. 26): Wiley New York.

Holdaway-Clarke, T. L., Weddle, N. M., Kim, S., Robi, A., Parris, C., Kunkel, J. G., & Hepler, P. K. (2003). Effect of extracellular calcium, pH and borate on growth oscillations in Lilium formosanum pollen tubes. *Journal of experimental botany, 54*(380), 65-72.

Honys, D., & Twell, D. (2003). Comparative analysis of the *Arabidopsis* pollen transcriptome. *Plant Physiology, 132*, 640-652.

Honys, D., & Twell, D. (2004). Transcriptome analysis of haploid male gametophyte development in *Arabidopsis*. *Genome Biology, 5*, R85.

Hossain, S., Packirisamy, M., & Rakheja, S. (2010). *Dynamic Behavior of Microcantilever under Periodic Flow of Viscous Fluids*. Paper presented at the Vetomac VI, New Delhi, India.

Howard, R. J., & Valent, B. (1996). Breaking and entering: host penetration by the fungal rice blast pathogen Magnaporthe grisea. *Annual Reviews in Microbiology, 50*(1), 491-512.

Huang, Y., & Rubinsky, B. (2001). Microfabricated electroporation chip for single cell membrane permeabilization. *Sensors and Actuators A: Physical, 89*(3), 242-249.

Hüsken, D., Steudle, E., & Zimmermann, U. (1978). Pressure probe technique for measuring water relations of cells in higher plants. *Plant Physiology, 61*(2), 158-163.

Jaalouk, D. E., & Lammerding, J. (2009). Mechanotransduction gone awry. *Nature reviews Molecular cell biology, 10*(1), 63-73.

Jo, B.-H., Van Lerberghe, L. M., Motsegood, K. M., & Beebe, D. J. (2000). Three-dimensional micro-channel fabrication in polydimethylsiloxane (PDMS) elastomer. *Microelectromechanical Systems, Journal of, 9*(1), 76-81.

Kang, J. H., Um, E., & Park, J.-K. (2009). Fabrication of a poly (dimethylsiloxane) membrane with well-defined through-holes for three-dimensional microfluidic networks. *Journal of Micromechanics and Microengineering, 19*(4), 045027.

Khademhosseini, A., Yeh, J., Jon, S., Eng, G., Suh, K. Y., Burdick, J. A., & Langer, R. (2004). Molded polyethylene glycol microstructures for capturing cells within microfluidic channels. *Lab Chip, 4*(5), 425-430.

Kim, D.-H., Wong, P. K., Park, J., Levchenko, A., & Sun, Y. (2009). Microengineered platforms for cell mechanobiology. *Annual review of biomedical engineering, 11*, 203-233.

Kim, M. C., Wang, Z., Lam, R. H. W., & Thorsen, T. (2008). Building a better cell trap: Applying Lagrangian modeling to the design of microfluidic devices for cell biology. *Journal of Applied Physics, 103*, 044701.

Kim, S. H., Yamamoto, T., Fourmy, D., & Fujii, T. (2011). Electroactive Microwell Arrays for Highly Efficient Single-Cell Trapping and Analysis. *small, 7*(22), 3239-3247.

Kim, T. K., Kim, J. K., & Jeong, O. C. (2011). Measurement of nonlinear mechanical properties of PDMS elastomer. *Microelectronic Engineering, 88*(8), 1982-1985.

Kloter, U., Schmid, H., Wolf, H., Michel, B., & Juncker, D. (2004). *High-resolution patterning and transfer of thin PDMS films: Fabrication of hybrid self-sealing 3D microfluidic systems.* Paper presented at the Micro Electro Mechanical Systems, 2004. 17th IEEE International Conference on (MEMS).

Ko, J.-M., Ju, J., Lee, S., & Cha, H.-C. (2006). Tobacco protoplast culture in a polydimethylsiloxane-based microfluidic channel. *Protoplasma, 227*(2-4), 237-240.

Kobel, S., Valero, A., Latt, J., Renaud, P., & Lutolf, M. (2010). Optimization of microfluidic single cell trapping for long-term on-chip culture. *Lab Chip, 10*(7), 857-863.

Kroeger, J., & Geitmann, A. (2012). The pollen tube paradigm revisited. *Current Opinion in Plant Biology, 15*, 618-624.

Kroeger, J. H., Zerzour, R., & Geitmann, A. (2011). Regulator or driving force? The role of turgor pressure in oscillatory plant cell growth. *PloS one, 6*(4), e18549.

Kuoni, A., Holzherr, R., Boillat, M., & de Rooij, N. F. (2003). Polyimide membrane with ZnO piezoelectric thin film pressure transducers as a differential pressure liquid flow sensor. *Journal of Micromechanics and Microengineering, 13*(4), S103.

Lee, H., Purdon, A., & Westervelt, R. (2004). Manipulation of biological cells using a microelectromagnet matrix. *Applied Physics Letters, 85*, 1063.

Lee, P., Helman, N., Lim, W., & Hung, P. (2008). A microfluidic system for dynamic yeast cell imaging. *Biotechniques, 44*, 91-95.

Lew, R. R. (2005). Mass flow and pressure-driven hyphal extension in Neurospora crassa. *Microbiology, 151*(8), 2685-2692.

Li, H., Lin, Y., Heath, R. M., Zhu, M. X., & Yang, Z. (1999). Control of pollen tube tip growth by a Rop GTPase–dependent pathway that leads to tip-localized calcium influx. *The Plant Cell Online, 11*(9), 1731-1742.

Lien, V., & Vollmer, F. (2007). Microfluidic flow rate detection based on integrated optical fiber cantilever. *Lab on a Chip, 7*(10), 1352-1356.

Lin, I., Liao, Y.-M., Liu, Y., Ou, K.-S., Chen, K.-S., & Zhang, X. (2008). Viscoelastic mechanical behavior of soft microcantilever-based force sensors. *Applied Physics Letters, 93*(25), 251907-251907-251903.

Lin, Y.-C., Jen, C.-M., Huang, M.-Y., Wu, C.-Y., & Lin, X.-Z. (2001). Electroporation microchips for continuous gene transfection. *Sensors and Actuators B: Chemical, 79*(2), 137-143.

Lintilhac, P. M., Wei, C., Tanguay, J. J., & Outwater, J. O. (2000). Ball tonometry: a rapid, nondestructive method for measuring cell turgor pressure in thin-walled plant cells. *Journal of plant growth regulation, 19*(1), 90-97.

Liu, M., Sun, J., Sun, Y., Bock, C., & Chen, Q. (2009). Thickness-dependent mechanical properties of polydimethylsiloxane membranes. *Journal of Micromechanics and Microengineering, 19*(3), 035028.

Liu, X., Kim, K., Zhang, Y., & Sun, Y. (2009). Nanonewton force sensing and control in microrobotic cell manipulation. *The international journal of robotics research, 28*(8), 1065-1076.

Lord, E. M. (2003). Adhesion and guidance in compatible pollination. *Journal of Experimental Botany, 54*, 47-54.

Lötters, J., Olthuis, W., Veltink, P., & Bergveld, P. (1997). The mechanical properties of the rubber elastic polymer polydimethylsiloxane for sensor applications. *Journal of Micromechanics and Microengineering, 7*(3), 145.

Mahoney, M. J., Chen, R. R., Tan, J., & Mark Saltzman, W. (2005). The influence of microchannels on neurite growth and architecture. *Biomaterials, 26*(7), 771-778.

Malhó, R. (2006). *The pollen tube: a cellular and molecular perspective* (Vol. 3). Berlin Heidelberg: Springer Verlag.

Malhó, R., Feijó, J. A., & Pais, M. S. S. (1992). Effect of electrical fields and external ionic currents on pollen tube orientation. *Sexual Plant Reprdocuction, 5*, 57-63.

Marcy, Y., Ouverney, C., Bik, E. M., Lösekann, T., Ivanova, N., Martin, H. G., . . . Relman, D. A. (2007). Dissecting biological "dark matter" with single-cell genetic analysis of rare and uncultivated TM7 microbes from the human mouth. *Proceedings of the National Academy of Sciences, 104*(29), 11889-11894.

Márton, M., & Dresselhaus, T. (2010). Female gametophyte-controlled pollen tube guidance. *Biochemical Society Transactions, 38*, 627-630.

Messerli, M., & Robinson, K. R. (1997). Tip localized $Ca^{2+}$ pulses are coincident with peak pulsatile growth rates in pollen tubes of *Lilium longiflorum*. *Journal of Cell Science, 110*, 1269-1278.

Messerli, M., & Robinson, K. R. (1998). Cytoplasmic acidification and current influx follow growth pulses of *Lilium longiflorum* pollen tubes. *Plant Journal, 16*, 87-91.

Messerli, M. A., Créton, R., Jaffe, L. F., & Robinson, K. R. (2000a). Periodic increases in elongation rate precede increases in cytosolic Ca $^{2+}$ during pollen tube growth. *Developmental biology, 222*(1), 84-98.

Messerli, M. A., & Robinson, K. R. (1998). Cytoplasmic acidification and current influx follow growth pulses ofLilium longiflorumpollen tubes. *The Plant Journal, 16*(1), 87-91.

Messerli, M. A., & Robinson, K. R. (2003). Ionic and osmotic disruptions of the lily pollen tube oscillator: testing proposed models. *Planta, 217*(1), 147-157.

Meyvantsson, I., & Beebe, D. J. (2008). Cell culture models in microfluidic systems. *Annu. Rev. Anal. Chem., 1*, 423-449.

Michard, E., Alves, F., & Feijó, J. A. (2009). The role of ion fluxes in polarized cell growth and morphogenesis: the pollen tube as an experimental paradigm. *International Journal of Developmental Biology, 53*(8), 1609.

Money, N. (2007). Biomechanics of invasive hyphal growth *Biology of the Fungal Cell* (Second ed., Vol. 8, pp. 237-249): Springer.

Money, N. P. (2001). Biomechanics of invasive hyphal growth. In R. J. Howard & N. A. R. Gow (Eds.), *The Mycota: Biology of the Fungal Cell* (Vol. 8, pp. 3-17). New York, New York, USA: Springer.

Money, N. P. (2004). The fungal dining habit: a biomechanical perspective. *Mycologist, 18*(2), 71-76.

Money, N. P., Davis, C. M., & Ravishankar, J. P. (2004). Biomechanical evidence for convergent evolution of the invasive growth process among fungi and oomycete water molds. *Fungal Genetics and Biology, 41*, 872-876.

Money, N. P., & Harold, F. M. (1992). Extension growth of the water mold Achlya: interplay of turgor and wall strength. *Proceedings of the National Academy of Sciences, 89*(10), 4245-4249.

Money, N. P., & Harold, F. M. (1993). Two water molds can grow without measurable turgor pressure. *Planta, 190*(3), 426-430.

Nezhad, A. S., Ghanbari, M., Agudelo, C., Packirisamy, M., & Bhat, R. (2012). *A new polydimethylsiloxane (PDMS) microcantilever with integrated optical waveguide for biosensing application.* Paper presented at the Photonics North 2012.

Nezhad, A. S., Naghavi, M., Packirisamy, M., Bhat, R., & Geitmann, A. (2013a). Quantification of cellular penetrative forces using lab-on-a-chip technology and finite element modeling. *Proceedings of the National Academy of Sciences, 110*(20), 8093-8098.

Nezhad, A. S., Naghavi, M., Packirisamy, M., Bhat, R., & Geitmann, A. (2013b). Quantification of the Young's modulus of the primary plant cell wall using Bending-Lab-On-Chip (BLOC). *Lab Chip*.

Nikkhah, M., Strobl, J. S., & Agah, M. (2007). *Geometry-Dependent Behavior of Fibroblast Cells in Three-Dimensional Silicon Microstructures.* Paper presented at the Engineering in Medicine and Biology Society, 2007. EMBS 2007. 29th Annual International Conference of the IEEE.

Nikkhah, M., Strobl, J. S., & Agah, M. (2009). Attachment and response of human fibroblast and breast cancer cells to three dimensional silicon microstructures of different geometries. *Biomedical microdevices, 11*(2), 429-441.

Nunes, L. (2011). Mechanical characterization of hyperelastic polydimethylsiloxane by simple shear test. *Materials Science and Engineering: A, 528*(3), 1799-1804.

Nuxoll, E., & Siegel, R. (2009). BioMEMS devices for drug delivery. *IEEE Engineering in Medicine and Biology Magazine, 28*, 31-39.

Oleschuk, R. D., Shultz-Lockyear, L. L., Ning, Y., & Harrison, D. J. (2000). Trapping of bead-based reagents within microfluidic systems: on-chip solid-phase extraction and electrochromatography. *Analytical chemistry, 72*(3), 585-590.

Orr, A. W., Helmke, B. P., Blackman, B. R., & Schwartz, M. A. (2006). Mechanisms of mechanotransduction. *Developmental cell, 10*(1), 11-20.

Ortega, J. K. (1990). Governing equations for plant cell growth. *Physiologia Plantarum, 79*(1), 116-121.

Ottesen, E. A., Hong, J. W., Quake, S. R., & Leadbetter, J. R. (2006). Microfluidic digital PCR enables multigene analysis of individual environmental bacteria. *science, 314*(5804), 1464-1467.

Palanivelu, R., & Johnson, M. A. (2011). Functional genomics of pollen tube-pistil interactions in *Arabidopsis*. *Biochemical Society Transactions, 38*, 593–597.

Palanivelu, R., & Preuss, D. (2000). Pollen tube targetting and axon guidance: Parallels in tip growth mechanisms. *Trends in Cell Biology, 10*, 517- 524.

Palanivelu, R., & Tsukamoto, T. (2011). Pathfinding in angiosperm reproduction: pollen tube guidance by pistils ensures successful double fertilization. *WIREs Developmental Biology, 1*, 96-113. doi: 10.1002/wdev.6

Park, J., Ryu, J., Choi, S. K., Seo, E., Cha, J. M., Ryu, S., . . . Lee, S. H. (2005). Real-time measurement of the contractile forces of self-organized cardiomyocytes on hybrid biopolymer microcantilevers. *Analytical chemistry, 77*(20), 6571-6580.

Parre, E., & Geitmann, A. (2005). More than a leak sealant - the physical properties of callose in pollen tubes. *Plant Physiology, 137*, 274-286.

Parre, E., & Geitmann, A. (2005). Pectin and the role of the physical properties of the cell wall in pollen tube growth of Solanum chacoense. *Planta, 220*(4), 582-592.

Petersen, N. O., McConnaughey, W. B., & Elson, E. L. (1982). Dependence of locally measured cellular deformability on position on the cell, temperature, and cytochalasin B. *Proceedings of the National Academy of Sciences, 79*(17), 5327-5331.

Peyton, S. R., Ghajar, C. M., Khatiwala, C. B., & Putnam, A. J. (2007). The emergence of ECM mechanics and cytoskeletal tension as important regulators of cell function. *Cell biochemistry and biophysics, 47*(2), 300-320.

Pierson, E., Miller, D., Callaham, D., Van Aken, J., Hackett, G., & Hepler, P. (1996). Tip-localized calcium entry fluctuates during pollen tube growth. *Developmental biology, 174*(1), 160-173.

Pina, C., Pinto, F., Feijó, J. A., & Becker, J. D. (2005). Gene family analysis of the *Arabidopsis* pollen transcriptome reveals biological implications for cell growth, division control, an gene expression regulation. *Plant Physiology, 138*, 744-756.

Pinto, S., Alves, P., Matos, C., Santos, A., Rodrigues, L., Teixeira, J., & Gil, M. (2010). Poly (dimethyl siloxane) surface modification by low pressure plasma to improve its characteristics towards biomedical applications. *Colloids and Surfaces B: Biointerfaces, 81*(1), 20-26.

Plyushch, T. A., Willemse, M., Franssen-Verheijen, M., & Reinders, M. (1995). Structural aspects of in vitro pollen tube growth and micropylar penetration inGasteria verrucosa (Mill.) H. Duval andLilium longiflorum Thunb. *Protoplasma, 187*(1-4), 13-21.

Prokop, A., Prokop, Z., Schaffer, D., Kozlov, E., Wikswo, J., Cliffel, D., & Baudenbacher, F. (2004). NanoLiterBioReactor: long-term mammalian cell culture at nanofabricated scale. *Biomedical microdevices, 6*(4), 325-339.

Qin, Y., & Yang, Z. (2011). Rapid tip growth: Insights from pollen tubes. *Seminars in Cell and Developmental Biology, 22*, 816-824.

Quist, A., Chand, A., Ramachandran, S., Cohen, D., & Lal, R. (2006). Piezoresistive cantilever based nanoflow and viscosity sensor for microchannels. *Lab on a Chip, 6*(11), 1450-1454.

Rasmussen, A., Mavriplis, C., Zaghloul, M., Mikulchenko, O., & Mayaram, K. (2001). Simulation and optimization of a microfluidic flow sensor. *Sensors and Actuators A: Physical, 88*(2), 121-132.

Raty, S., Davis, J., Beebe, D., Rodriguez-Zas, S., & Wheeler, M. (2001). Culture in microchannels enhances in vitro embryonic development of preimplantation mouse embryos. *Theriogenology, 55*(1), 241.

Raty, S., Walters, E. M., Davis, J., Zeringue, H., Beebe, D. J., Rodriguez-Zas, S. L., & Wheeler, M. B. (2004). Embryonic development in the mouse is enhanced via microchannel culture. *Lab on a Chip, 4*(3), 186-190.

Rojas, E., Hotton, S., & Dumais, J. (2011). Chemically mediated mechanical expansion of the pollen tube cell wall. *Biophysical Journal, 101*, 1844–1853.

Saif, M. T. A., Sager, C. R., & Coyer, S. (2003). Functionalized biomicroelectromechanical systems sensors for force response study at local adhesion sites of single living cells on substrates. *Annals of Biomedical Engineering, 31*(8), 950-961.

Sanati Nezhad, A., Ghanbari, M., Agudelo, C., Packirisamy, M., Bhat, R., & Geitmann, A. (submitted). PDMS microcantilever-based flow sensor integration for lab-on-a-chip. *IEEE Sensors Journal*.

Sanati Nezhad, A., Ghanbari, M., Agudelo, C. G., Naghavi, M., Packirisamy, M., Bhat, R. B., & Geitmann, A. (2013). Optimization of flow assisted entrapment of pollen grains in a microfluidic platform for tip growth analysis. *Biomedical Microdevices*.

Sanati Nezhad, A., Ghanbari, M., Agudelo, C. G., Packirisamy, M., Bhat, R. B., & Geitmann, A. (2013). PDMS microcantilever-based flow sensor integration for lab-on-a-chip. *IEEE Sensors, 13*, 601-609.

Sanati Nezhad, A., Naghavi, M., Packirisamy, M., Bhat, R., & Geitmann, A. (2013). Quantification of cellular penetrative forces using lab-on-a-chip technology and finite element modeling. *Proceedings of the National Academy of Sciences, 110*(20), 8093-8098.

Sanati Nezhad, A., Naghavi, M., Packirisamy, M., Bhat, R., & Geitmann, A. (2013). Quantification of the Young's modulus of the primary plant cell wall using Bending-Lab-On-Chip (BLOC). *Lab Chip, 13*, 2599-2608.

Sasoglu, F. M., Bohl, A. J., & Layton, B. E. (2007). Design and microfabrication of a high-aspect-ratio PDMS microbeam array for parallel nanonewton force measurement and protein printing. *Journal of Micromechanics and Microengineering, 17*(3), 623.

Schopfer, P. (2006). Biomechanics of plant growth. *American Journal of Botany, 93*(10), 1415-1425.

Seger, U., Gawad, S., Johann, R., Bertsch, A., & Renaud, P. (2004). Cell immersion and cell dipping in microfluidic devices. *Lab Chip, 4*(2), 148-151.

Sherwood, T. K., Pigford, R. L., & Wilke, C. R. (1975). *Mass transfer* (Vol. 23): McGraw-Hill New York.

Skelley, A. M., Kirak, O., Suh, H., Jaenisch, R., & Voldman, J. (2009). Microfluidic control of cell pairing and fusion. *Nature methods, 6*(2), 147-152.

Strömberg, A., Karlsson, A., Ryttsén, F., Davidson, M., Chiu, D. T., & Orwar, O. (2001). Microfluidic device for combinatorial fusion of liposomes and cells. *Analytical chemistry, 73*(1), 126-130.

Taiz, L., & Zeiger, E. (2010). *Plant Physiology* (Fifth ed.): Sinauer Associates.

Tan, J. L., Tien, J., Pirone, D. M., Gray, D. S., Bhadriraju, K., & Chen, C. S. (2003). Cells lying on a bed of microneedles: an approach to isolate mechanical force. *Proceedings of the National Academy of Sciences, 100*(4), 1484-1489.

Tan, W. H., & Takeuchi, S. (2007). A trap-and-release integrated microfluidic system for dynamic microarray applications. *Proceedings of the National Academy of Sciences, 104*(4), 1146.

Taylor, M. T., Belgrader, P., Furman, B. J., Pourahmadi, F., Kovacs, G. T., & Northrup, M. A. (2001). Lysing bacterial spores by sonication through a flexible interface in a microfluidic system. *Analytical chemistry, 73*(3), 492-496.

Terao, M., Akutsu, T., & Tanaka, Y. (2007). *Non-wetted thermal micro flow sensor.* Paper presented at the SICE, 2007 Annual Conference.

Thomas, C., Zhang, Z., & Cowen, C. (2000). Micromanipulation measurements of biological materials. *Biotechnology letters, 22*(7), 531-537.

Timoshenko, S., & Gere, J. (1972). *Mechanics of Materials. van Nordstrand Reinhold Company*.

Tomos, A. (1988). Cellular water relations of plants. *Water Sci. Rev, 3*, 186-277.

Vogler, H., Draeger, C., Weber, A., Felekis, D., Eichenberger, C., Routier-Kierz-kowska, A.-L., Smith, R. S. (2013). The pollen tube: a soft shell with a hard core. *The Plant Journal, 73*, 617-627.

Voldman, J., Gray, M. L., Toner, M., & Schmidt, M. A. (2002). A microfabrication-based dynamic array cytometer. *Analytical chemistry, 74*(16), 3984-3990.

Walker, G., Ozers, M., & Beebe, D. (2002). Insect cell culture in microfluidic channels. *Biomedical microdevices, 4*(3), 161-166.

Walker, G. M., Zeringue, H. C., & Beebe, D. J. (2004). Microenvironment design considerations for cellular scale studies. *Lab on a Chip, 4*(2), 91-97.

Wang, F., Wang, H., Wang, J., Wang, H. Y., Rummel, P. L., Garimella, S. V., & Lu, C. (2008). Microfluidic delivery of small molecules into mammalian cells based on hydrodynamic focusing. *Biotechnology and bioengineering, 100*(1), 150-158.

Wang, L., Hukin, D., Pritchard, J., & Thomas, C. (2006). Comparison of plant cell turgor pressure measurement by pressure probe and micromanipulation. *Biotechnology letters, 28*(15), 1147-1150.

Wang, N., Tytell, J. D., & Ingber, D. E. (2009). Mechanotransduction at a distance: mechanically coupling the extracellular matrix with the nucleus. *Nature reviews Molecular cell biology, 10*(1), 75-82.

Wang, Y.-H., Lee, C.-Y., & Chiang, C.-M. (2007). A MEMS-based air flow sensor with a free-standing micro-cantilever structure. *Sensors, 7*(10), 2389-2401.

Wang, Y., Zhang, W.-Z., Song, L.-F., Zou, J.-J., Su, Z., & Wu, W.-H. (2008). Transcriptome analyses show changes in gene expression to accompany pollen germination and tube growth in *Arabidopsis*. *Plant Physiology, 148*, 1201-1211.

Wheeler, A. R., Throndset, W. R., Whelan, R. J., Leach, A. M., Zare, R. N., Liao, Y. H., . . . Daridon, A. (2003). Microfluidic device for single-cell analysis. *Analytical chemistry, 75*(14), 3581-3586.

Wilding, P., Kricka, L. J., Cheng, J., Hvichia, G., Shoffner, M. A., & Fortina, P. (1998). Integrated cell isolation and polymerase chain reaction analysis using silicon microfilter chambers. *Analytical biochemistry, 257*(2), 95-100.

Winship, L. J., Obermeyer, G., Geitmann, A., & Hepler, P. K. (2010). Under pressure, cell walls set the pace. *Trends in plant science, 15*(7), 363-369.

Winship, L. J., Obermeyer, G., Geitmann, A., & Hepler, P. K. (2011). Pollen tubes and the physical world. *Trends in Plant Science, 16*, 353-355

Wu, M.-H., Huang, S.-B., & Lee, G.-B. (2010). Microfluidic cell culture systems for drug research. *Lab on a Chip, 10*(8), 939-956.

Xia, Y., & Whitesides, G. M. (1998). Soft lithography. *Annual review of materials science, 28*(1), 153-184.

Xiang, Y., & LaVan, D. A. (2007). Analysis of soft cantilevers as force transducers. *Applied Physics Letters, 90*(13), 133901-133901-133903.

Yang, M., Li, C. W., & Yang, J. (2002). Cell docking and on-chip monitoring of cellular reactions with a controlled concentration gradient on a microfluidic device. *Analytical chemistry, 74*(16), 3991-4001.

Yang, S., & Saif, T. (2005). Reversible and repeatable linear local cell force response under large stretches. *Experimental cell research, 305*(1), 42-50.

Yetisen, A., Jiang, L., Cooper, J., Qin, Y., Palanivelu, R., & Zohar, Y. (2011b). A microsystem-based assay for studying pollen tube guidance in plant reproduction. *Journal of Micromechanics and Microengineering, 21*(5), 054018.

Young, E. W., & Beebe, D. J. (2010). Fundamentals of microfluidic cell culture in controlled microenvironments. *Chemical Society Reviews, 39*(3), 1036-1048.

Yu, H., Meyvantsson, I., Shkel, I. A., & Beebe, D. J. (2005). Diffusion dependent cell behavior in microenvironments. *Lab on a Chip, 5*(10), 1089-1095.

Zahalak, G., McConnaughey, W., & Elson, E. (1990). Determination of cellular mechanical properties by cell poking, with an application to leukocytes. *Journal of biomechanical engineering, 112*(3), 283-294.

Zare, R. N., & Kim, S. (2010). Microfluidic platforms for single-cell analysis. *Annual review of biomedical engineering, 12*, 187-201.

Zerzour, R., Kroeger, J., & Geitmann, A. (2009). Polar growth in pollen tubes is associated with spatially confined dynamic changes in cell mechanical properties. *Developmental biology, 334*(2), 437-446.

Zhang, Y., Lo, C.-W., Taylor, J. A., & Yang, S. (2006). Replica molding of high-aspect-ratio polymeric nanopillar arrays with high fidelity. *Langmuir, 22*(20), 8595-8601.

Zhang, Z., Ferenczi, M., Lush, A., & Thomas, C. (1991). A novel micromanipulation technique for measuring the bursting strength of single mammalian cells. *Applied microbiology and biotechnology, 36*(2), 208-210.

Zimmermann, U., & Steudle, E. (1979). Physical aspects of water relations of plant cells. *Advances in Botanical Research, 6*, 45-117.

Zonia, L. (2010). Spatial and temporal integration of signalling networks regulating pollen tube growth. *Journal of experimental botany, 61*(7), 1939-1957.

Zonia, L., Müller, M., & Munnik, T. (2006). Hydrodynamics and cell volume oscillations in the pollen tube apical region are integral components of the biomechanics of Nicotiana tabacum pollen tube growth. *Cell biochemistry and biophysics, 46*(3), 209-232.

Zou, H., Mellon, S., Syms, R., & Tanner, K. (2006). 2-dimensional MEMS dielectrophoresis device for osteoblast cell stimulation. *Biomedical Microdevices, 8*, 353–359.